Technical Report 80-2

CALIBRATION CHARACTERISTICS OF IRAD GAGE VIBRATING WIRE STRESSMETER AT NORMAL AND HIGH TEMPERATURE

VOLUME 1

Prepared for

University of California
Lawrence Livermore Laboratory
P. O. Box 5012
LIVERMORE, California 94550

by

Piyush K. Dutta
Robert W. Hatfield
Peter W. Runstadler, Jr.

IRAD GAGE
(Creare Products Inc.)
Etna Road
LEBANON, New Hampshire 03766 USA
(603) 448-4445

October, 1981

DISCLAIMER

NOTICE

Work performed under the auspices of the U.S. Department of Energy by the Lawrence Livermore Laboratory under contract number W-7405-ENG-48.

"This report is an account of work performed by IRAD for the University of California, Lawrence Livermore National Laboratory. The intent of the work was to obtain laboratory calibration data for the vibrating wire stress meter in Climax Stock Quartz Monzonite. The theoretical development contained in this report is incidental to the main task, is incomplete at this stage, and is included in this report only to indicate avenues so far explored in understanding the gage-rock interaction problem."

DISCLAIMER

Portions of this document may be illegible in electronic image products. Images are produced from the best available original document.

UCRL--15426 Vol. 1

DE82 005512

Technical Report 80-2

CALIBRATION CHARACTERISTICS OF IRAD GAGE VIBRATING WIRE STRESSMETER AT NORMAL AND HIGH TEMPERATURE

VOLUME 1

Prepared for

University of California
Lawrence Livermore Laboratory
P. O. Box 5012
LIVERMORE, California 94550

by

Piyush K. Dutta
Robert W. Hatfield
Peter W. Runstadler, Jr.

IRAD GAGE
(Creare Products Inc.)
Etna Road
LEBANON, New Hampshire 03766 USA
(603) 448-4445

October, 1981

CONTENTS

VOLUME 1

CONTENTS

LIST OF ILLUSTRATIONS

LIST OF ILLUSTRATIONS

LIST OF TABLES

FOREWARD

This report was prepared by IRAD GAGE (Division of Creare Products Inc.) under the University of California, Lawrence Livermore Laboratory Contract P. O. No. 7989009. The contract was initiated by the Lawrence Livermore Laboratory under the auspices of the U. S. Department of Energy's UCLL Contract No. W-7405-ENG-48. The University's Technical Representative under this contract was Dr. R. C. Carlson. Mr. H. L. Halunen was the Contract Administrator.

This report is a summary of the work completed as part of this contract during the period of February, 1980 to September, 1980.

The authors wish to acknowledge the assistance of Dr. R. C. Carlson, who provided valuable guidance for the test program, and also that of Dr. Bert Abbey of Lawrence Livermore Laboratory, who arranged for the Climax granite test samples. Dr. Malcolm Mellor, U. S. Army Cold Regions Research and Engineering Laboratory, Hanover, New Hampshire, acted as a consultant. Mr. M. Hughes and Mr. J. B. McRae of IRAD GAGE provided material and equipment support from the IRAD GAGE production facility and reviewed the report. Robert Tutwiler assisted in all experimental work.

EXECUTIVE SUMMARY

This report describes calibration studies of the IRAD GAGE Vibrating Wire Stressmeter. The work has been performed for the University of California, Lawrence Livermore Laboratory, to understand and interpret the behavior and performance of the stressmeter in Climax granite. To help interpret the results obtained in Climax granite, the study also included calibration tests of the gage in other materials: Barre granite, aluminum, and Lucite.

Stressmeter calibrations were carried out in thin rock slabs by determining the relation between the stressmeter readings and uniaxial plane stresses. Calibrations were also conducted under biaxial and triaxial stress fields. The biaxial tests were made by setting stressmeters into cylindrical rock cores loaded hydrostatically around their periphery, leaving the ends unloaded. Triaxial tests were made by repeating the biaxial tests, with the addition of end loading. The effects of temperature on calibration characteristics were also evaluated by conducting uniaxial, biaxial and triaxial tests between room temperature and approximately 100°C.

The Vibrating Wire Stressmeter is a highly sensitive gage which can detect minute changes in the diameter of the gage (as small as 0.1×10^{-6} in.) induced by stress changes in the material surrounding the borehole into which it is set. The relation between changes in gage output and stress changes in the surrounding material — i.e., the gage calibration characteristics — commonly referred to as the stress sensitivity factor* of the stressmeter — are governed by:

- the host material physical characteristics,
- gage design and construction
- the stress environment.

The stress sensitivity factor of the Vibrating Wire Stressmeter is dependent upon Young's Modulus of the host material. This study clearly displays this dependence for the four materials investigated.

For Climax granite, the variation in the stress sensitivity factor is further compounded by the large variation in physical properties of this material. Young's Modulus can vary by as much as 12% and porosity by about 40%. Bulk anisotropy is also important in interpreting stressmeter behavior in Climax granite — the Climax granite specimens used in this study contained a variable number and orientation of micro and macro cracks and assorted sizes of feldspar crystals. The variability of rock properties and bulk anisotropy of the material must be taken into consideration when interpreting stressmeter data in Climax granite.

---

* The stress sensitivity factor of the vibrating wire stressmeter is the number by which a uniaxial rock stress change is multiplied to obtain the change of stress in the vibrating wire element.

The stressmeters prepared for Lawrence Livermore Laboratory have a slightly greater gage body stiffness than the standard IRAD GAGE VBS-1HT stressmeter. This is caused by heat treatment and electroplating of the gage body. All other design and construction characteristics of the gages are identical to the standard stressmeter.

The contact geometry of the stressmeter platen, which is used to wedge the gage in the borehole, has an effect on gage sensitivity. This was demonstrated by analysis and tests in this investigation. The analysis and tests show that a large platen contact area increases the stress sensitivity factor.

The stress environment, which also determines the response of the stressmeter, depends upon the factors of:

- gage setting preload,
- initial in-situ stress,
- loading range,
- gage orientation to the applied load,
- biaxial and triaxial stress fields, and
- the influence of elevated temperature.

Preload - The calibration tests on all four materials showed that the gage sensitivity factor increased with higher gage preload, and that a minimum preload value should be used for each material, above which the sensitivity factor of the gage is essentially constant.

Initial Stress Field - Tests in Climax granite showed initial uniaxial stress fields up to 1300 psi had a negligible effect on gage calibration.

Load Range - Load range has a slight effect on the gage stress sensitivity factor. In all materials the factor increased slightly with load up to the maximum load measured.

Gage Orientation - Gage orientation tests conducted in Climax granite showed a very close correlation with results expected from classical elasticity theory.

Biaxial and Triaxial Stress Fields - The wide range of tests conducted in Climax granite slabs under uniaxial stress loading correlated well with the biaxial and triaxial loading tests indicating that biaxial and triaxial loading did not significantly affect the stress sensitivity factor of the stressmeter.

Influence of Elevated Temperature - Analysis of the influence of temperature on stressmeter response predicts only a very small increase of sensitivity factor with temperature; this has been borne out by the tests conducted in Climax and Barre granites.

Under biaxial and triaxial loading, however, the data display a more pronounced increase in stressmeter sensitivity factor (approximately 25%) at temperatures of approximately 100°C. No attempt was made in this report to analyze the temperature problem under biaxial and triaxial loading conditions.

Of the number of specific factors discussed above that were investigated during the course of this study, the important results are summarized as follows:

1) Existing stress fields appear to have negligible effect on the stressmeter gage calibration.

2 In setting the stressmeter, a minimum preload value should be used above which the stressmeter sensitivity factor is constant. This value has been determined for Climax granite.

3) The amount of surface contact between the gage (gage platen) and the borehole controls gage sensitivity. It is important to control borehole size, shape and surface condition at those locations where the Vibrating Wire Stressmeter is used.

4) Local variations of rock elastic modulus and rock anisotropy — macro and micro cracks and heterogeneous inclusions — can have a relatively large influence on stressmeter sensitivity. Both of these factors are very pronounced in Climax granite. The variability of the physical factors must be taken into account in interpreting stressmeter behavior in Climax granite.

5) Calibration tests conducted in this study indicated that biaxial and triaxial loading do not significantly affect the stress sensitivity factor.

6) A very small increase of stressmeter sensitivity factor occurs with increasing temperature up to 100°C and this is predicted by theory. Under biaxial and triaxial loadings, however, the test data show a more pronounced increase in stress sensitivity factor of approximately 25% at 100°C.

NOMENCLATURE

b	Width of the platen contact, in.
B	Diameter of the cylindrical triaxial test sample, in.
D	Borehole diameter, in.
d	Stressmeter diameter, in.
d_1^o, d_2	Contact surface curvature diameters, in.
d_i	Stressmeter body inside diameter, in.
E^i	Young's modulus of wire material
E^w	Young's modulus of rock
f^r	Frequency
g	Acceleration due to gravity
h	Stressmeter height to flat, in.
K	Constant
K_g	Stiffness of gage body, lb/in.
K^{ga}	Stiffness of gage assembly, lb/in.
ℓ^{ga}	Wire length, in.
L^w	Stressmeter length, in.
L^g	Platen length, in.
p^p	Force on gage body per linear in.
P	Force on gage body, lb
P_o	Hydrostatic pressure, psi
P^o	Stress due to end loading, psi
r^z	Hole radius, in.
t^o	Gage width
t_o	Initial gage temperature °F
t_1^o	Current gage temperature °F
T	MB-6 (Stressmeter Readout) reading

α	Uniaxial Stress Sensitivity Factor
β	Half contact angle (radian)
δ	Hole closure (in.)
δ_w	Wire deformation (in.)
δ^w	Empty hole closure (in.)
δ^e	Hole opening by preloading the gage (in.)
ε^p	Strain (in./in.)
ε_w	Wire strain (in./in.)
ε^w	
ε_{w_o}	Wire strain of unset gage for reading T_o, @ temperature t_o °F
ε_{w_1}	Wire strain of unset gage for reading T_1, @ temperature t_1 °F
ε_{w_2}	Wire strain of set gage, reading T_2, @ temperature t_2°F
θ_w	Coefficient of thermal expansion of wire, in./in./°F
θ^w	Coefficient of thermal expansion of gage body in./in./°F
θ^B	Coefficient of thermal expansion of rock, in./in./°F
ρ^r	Density, lb/in.^{3}
σ	Stress, psi (MPa)
σ_w	Wire stress, psi (MPa)
υ^w	Poisson's ratio

1. INTRODUCTION

This report presents the results of a study of the calibration characteristics of the IRAD GAGE vibrating wire stressmeter in Climax granite. The study also includes the investigation of the gage in other materials including Barre granite. This investigation was sponsored by Lawrence Livermore Laboratory, University of California, to interpret data to be obtained from the Nevada Test site and, in particular, to resolve several questions related to stress response of the gage and thermal effects on the stressmeter readings.

The vibrating wire stressmeter was initially developed by IRAD GAGE as a borehole gage to indicate changes in the stress field around underground excavations. The stressmeter is highly sensitive and if meter readings do not change, then conditions are stable around the area of the meter. Calibration data are normally supplied with the gage instruction manual to provide a rough correlation between the magnitude of the gage readings and the stress changes, both for uniaxial and biaxial stress fields. In recent years, there has been a growing use of the vibrating wire stressmeter in scientific studies; this requires a more precise correlation between the stressmeter readings and the stresses causing them, and has been a central purpose of this study.

The vibrating wire stressmeter is a very stiff unidirectional deformation gage. It enables extremely minute diametral changes (as small as 0.1×10^{-6} in., 2.54×10^{-6} mm) to be measured in a direction parallel to a highly tensioned steel wire mounted across a hollow steel cylinder preloaded in a borehole. Because the steel cylinder is relatively stiff compared to many of the materials (usually rock) into which it is set, any deformations of the borehole induced by stress changes in the surrounding material are resisted by the cylinder. The essential difference between a true stressmeter and a borehole deformation gage is that, in the case of a true stressmeter, the stress change is measured directly from the stressmeter output whereas, in the case of a borehole deformation gage, the stress change is determined from a knowledge of the modulus of elasticity of the rock and the deformation output of the gage. Ideally, the output of a true stressmeter should not be influenced by Young's Modulus — and it follows that the borehole cannot be allowed to deform. However, construction of such an ideal rigid inclusion stressmeter is not practical. In reality, the design of a stressmeter seeks a compromise between a very small deformation of the hole, in order for the transducer to sense the stress change, and a relatively small influence of the elastic modulus of the host material on the gage output. Normally, the very small deformation allows only a poor sensitivity of the gage to be realized, but the vibrating wire stressmeter allows a high resolution, ruggedness, temperature stability, and remote reading capability.

A detailed discussion of this subject, known as "Inclusion Theory", is given by Coutinho (1949). Basically, applying this theory to the vibrating wire stressmeter shows that a non-linear relation exists between the applicable host material moduli (Young's Modulus, Poisson's Ratio) and the gage readings. The theory shows that for a given gage stiffness, as host material modulus decreases, the gage sensitivity becomes less

dependent on its value. For a perfect thick-walled annular cylinder inclusion, with a material modulus of 10 x 10^6 psi (69.0 GPa) and bounded around its periphery into a borehole, the deformation induced in the inclusion is completely independent of the host material modulus once this has fallen below 10^6 psi (6.9 GPa). The IRAD GAGE vibrating wire stressmeter response is found to be dependent on host material modulus for common granite materials such as those tested in this study. The current test program measured uniaxial gage sensitivity factor using four materials; included were two granites (Climax and Barre), aluminum (Young's Modulus = 10 x 10^6 psi; 69.0 GPa) and Lucite (Young's Modulus = 0.5 x 10^6 psi; 3.5 GPa). The sensitivity factor was found to change around 44% over this range. For comparison, the sensitivity of a borehole deformation meter would change by another order of magnitude over a similar range of modulus change (Hawkes 1973). Because physical and elastic rock properties are not easy to obtain and they vary with such factors as time and rate of loading, stress, anisotropy, temperature and the presence of moisture, the precise correlation between meter readings and stress must be obtained by direct calibration. Other secondary factors that make a direct calibration approach mandatory involve the physical interaction of the gage with the borehole, i.e., curvature of the loading platens relative to the borehole diameter and their area of contact with the borehole walls. An analytical description of these factors useful in understanding the correlating data is given in Section 2 of this report.

The stressmeter calibrations were carried out in thin rock slabs by determining the relationship between the stressmeter readings and uniaxial plane stresses. Biaxial and triaxial behavior were predicted from the uniaxial test data using the principle of stress superposition and these predictions are compared to calibration factors obtained from biaxial and triaxial tests. The biaxial tests were made by setting stressmeters into 5½ in. diameter rock cores loaded hydrostatically around their periphery, leaving the ends unloaded. Triaxial tests were made by repeating the biaxial tests, with the addition of end loading. The test equipment and procedures used are discussed in detail in Section 3.

The several specific factors that were investigated during the course of this study are:

(1) The influence of existing stress fields and of gage preload on the calibration factors.

(2) The influence of platen form and matching of borehole and platen shape on the calibration factors.

(3) The influence of temperature on gage readings both at constant stress and under changing stress fields.

(4) The influence of rock anisotropy on the calibration values.

Because of the heterogeneity of the Climax granite test samples and smallness of their size, some additional studies on strain perturbation effect were conducted using foil strain gages. The results of all tests are summarized and presented in graphical form in Section 4. The test case numbers are shown in parentheses on the data points of the graphs. The raw data has been attached as Appendix 9 to this report.

In Section 5, the results are discussed in brief and specific conclusions are summarized. The principal results are that the uniaxial stress sensitivity factor for the material Climax granite varied over a wide margin — from 2.7 to 4.5. The stressmeter setting preload has been observed to have a major influence on the sensitivity factor and, to reduce this influence when the gage is set, an optimum preloading of the stressmeter must be ensured. The influence of a temperature rise of up to 100°C indicated an increase of up to 25% on the sensitivity factor under biaxial and triaxial loading. Test data for uniaxial loading at high temperature, however, does not show any perceptible increase over a similar temperature range, and is in agreement with analytical predictions of the behavior.

2. PREDICTED BEHAVIOR OF THE STRESSMETER

This section of the report has been prepared to help understand the vibrating wire stressmeter characteristics by predicting gage performance using analytical models of the gage and of the host material behavior. The various equations and graphical results describing gage behavior are used later to explain and interpret test results.

2.1 Background

The IRAD GAGE vibrating wire stressmeter uses a tensioned wire across a hollow steel cylinder which is preloaded diametrically across the sides of a 1.5 in. (3.8 cm) borehole by means of a sliding wedge platen assembly. Because of the wedge platen loading system, the vibrating wire stressmeter is, in the strictest sense, neither a borehole inclusion stressmeter — in which continuity of stresses and displacements is maintained across the entire interface between the stressmeter and the surrounding rock — nor a borehole deformation gage — in which the gage modulus of elasticity is much lower than that of the rock. As such, the vibrating wire stressmeter is a separate class of instrument, which we call a semi-rigid stressmeter. The three classes of borehole type measuring devices can, therefore, be summarized as in Figure 1. These classes are:

(a) Rigid and elastic inclusion gages (stress continuity through interface).

(b) Borehole deformation gages (borehole diameter measuring instruments).

(c) Semi-rigid inclusion gages (partial contact to borehole surface).

Classical theories to correlate rock stress change to the stressmeter readings are available for both the rigid inclusion type and the deformation type stress gages where the gages do not preload the borehole wall. The IRAD GAGE stressmeter, however, is set with a preload which interferes with the free deformation of the borehole in a complex way and complicates the analytical treatment of the behavior of this gage. While developing the gage, Hawkes (1973) primarily relied on direct calibration of the gage in the range of rocks typically encountered in mines. Later, analytical approximations to predict the gage response were developed by Fossum (1976) and Pariseau (1977). In the following sections, the principle of vibrating wire frequency changes related to gage deformation and the behavior of the gage deformation related to rock stress changes will be explained. The analyses of Fossum and Pariseau will be used and extended to explain the trend and nature of the data obtained during this study. In the final portions of this section, these analyses are extended to relate uniaxial stress behavior to both biaxial and triaxial stressmeter characteristics and to predict and interpret the elevated temperature characteristics for the uniaxial stress loading.

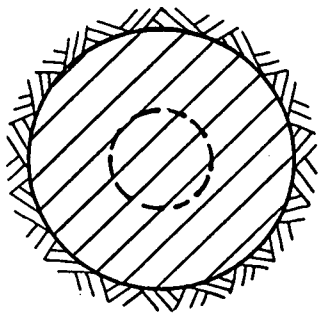	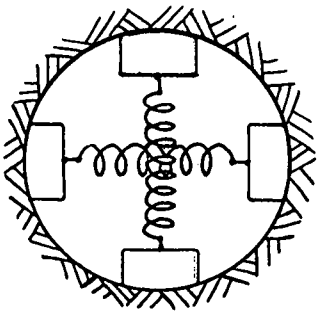	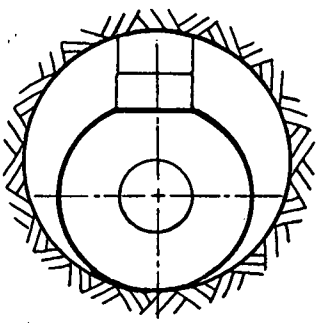
Borehole Inclusion Stressmeter (Solid and Hollow)	**Deformation Gage**	**Semi-rigid Inclusion Gage**
(a) Photoelastic hollow cylinder inclusions (Hawkes, 1967) (b) Strain gaged rigid inclusion probe (Nichols et al 1968) (c) Solid metal plug (Jaeger and Cook (1969)) (Jordan (1965)) (d) Plastic plug with elastic strain gages (Rocha (1969)) (e) End of borehole strain gage device (CSIR electric resistance "doorstopper") (f) Borehole sidewall strain gage device (CSIR triaxial strain cell)	(a) USBM borehole deformation gage (b) Hollow borehole deformation transducer (Rocha (1969)) (c) Pneumatic profile gage (Roberts (1969))	(a) Hast's strain cell (b) IRAD GAGE vibrating wire stressmeter

Figure 1. Major Types of Borehole Stressmeters

2.2 Theory of the Vibrating Wire Stressmeter

The operation of the vibrating wire stressmeter is based on the fact that the fundamental frequency of a stressed wire is proportional to the applied stress in the wire. Figure 2 shows the cross section of a stressmeter set in a borehole. Any deformation of the borehole will change the compression in the gage body and, through deformation of the body, change the stress in the wire. The wire is pretensioned in the gage during manufacture to a predetermined value. When the gage is set into a borehole under preload, using the wedge platen system, the tension in the wire decreases. Later, if the stress in the rock increases, causing compression of the gage body, the wire tension will decrease still further. The output of the stressmeter is the vibration frequency of the wire and is given by the following formula:

$$f = \frac{1}{2\ell_w}\sqrt{\frac{\sigma_w g}{\rho}} \tag{1}$$

where:

f is the natural frequency, (sec^{-1})
ℓ_w is the length of vibrating wire, (in.)
σ_w is the stress in the wire (psi)
ρ is the density of the wire material, $(lb/in.^3)$
g is the acceleration due to gravity, $(in./sec^2)$

For the IRAD GAGE stressmeter, $\ell_w = 0.780$ in. and $\rho = 0.283$ lb/in.^{3}, therefore,

$$f = 23.674\sqrt{\sigma_w}\ (sec^{-1}) \tag{2}$$

Defining T as the 4 digit display of the IRAD GAGE vibrating wire readout unit, T is given by

$$T = \frac{10^7}{f} \tag{3}$$

then

$$\sigma_w = 1.78422 \times 10^{11} \times \frac{1}{T^2}\ (psi) \tag{4}$$

Equation (1) can also be cast in terms of the strain of the wire:

$$f = \frac{1}{2\ell_w}\sqrt{\frac{E_w\, g\varepsilon_w}{\rho}} \tag{5}$$

where:

E_w is the modulus of the wire material (psi), and
ε_w is the wire strain (in./in.)

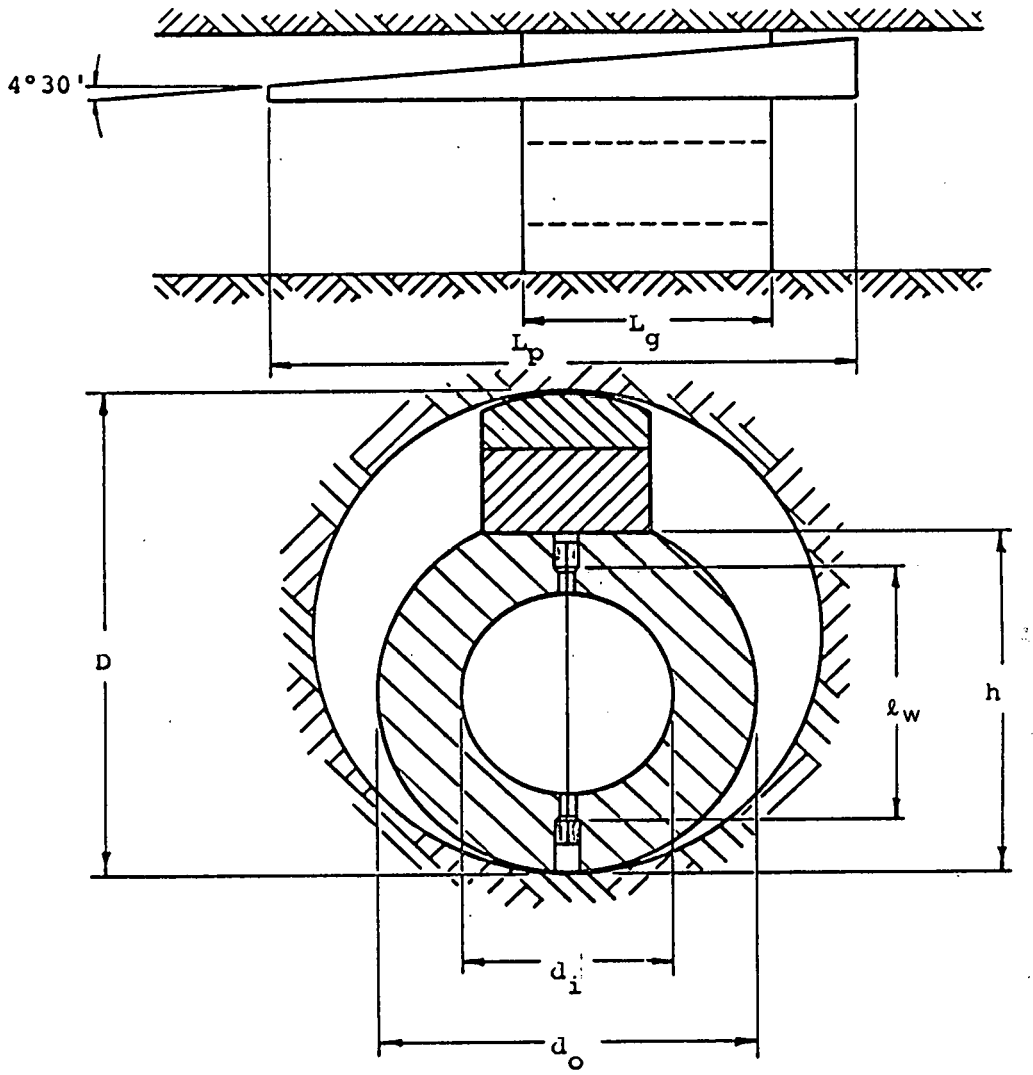

D = bore hole diameter - 1 1/2 ± 1/16 in. (gauge range 1/8")
d_o = gauge diameter - 1.125 ± 0.003 in.
D_i = gauge bore - 0.500, + 0.002, - 0.000 in.
h = gauge height to flat - 1.064 ± 0.002 in.
ℓ_w = wire length - 0.780 ± 0.002 in.
L_g = gauge length - 1.500 ± 0.050 in.
L_p = wedge length - 3 1/2 in. ± 0.050 in.

Figure 2. Critical Dimensions of Vibrating Wire Stressmeter

Rearranging equation (5)

$$\varepsilon_w = \frac{4\ell_w^2 f^2 \rho}{E_w g} = Kf^2 \tag{6}$$

where:

$$K = \frac{4\ell_w^2 \rho}{E_w g}$$

The wire deformation δ_w equals $\ell_w \varepsilon_w$ and hence

$$\delta_w = K\ell f^2 \tag{7}$$

For the vibrating wire stressmeter, where $E_w = 30 \times 10^6$ lb/in.^{2}, $\ell_w = 0.780$ in. and $\rho = 0.283$ lb/in.^{3}, the numerical value of the constant K is calculated to be 5.947×10^{-11} and the wire deformation, δ_w, is given by:

$$\delta_w = 4.639 \times 10^{-11} \times f^2 = \frac{4639}{T^2} \text{ in.} \tag{8}$$

The stressmeter readings on the IRAD GAGE readout unit typically vary between T = 1500 (10^{-7} sec) and T = 4000 (10^{-7} sec. (The operating range of the gage has been set at between 1500-4000 (10^7 sec) to maintain a reasonable gage sensitivity range.) Thus, using equation (8), when T = 1500 (10^{-7} sec), $\delta_w = 2.06 \times 10^{-3}$ in. and when T = 4000 (10^{-7} sec), $\delta_w = 0.29 \times 10^{-3}$ in. From these numerical values, we see that the theoretical deformation range of the wire is indeed very small, being approximately 1.77×10^{-3} in. (2 mils). This very small deformation and relatively large numerical range of readout units give the IRAD GAGE stressmeter a classification as a semi-rigid stressmeter with very high sensitivity.

2.3 Uniaxial Calibration Theory—Stressmeter/Rock Interaction Mechanics

The relation between stressmeter frequency output and gage body deformation has been described in the preceding section. The relation between stressmeter output (wire vibration period) and changes in the rock stress are governed by the mechanics of the gage/rock interaction. The stressmeter output (period of wire vibration) is a function of the wire stress (σ_w) in the stressmeter body. The ratio of the wire stress change ($\Delta\sigma_w$) to the change in rock stress ($\Delta\sigma_r$) provides a simple factor to characterize the stressmeter response in various rocks. This ratio is defined as the 'stress sensitivity factor', and should not be confused with the 'gage uniaxial sensitivity' which gives the rock stress change per unit change in readout meter reading.

The factors which influence the response of the gage to the applied stresses in the borehole can be classified in three categories as given in Table 1.

Table 1. Factors Influencing Stressmeter Sensitivity

Host Material Characteristics	Gage Characteristics	Gage Setting Conditions
Young's modulus	Gage body stiffness	Setting Preload
Poisson's ratio	Gage assembly stiffness	Hole diameter
Anisotropy	Platen geometry	Surface Roughness
Petrofabric		Initial stress level
Creep Property		Gage orientation
		Load range
		Temperature

In the analysis that follows, we will examine the influence of the following factors on the 'stress sensitivity factor': Young's Modulus and Poisson's Ratio of the host material, the gage body and assembly stiffness, platen geometry, and the gage setting conditions of preload and initial stress level.

For modelling the stressmeter setting in rock:

let D_1 = diameter of the empty boreole in rock before setting of the stressmeter;
D_2 = expanded diameter of the borehole after setting and preloading the hole in the process of setting the stressmeter;
D_3 = changed diameter of the hole after a change of rock stress $\Delta\sigma_r$ has occurred;
D_4 = assumed collapsed diameter of the empty hole if the stressmeter was not set in the hole.

From the above, it follows that

if δ_{p_o} = increase in hole diameter by preloading the gage;
δ_p = decrease in diameter because of an increase of stress on rock $\Delta\sigma_r$ after gage setting;
δ_e = decrease in diameter by rock stress change $\Delta\sigma_r$, if the hole was empty;
and δ = amount of hole diameter which remained open because of gage set in hole;

then, referring to Figure 3

$$\delta_{p_o} = D_2 - D_1$$
$$\delta^p = D_2 - D_3$$
$$\delta^e = D_1 - D_4$$
and $$\delta = D_3 - D_4$$

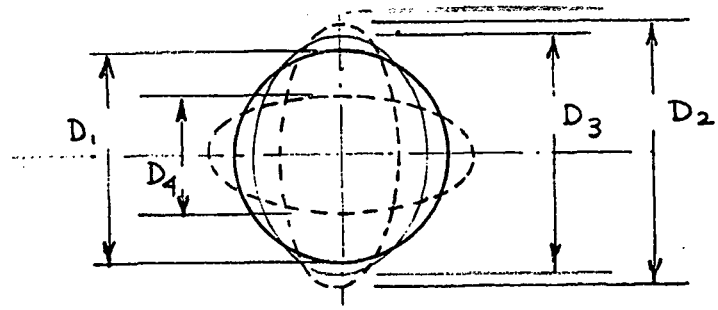

Figure 3. Deformation of a Circular Hole.

From the above, it follows that

$$\delta = \delta_e - \delta_p + \delta_{p_o} \tag{9}$$

The placement of the gage at the preloading stage produces two opposing forces P_o parallel to the direction of σ_r. Assuming that preloading of the gage produces a uniform pressure distribution symmetrically about the gage over the contact angle $2\beta_o$, the deformation, δ_{p_o}, produced by this force (Jaeger and Cook, 1969; also see Appendix 1) is

$$\delta_{p_o} = D_2 - D_1 = \frac{P_o}{E_r} f(\beta_o, \upsilon_r, t) \tag{10}$$

where

$$f(\beta_o, \upsilon_r, t) = \frac{2}{\pi t}\left\{1 + \upsilon_r + \frac{(1-\upsilon_r)}{\beta_o}\left[\frac{\Pi}{2}\cos(\beta_o) - \left(\frac{\Pi}{2}\right) + (\beta_o)\right] + \frac{2}{\beta_o}\sin(\beta_o)\,\ell n\left[\cot\frac{\beta_o}{2}\right]\right\} \tag{11}$$

$2\beta_o$ = contact angle for force P_o on the stressmeter (radian)
υ_r = Poisson's ratio, and
t = gage width (in.)

A change of rock stress (assuming this is compessive) will provide additional compressive force, say P, on the stressmeter when the diameter changes from D_2 to D_3, so that,

$$D_2 - D_3 = \delta_p = \frac{P}{K_{ga}} = \frac{K_g \Delta\delta_w}{K_{ga}} = \frac{K_g \ell_w \Delta\sigma_w}{K_{ga} E_w} \tag{12}$$

where

K_{ga} = stiffness of the gage assembly
K_g^{ga} = stiffness of the gage body
$\Delta\delta_w$ = deformation of the stressmeter wire under load P
ℓ_w = wire length
$\Delta\sigma_w^w$ = change in wire stress corresponding to a change of rock stress $\Delta\sigma_r$

On the otherhand, if the gage were not placed in the hole, the hole would have collapsed from D_1 to D_4, so that,

$$D_1 - D_4 = \delta_e = \frac{3D_1\sigma_r}{E_r} \tag{13}$$

The final diameter of the hole under the combined action of preload and rock stress change is D_3. The difference in diameter, $D_3 - D_4$, arises because the combined P_o and P forces have resisted the complete collapse of the hole diameter, such that,

$$D_3 - D_4 = \delta = \frac{P_o + P}{E_r} f(\beta, \upsilon_r, t) \tag{14}$$

where 2β = platen contact angle for force $P_o + P$.

Substituting for δ, δ_e, δ_p and δ_{p_o} from Eq. (14), (13), (12) and (10), respectively, and also substituting F_o for $f(\beta_o, \upsilon_r, t)$ and F for $f(\beta, \upsilon_r, t)$, it can be shown (see Appendix 2) that,

$$\alpha = \frac{\sigma_w}{\sigma_r} = \frac{3D_1E_w}{K_g \ell_w E_r \left[\frac{\phi(F_1-F_o)+F_1}{E_r} + \frac{1}{K_{ga}} \right]} \tag{15}$$

where,

$$\phi = \frac{P_o}{P} = \frac{\Delta\sigma_{w_o}}{\Delta\sigma_w} = \frac{\text{Change of wire stress at preloading}}{\text{Change of wire stress because of rock stress change}}$$

Substituting

D_1 = 1.5 in.
E_w = 30×10^6 psi
K_g = 7.5×10^6 lb/in.*
K_{g_a} = 5.7×10^6 lb/in.**
ℓ_w = 0.78 in.

in Eq. (15)

$$\alpha = \frac{131.58}{E_r \times 10^{-6} + 5.7[F_1+\phi(F_1-F_o)]} \tag{16}$$

2.3.1 Contact pressure distribution and contact angle

A realistic model of the gage/borehole contact includes a proper analysis of the platen contact with the borehole and the change in this boundary condition as the gage is preloaded or rock stresses change. For the standard hard rock (HR) type platen, the contacting radius is made slightly less than that of the borehole (0.56R for the platen) to eliminate outer boundary stress concentrations. This HR platen shape defines a dome-shaped contact pressure distribution, (Hast, 1958), with a maximum pressure centered over the wire and decreasing pressure towards the platen edge (Figure 4). This contact angle should progressively increase with increased loading of the stressmeter. The analysis is as follows:

---

* This value has been measured experimentally and details are given in Appendix 3.

** This value has been measured by Ivor Hawkes (1973); see Reference (7).

For two cylindrical surfaces, the width of the platen contact, b (in.) is given by the following formula (Roark 1975):

$$b = 1.6\sqrt{pK_D C_E}$$

where p = load on the stressmeter (per linear inch),

$$K_D = \frac{d_1 d_2}{d_1 - d_2}$$ (d_1 = hole diameter, and d_2 = 2 x platen radius of curvature)

and $$C_E = \frac{1-\upsilon_r^2}{E_r} + \frac{1-\upsilon_g^2}{E_g}$$ (υ = Poisson's Ratio, subscript g for gage material, r for rock or sample material)

The contact surface of the stressmeter is 1.5 in. long. Hence, P = 1.5p and the above equation reduces to

$$b = 1.6\sqrt{\frac{PK_D C_E}{1.5}} \qquad (17)$$

For 1.5 in. diameter boreholes used with the HR platen (platen curvature radius = 0.56 in.), the values of b are determined in Table 2. [Assumed values are υ_g = 0.3 and P (load on stressmeter body) = 1.5p (applied load per linear inch).]

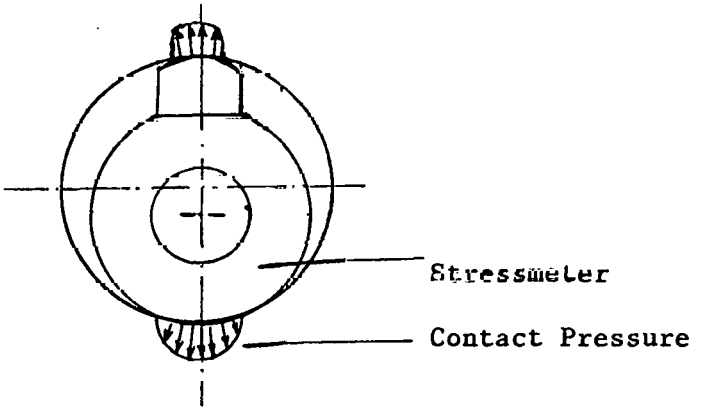

Figure 4. Contact Pressure Distribution Across the Stressmeter

Table 2. Contact Width "b" of Stressmeter Set in Various Materials

Parameter	Material: Aluminum	Barre Granite	Climax Granite	Lucite
υ_r	0.34	0.20	0.21	0.30
E_r (psi)	10×10^6	6×10^6	10×10^6	0.4×10^6
C_E*	1.18×10^{-7}	1.92×10^{-7}	1.26×10^{-7}	2.3×10^{-6}
K_D**	4.5	4.5	4.5	4.5
b***(in.)	$0.951\times10^{-3}\sqrt{P}$	$1.214\times10^{-3}\sqrt{P}$	$0.984\times10^{-3}\sqrt{P}$	$4.203\times10^{-3}\sqrt{P}$

$$* \; C_E = \frac{1-\upsilon_r^2}{E_r} + \frac{1-\upsilon_g^2}{E_g}$$

$$** \; K_D = \frac{d_1 d_2}{d_1 - d_2} = \frac{1.5 \times 1.125}{1.5 - 1.125} = 4.5$$

$$*** \; b = 1.6\sqrt{\frac{PK_D C_E}{1.5}}$$

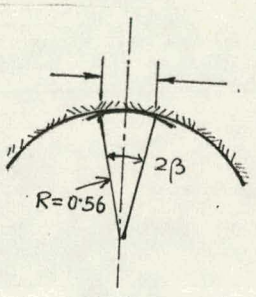

Figure 6.
Geometry of Contact Width

Figure 5 is a plot of contact width vs. applied load for the four materials tested in the current study.

Geometrically, the contact width can be related to contact angle 2β (see Figure 6).

$$\beta = \sin^{-1}\left[\frac{b/2}{0.56}\right]$$

The contact load P, for a typical stressmeter can be calculated as below:

If T_o = initial gage reading before setting
T_1 = gage reading after setting
and T_2 = gage reading after changing stress field

then from equation (4), the total change in wire stress $\Delta\sigma_w$,

$$\Delta\sigma_w = 1.78422\times10^{11}\left[\frac{1}{T_2^2} - \frac{1}{T_o^2}\right]$$

The total change in wire strain $\Delta\varepsilon_w = \frac{\Delta\sigma_w}{E_g}$

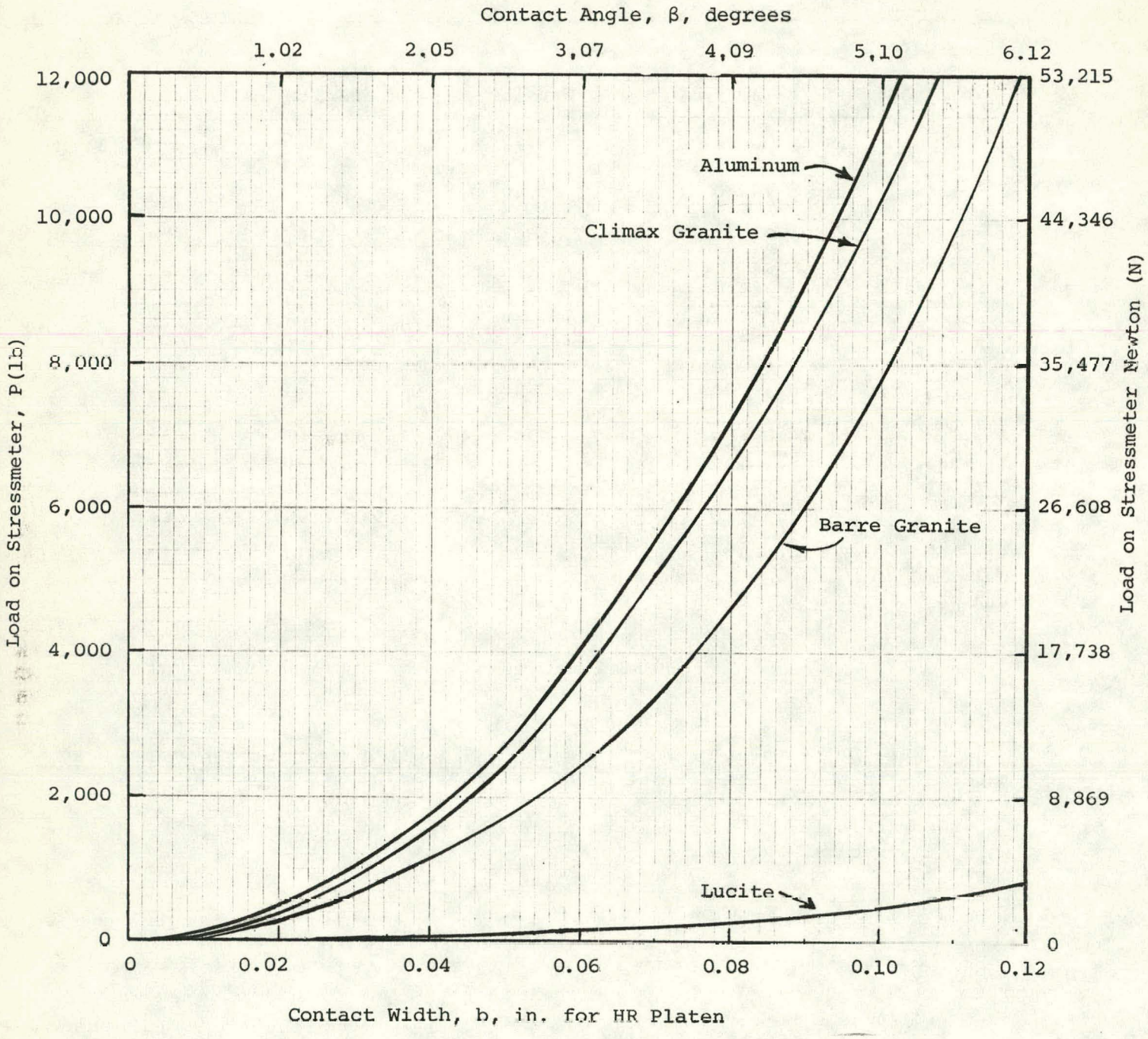

Figure 5. Computed HR Platen Contact Width vs Applied Load

Total wire deformation is $\delta_w = \frac{\Delta\sigma_w}{E_g} \times \ell_w = \frac{1.78422 \times 10^{11}}{30 \times 10^6} \times .78 \left[\frac{1}{T_2^2} - \frac{1}{T_o^2}\right]$

$$= 4638.97 \left[\frac{1}{T_2^2} - \frac{1}{T_o^2}\right]$$

Assuming that the gage body deformation is the same as the wire deformation, (ignoring platen, and wedge deformation), the contact load, P, is given by

$$P = 4638.97 \cdot K_g \cdot \left[\frac{1}{T_2^2} - \frac{1}{T_o^2}\right] \text{ (lb)} \qquad (18)$$

where gage body stiffness, $K_g = P/\delta_w$.

Substituting $K_g = 7.5 \times 10^6$ lb/in. in Equation (23), the contact load on the gage body is given by

$$P = 3.4792 \times 10^{10} \left[\frac{1}{T_2^2} - \frac{1}{T_o^2}\right] \qquad (19)$$

The influence of the variable contact angle with gage load can now be examined in detail using the basic equation for gage sensitivity factor, Equation (16).

Values of $f(\beta, \upsilon_r, t)$ derived from Equation (11) are plotted in Figure 7 for various values of β.

Using Equation (19), just derived, stressmeter readings can be related to gage load and used in Equation (17) to calculate the width of the platen contact, b. This contact width can be related to contact angle β and $f(\beta, \upsilon, t)$ and then used in Equation (16) to calculate the stressmeter sensitivity factor (which now includes the variation of contact angle, β, with stressmeter load).

Figures 8a, b, c and d show the theoretically predicted values of α calculated as per Equation (16) over a range of rock stress for the sample materials investigated during the program. The general trend of the α-curve is to rise with increasing rock stress initially and then a tendency to a constant value at sufficiently high stress. The experimental data points plotted on these graphs show the same trends. Similar trends of α-curves are also observed in the study of gage-preloading influence on α discussed in detail later in Section 4.5 and given in Figure 28. Both series of curves show the influence of variable load and, therefore, variable contact angle on the α-value of the stressmeter.

2.4 Relation of Uniaxial Sensititivy to Biaxial and Triaxial Sensitivity

A part of the scope of the present investigation included correlating uniaxial sensitivity factor with the sensitivity factor obtained under biaxial and triaxial loading.

In the test program, the biaxial test was effected by applying a uniform hydrostatic pressure to the curved surface of the cylindrical specimen; for triaxial loading a compressive axial load was applied to the ends of the specimen simultaneously with the hydrostatic pressure.

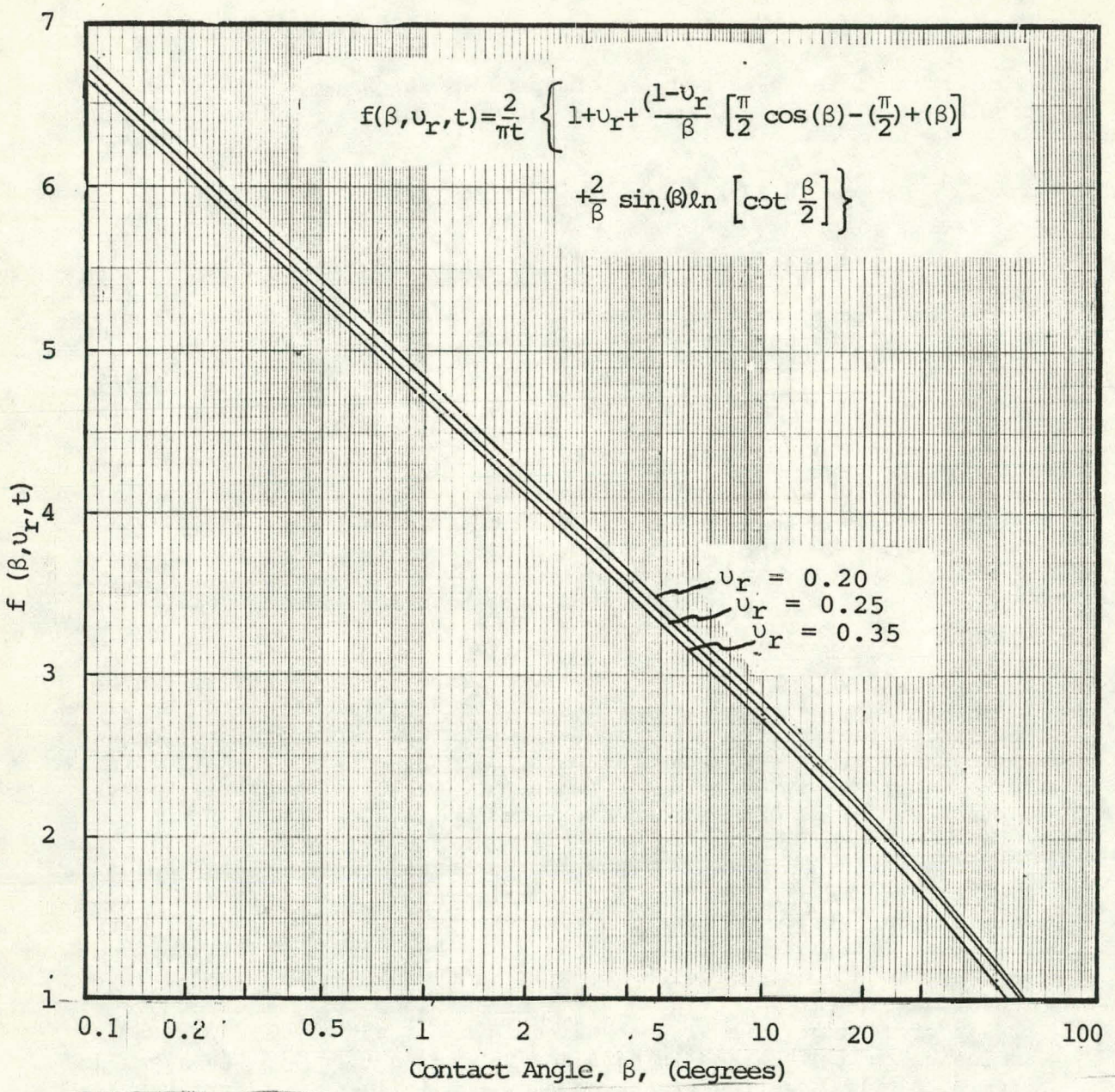

Figure 7. Computed Contact Angle, β, vs fβ, υ_r, t)

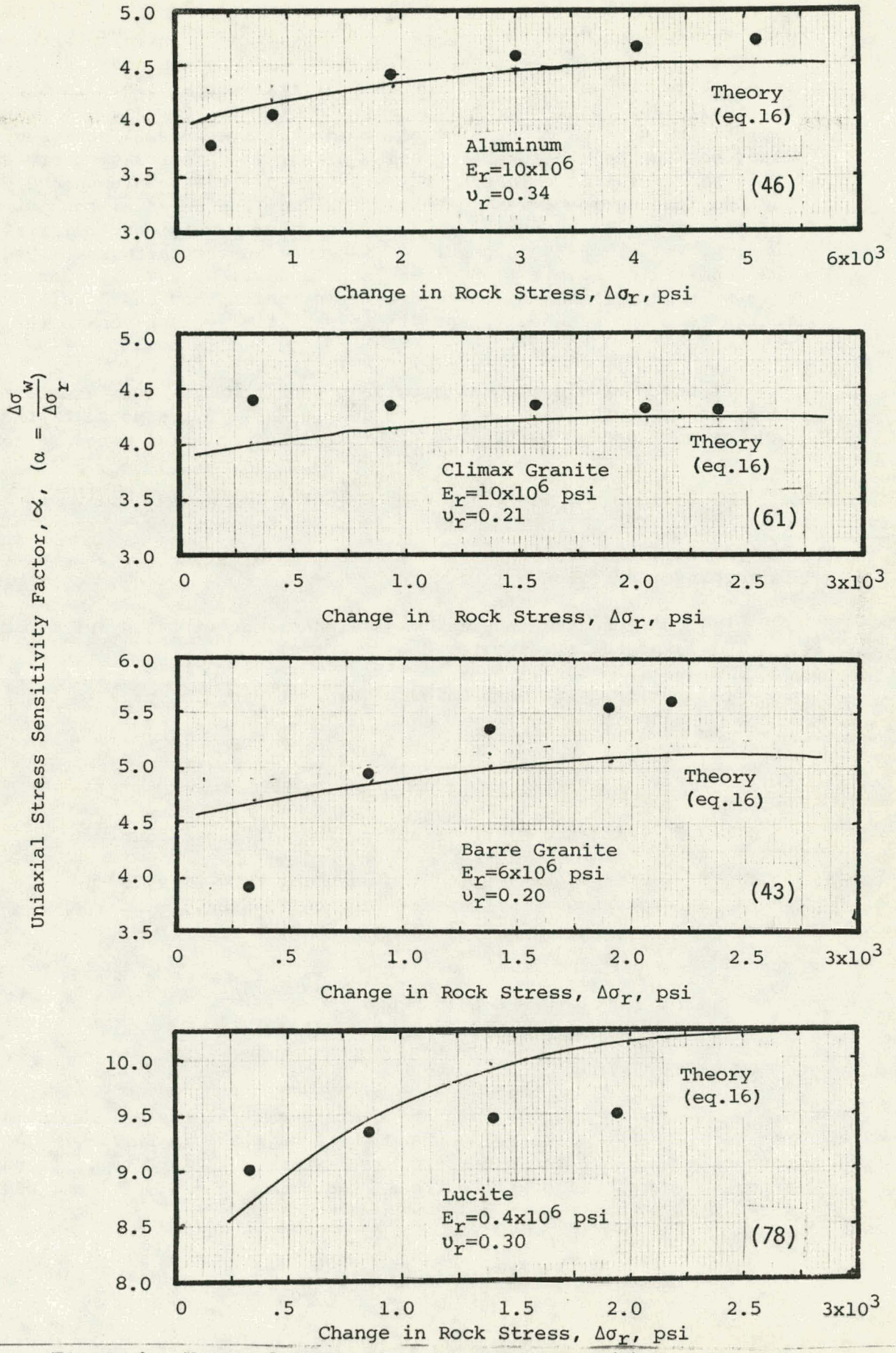

Figure 8. Uniaxial Stress Sensitivity Factor (α) for Four Different Materials. Theory and Experimental Data.

The response of the gage to the biaxial and triaxial stress fields was determined from the mechanics of hole deformation and gage interaction in the same way as discussed for the uniaxial stress field in the last section. Table 3 summarizes the results of this analysis. This table depicts the various modes of loading in the first row. The second row describes the hole deformation using classical elasticity theory where P_o is the hydrostatic loading for biaxial and triaxial tests and P_z is the end loading for triaxial tests. Calling the uniaxial rock stress σ_r, the equivalent uniaxial rock stress under biaxial and triaxial loading, as derived in Appendix 4, is given in the third row. Using the geometry of the test specimens, the equivalent uniaxial rock stress is expressed in terms of the hydrostatic loading and end loadings in the fourth row, and the equivalent stress sensitivity is given in the fifth row.

If the equivalent uniaxial stress sensitivity values α determined under test are the same as those shown in Table 3, response of the gage can be concluded as unaffected by biaxial and triaxial modes of loading.

2.5 Influence of Temperature

An elevated temperature environment changes the stressmeter response. This change in response is caused by:

(1) Differential thermal expansion of the vibrating wire material and the stressmeter body material.

(2) Differential expansion of the rock and the gage in the borehole; and

(3) Change of elastic modulus of the rock with temperature.

2.5.1 Influence of differential thermal expansion

Using Equation (4) and assuming $E_w = 30 \times 10^6$ psi, it can be shown that for an unset stressmeter bench reading, T_o, the wire strain ε_{w_o} is given by

$$\varepsilon_{w_o} = \frac{\sigma_{w_o}}{E_w} = \frac{1.78422 \times 10^{11}}{30 \times 10^6 \times T_o^2} = \frac{5947.4}{T_o^2} \text{ (in./in.)} \qquad (20)$$

If θ_w, θ_B, θ_r are the coefficients of thermal expansion of the wire, the stressmeter body and the rock, (all in in./in./°F), respectively, then for a temperature rise from t_o to t_1°F in an unset gage, the wire strain will decrease (assuming $\theta_w > \theta_B$). The final unset wire strain ε_{w_1} is

$$\varepsilon_{w_1} \text{ (unset)} = \frac{5947.4}{T_o^2} - (\theta_w - \theta_B)(t_1 - t_o) \qquad (21)$$

Table 3. Hole Closure and Equivalent Uniaxial Stress Sensitivity Under Uniaxial, Biaxial and Triaxial Loading

Mode of Loading	Uniaxial	Biaxial	Triaxial
Model	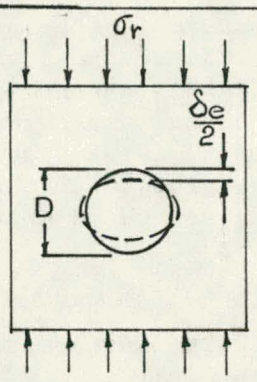	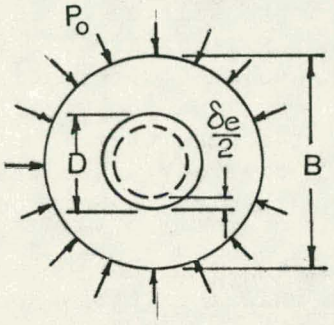	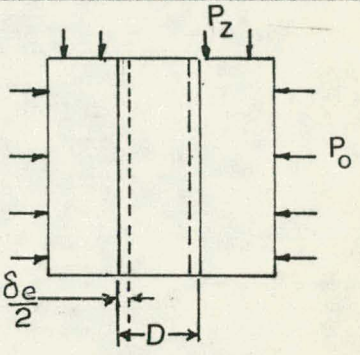
Hole deformation in line with the stress-meter wire	$\delta e = \frac{3D\ \sigma_r}{E_r}$	$\delta e = \frac{2D\ B^2 P_o}{E_r(B^2 - \frac{D^2}{4})}$	$\delta e = \frac{2D\ B^2 P_o}{E_r(B^2 - \frac{D^2}{4})} - \frac{\upsilon D\ P_z}{E_r}$
Equivalent uniaxial rock stress σ_r	σ_r	$\sigma_r = \frac{2P_o B^2}{3(B^2 - \frac{D^2}{4})}$	$\sigma_r = \frac{1}{3}\left[\frac{2P_o B^2}{B^2 - \frac{D^2}{4}} - \upsilon P_z\right]$
For B=5.50 in. and D = 1.5 in. σ_r	σ_r	$\sigma_r = 0.72\ P_o$	$\sigma_r = 0.72P_o - .07P_z$
Equivalent uniaxial stress sensitivity $\alpha = \frac{\sigma_w}{\sigma_r}$	$\frac{\sigma_w}{\sigma_r}$	$\frac{\sigma_w}{0.72\ P_o}$	$\frac{\sigma_w}{0.72\ P_o - .07\ P_z}$

And the new corrected bench reading T_1 for the temperature rise is given by:

$$T_1 \text{ (unset)} = \sqrt{\left(\frac{5947.4}{\varepsilon_{w_1} \text{(unset)}}\right)} = \sqrt{\left[\frac{5947.4}{\frac{5947.4}{T_o^2} - (\theta_w - \theta_B)(t_1 - t_o)}\right]} \qquad (22)$$

For a gage set in a borehole at ambient temperature, as temperature increases, there will be an additional compressive load (assuming $\theta_B > \theta_r$), and the final wire strain ε_w (set) will depend on the elastic deformation of the rock and the differential thermal expansions of the three bodies, rock, gage body, and the wire. Experimental results of the thermal offsets of a set stressmeter in Climax granite test block were obtained and are shown in Figure 9. The testing method is described later in Section 3.7, and the results in Section 4.8.

2.5.2 Uniaxial stress sensitivity factor at elevated temperatures

A rise of temperature will influence the uniaxial stress sensitivity factor α in two ways:

(1) The expansion of the gage body will increase the contact angle 2β of the platen, and

(2) There will be a decrease in rock modulus E_r at higher temperatures.

The effect of both of these factors upon α can be seen by examination of Equation (16). Both terms in the denominator of Equation (16) will decrease at higher temperatures, and the uniaxial stress sensitivity factor α will, therefore, increase.

Assuming that there is no significant change of E_r within the range of the test program, we can consider only the effect of contact angle change with temperature rise.

If T_3 (set) is the elevated temperature reading of a set stressmeter and T_o is the initial reading, then loading on the gage is given by Equation (19) as:

$$P = 3.4792 \times 10^{10} \left(\frac{1}{T_3^2 \text{(set)}} - \frac{1}{T_o^2 \text{(set)}}\right)$$

and the contact width 'b' by Equation (22) as:

$$b = 1.6 \sqrt{PK_D C_E}, \text{ and}$$

$$\beta = \sin^{-1} \frac{b/2}{0.56}$$

These relations, together with $f(\beta, \upsilon, t)$ can then be used to evaluate α at elevated temperatures.

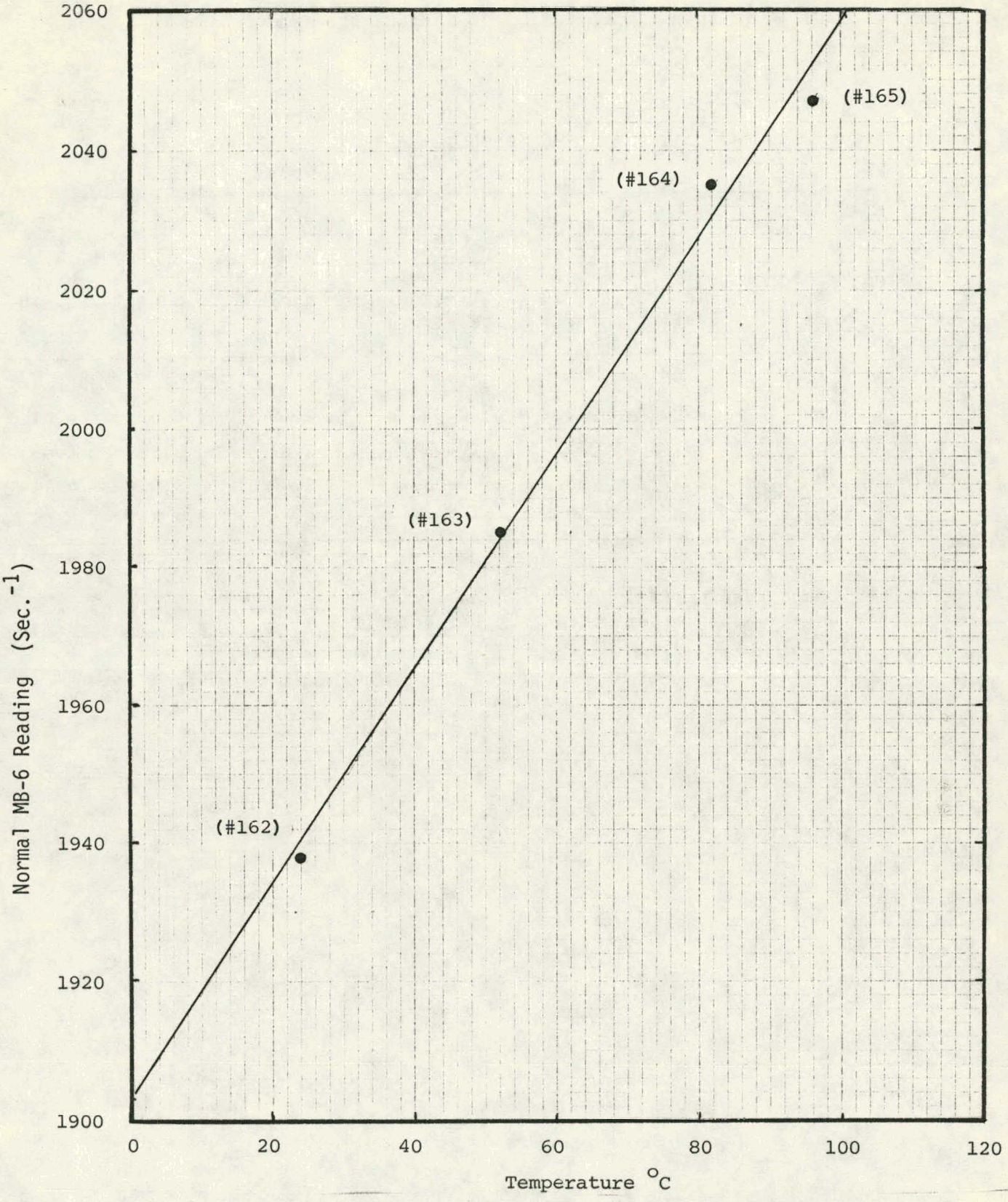

Figure 9. Temperature Offset for the Stressmeter Readings in Climax Granite.

Table 4 is such a computation of α for a stressmeter set in Climax granite.

Table 4. Predicted Uniaxial Stress Sensitivity Factor at Elevated Temperature - Climax Granite

Temperature Change °F	Stress-meter Reading	Load on Stress-meter Eq. 19 (psi)	Contact Width b From Table 2 (Climax Granite) (in.)	½ Contact Angle β_o	$f(\beta,\upsilon,t)$	α From Eq. 16
0	1700*	0	0	0		
0	1900**	2401	0.048	2.45	4.00	4.01
50	1974	3110	0.055	2.81	3.88	4.09
100	2027	3571	0.059	3.00	3.82	4.14
200	2183	4738	0.068	3.45	3.69	4.24

* Bench reading (T_o)
** Gage reading after setting in borehole (T_2)

3. TEST PROGRAM

The testing program required three modes of stress application to test specimens under ambient and elevated temperature. This section will document the testing equipment and the procedures used under each mode (uniaxial, biaxial and triaxial states of stress).

3.1 Uniaxial Tests: Equipment and Samples

Uniaxial testing was performed with a recently calibrated Baldwin Universal Loading Machine, which had the following specifications:

Full Range (upper scale)	120,000 lb (533 KN)
Minimum Resolution (upper scale)	100 lb (443 N)

Appendix 5 gives the calibration and the error band results for the Baldwin Machine. The maximum applied rock stress error was ± 3 psi. The test setup is shown in Figure 10. The load column included a 9 in. diameter spherical seat to aid alignment, and ground stock steel load platens on the ends, to assure intimate contact over the entire loading surfaces.

For uniaxial loading, test slabs from four different materials were prepared. Their sizes are given in Table 5.

Table 5. Uniaxial Loading Test Samples

Material	Sample No.	Size (in.) Length	Width	Thickness	Perpendicularity to the Loading Platen (°)
Climax Granite	C1	9.982±0.010	9.982±0.008	1.363±0.024	0.12
	C2	10.027±0.030	10.100±0.020	1.414±0.009	0.48
	C3	9.636±0.022	9.556±0.020	1.429±0.017	-
	C4	10.071±0.018	9.959±0.032	1.388±0.004	0.50
Barre Granite	B1	14.825±0.010	9.800±0.002	1.551±0.031	0.33
	B2	14.900±0.010	9.750±0.002	1.550±0.041	0.09
	B3	14.844±0.010	9.969±0.002	1.539±0.006	0.44
	B4	10.010±0.002	10.063±0.002	1.522±0.010	0.67
Aluminum	A1	10.000±0.005	10.000±0.005	1.500±0.005	
	A2	12.000±0.005	8.000±0.005	1.500±0.005	0.00
	A3	20.000±0.005	10.000±0.005	1.500±0.005	
Lucite	L1	10.000±0.005	10.000±0.005	1.500±0.005	
	L2	15.000±0.005	10.000±0.005	1.500±0.005	0.00
	L3	20.000±0.005	10.000±0.005	1.500±0.005	

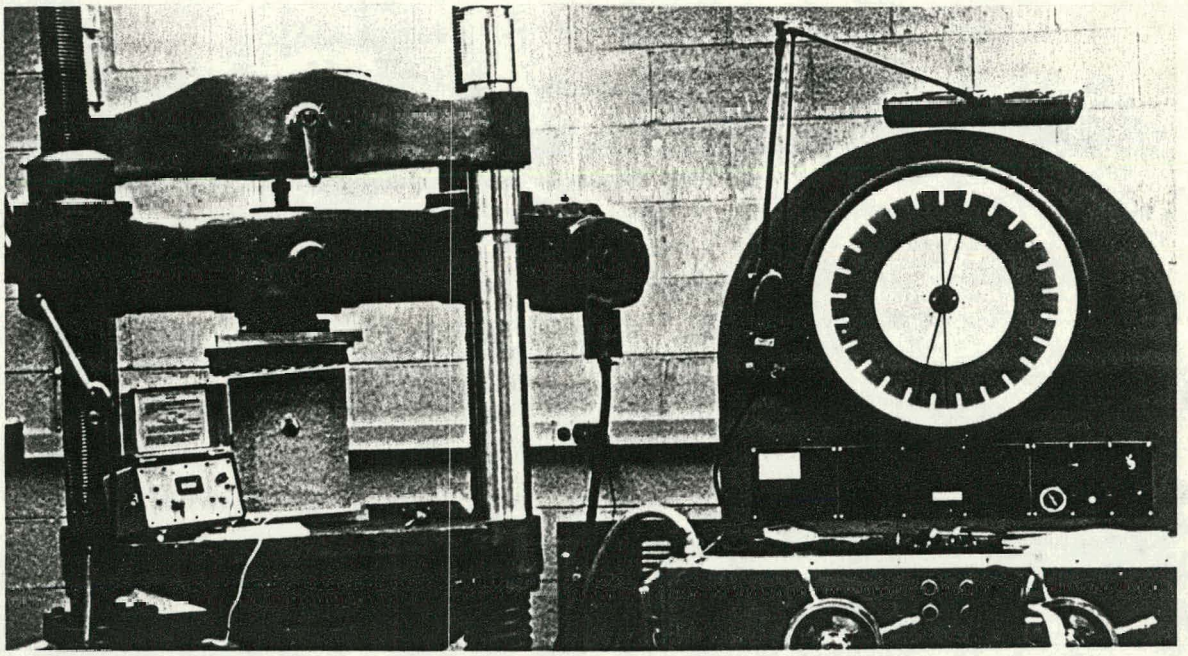

Figure 10. Uniaxial Calibration Test Setup at Room Temperature.

To check the straightness and alignment of contact surfaces, single sheets of carbon paper and typing paper were placed between load platens and slab end planes, and a nominal load (5,000 lb; 22-24 KN) applied through the load column. Impressions on the two pieces of paper were required to be uniform. This test was performed prior to uniaxial loading for all the slabs tested.

3.2 Loading Platen and Stress Uniformity

In an ideal uniaxial test setup, there would be, at all points in the specimen, one finite principal stress in a direction parallel to the loading and sample axes and equal in magnitude to the applied load divided by the cross-sectional area.

In practice, it is extremely difficult to produce a perfectly uniform stress field, and it is usually necessary to reach some compromise on perturbations of the stress field near the platen/sample contact area.

A variation of the stress field in the Climax granite samples was suspected for two reasons: (1) the samples contained a large number of strongly oriented macro-cracks and inclusions of ½ in. to 1 in. diameter Feldspar crystals. Figure 11 is a photograph of one of the Climax granite samples received from the Lawrence Livermore Laboratory, and (2) the sample size was small, only 10 in. square. Normally, lack of uniform pressure distribution due to inadequate sample flatness, squareness and parallelism are avoided by large length (L) to width (W) ratios usually 2 to 2.5. With 10 x 10 x 1½ (in.) Climax granite samples, this was not ensured.

In order to reduce the stress perturbation, initial trials were made using hydrostatic loading principles and compliant load platens constructed of a 0.125 in. (0.318 cm) thick layer of constrained silicone rubber. The strain measurement on the test block showed inconsistent and erratic results; so the technique was abandoned. A second configuration was constructed, substituting a single 0.011 in. (0.028 cm) manila sheet at the test slab/load platen interface. The results were more consistent and predictable. During all room temperature tests, the manila paper was used at the testing machine platen/rock interface. (Manila paper was also used by Hawkes (1973) in the original development tests of the stressmeter.) Later tests with and without manila paper showed no perceptible difference in uniaxial stress sensitivity results. Therefore, all later and high temperature tests were conducted without any interface material.

3.3 Strain Gage Study

In order to study the stress perturbation effect, four rows of foil strain gages (Micro Measurement precision strain gage type WA-13-250BG-120) were mounted on the front and back surfaces of one of the Climax granite slabs (see Figure 12). For tests, the slab was positioned in the standard uniaxial test setup; a stressmeter with HR (hard rock type) platen was installed, and the applied rock load was increased through three levels of rock stress with the strain gage output recorded at each level. Figure 13 shows the test arrangement. Table 6 summarizes the results. The microstrain reported is the average of 4-5 separate strain gages in each row.

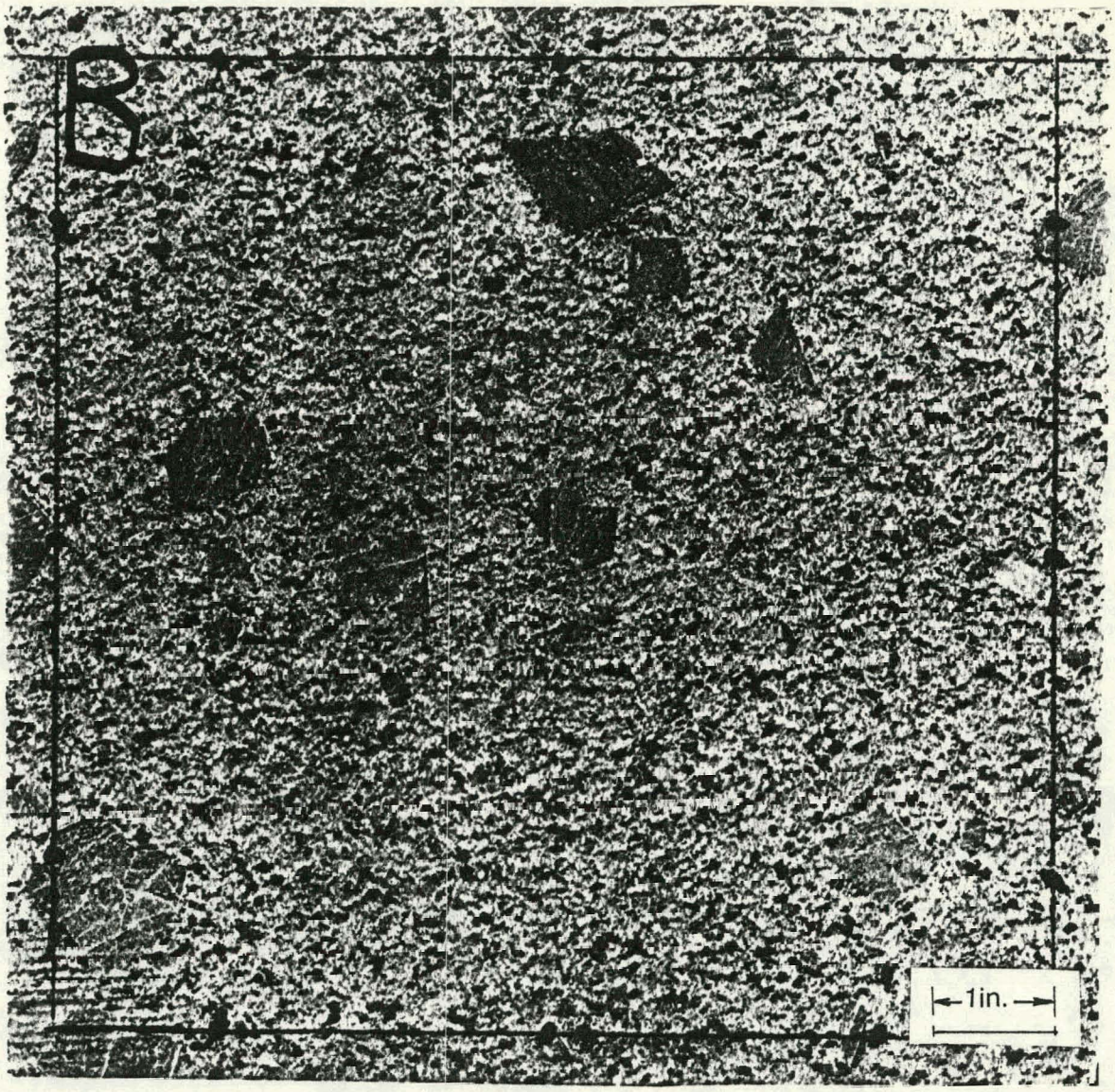

Figure 11. Climax Granite Sample with Large Inclusions of Feldspar

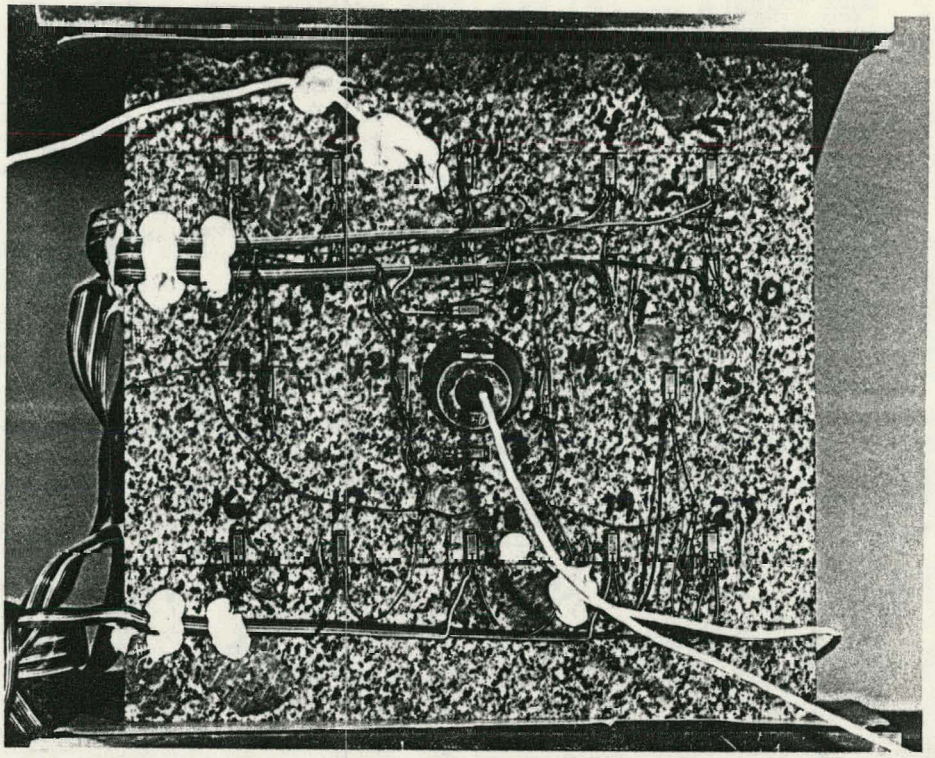

Figure 12. Strain Gaged Climax Granite Slab

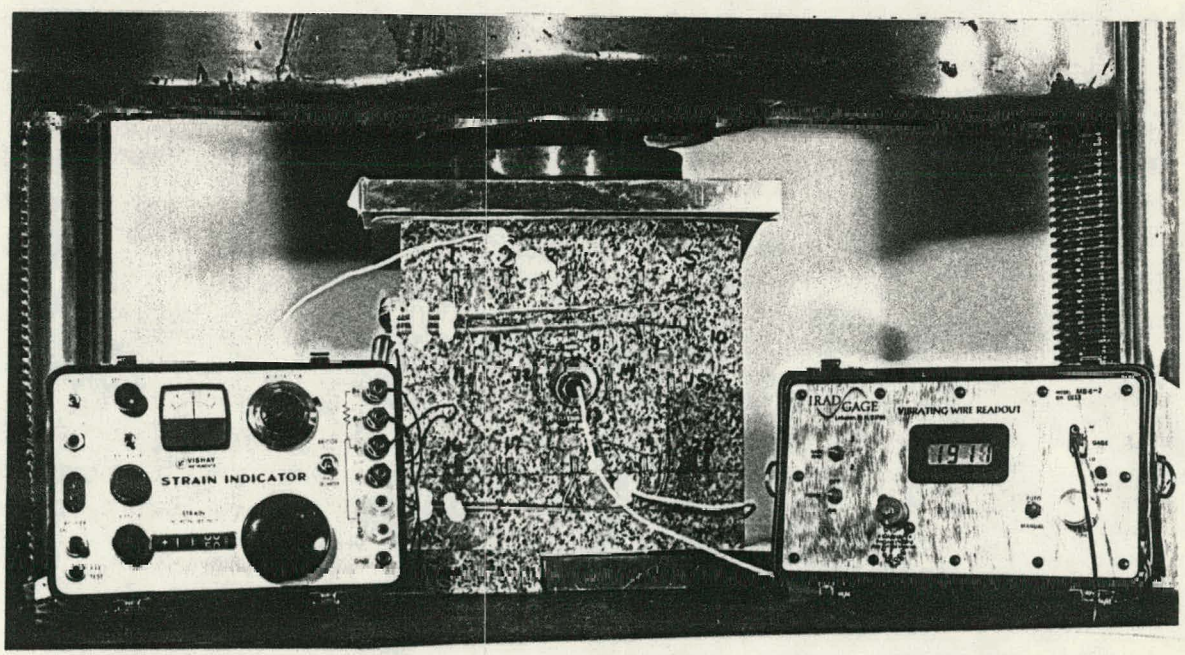

Figure 13. Test Setup of the Strain Gaged Climax Granite

The results show that average strain measured by the foil strain gages corresponded well with the calculated strain on the slab.

Table 6. Summary of Foil Strain Gage Test Results

Applied Rock Stress σ_r		Measured Strain by the Foil Gage, με					Calculated Strain (με) with (E_r=10x10^6 psi)	% Deviation [$\frac{\text{Meas.}}{\text{Calc.}}$x100]
		1st Row	2nd Row	3rd Row	4th Row	Average Measured Strain (με)		
psi	(MPa)							
636	(4.39)	51	52	61	44	52±9	64	81
1239	(8.54)	113	109	111	103	109±6	124	88
1679	(11.58)	155	146	154	140	149±9	168	89

3.4 Uniaxial Test Procedure

The uniaxial testing protocol was as follows:

(1) Load was applied on the sample to achieve the desired initial stress level.

(2) Using an IRAD GAGE standard manual setting tool (see Figure 14), the stressmeter was set in the test slab. An MB-6 readout box was used to achieve the desired level of gage preload.

(3) The applied rock stress was increased and readings were taken in increments of 250-500 psi (1.7-3.4 MPa). The maximum applied rock stress was 2000 psi (13.8 MPa) for the granites and Lucite, and 6000 psi (41.4 MPa) for aluminum. The loading rate was approximately 100 psi/sec (0.7 MPa/sec).

(4) The test slab was unloaded to the initial stress level (same as (1)). The load-unload cycles were repeated three more times, recording data on the load cycle. (During hysteresis studies, the unload cycle was also recorded).

(a) Manual Setting Tool

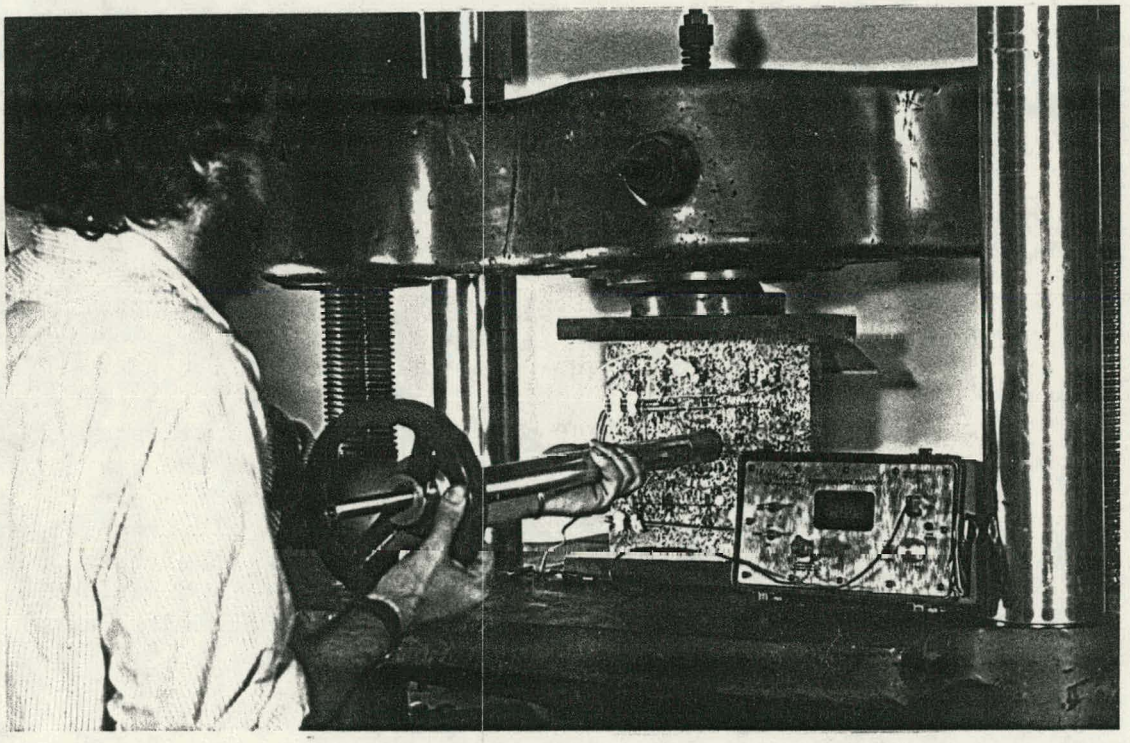

(b) Installing a Stressmeter

Figure 14. Installing a Stressmeter with a Manual Setting Tool

3.5 Biaxial Tests

Biaxial testing was carried out with the IRAD GAGE Model MC-1 Biaxial Modulus Chamber. Table 7 gives the chamber specifications; Figure 15 shows the biaxial test setup.

Table 7. Biaxial Testing Chamber Specifications

Full Range	0-3000 psi (20.7 MPa)
Minimum Resolution	50 psi (0.35 MPa)
Core Diameter	5.625 in. (nominal) (14.3 cm)

The biaxial chamber is a hydraulic device controlling applied pressure with a hand-operated jack. The Climax granite overcore sample (5.50 in. outer diameter) was mounted in the chamber so that rock/chamber contact was only through the membrane rubber housing. (The core O.D. was built up with silicone rubber to fit test chamber.) The stressmeter was installed in the sample's central hole, with the core under zero initial load, and the hydrostatic load was applied to the overcore exterior via the rubber membrane.

The biaxial test procedure was essentially identical to the uniaxial case. Following stressmeter installation, the core was load cycled four times with the stress output recorded every 200 psi (1.4 MPa) increase in hydrostatic pressure.

3.6 Triaxial Tests

The triaxial test was effected by applying a uniform hydrostatic pressure to the outer surface of the cylindrical specimen in the biaxial modulus chamber, while simultaneously applying a compressive axial load to the end of the specimens with the Baldwin uniaxial loading machine. The general test setup is shown in Figure 16. All tests were done on a 5.50 in. diameter 8 in. long Climax granite sample. After mounting the stressmeter to a predetermined preload in the central portion of the 1.5 in. diameter hole, the core was placed inside the biaxial chamber. Then the unit was transferred to the Baldwin tester where the ends of the core were in contact with ground stock platens. The end loading on the core was maintained constant while the hydrostatic pressure was cycled. Stressmeter readings were taken every 200 psi (1.4 MPa) (hydrostatic pressure). As with all the previous testing, each stressmeter setting was load cycled four times.

3.7 Elevated Temperature Tests

Elevated temperature tests used a closed loop, forced-air heating arrangement with a BLUE-M Model No. OV-490A-2 (38°C-260°C) oven heat source in series with an insulated enclosure surrounding the load column

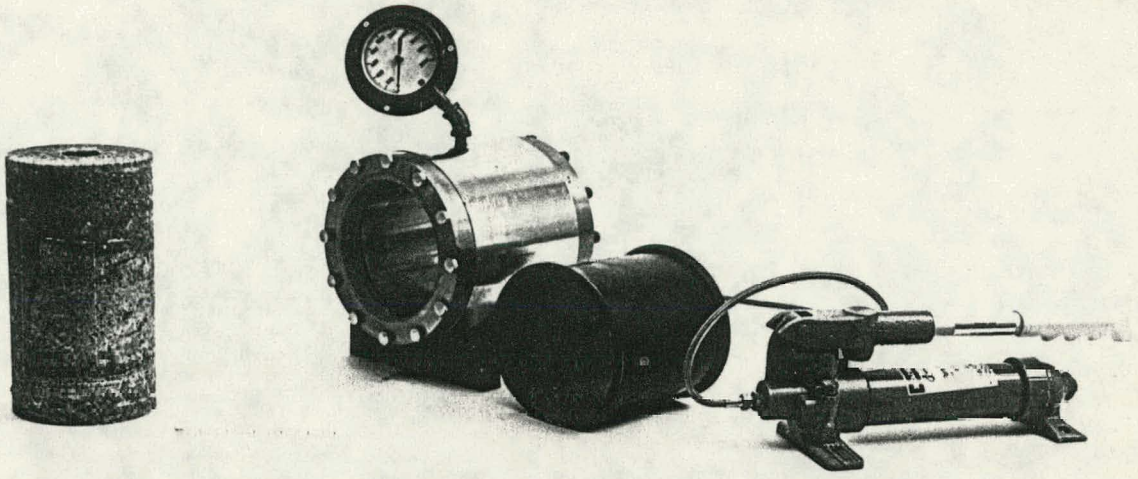

(a) Components of Biaxial Test Apparatus

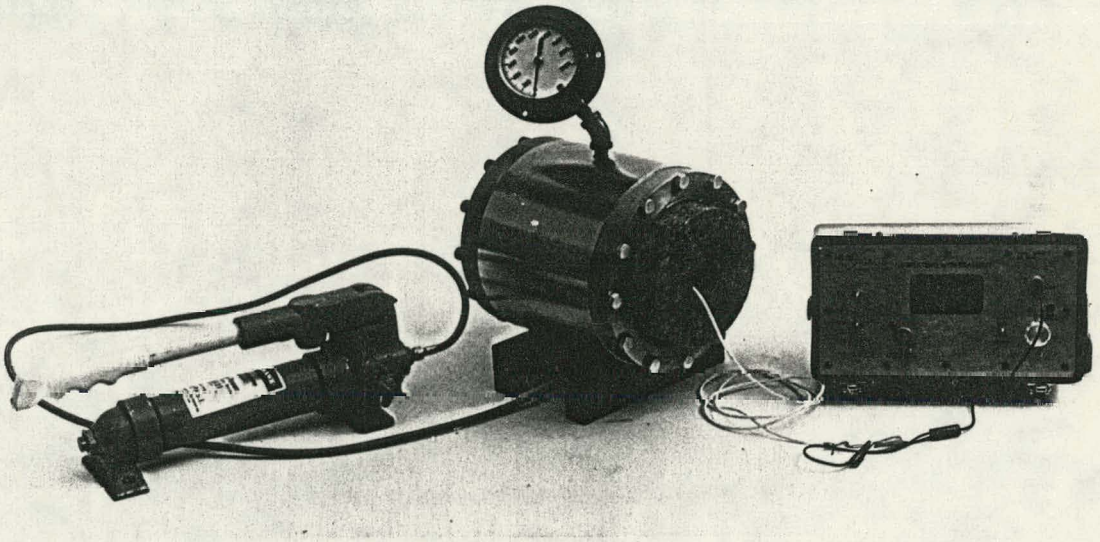

(b) Biaxial Testing of Stressmeter in IRAD GAGE Model MC-1 Biaxial Modulus Chamber

Figure 15. Biaxial Test Setup

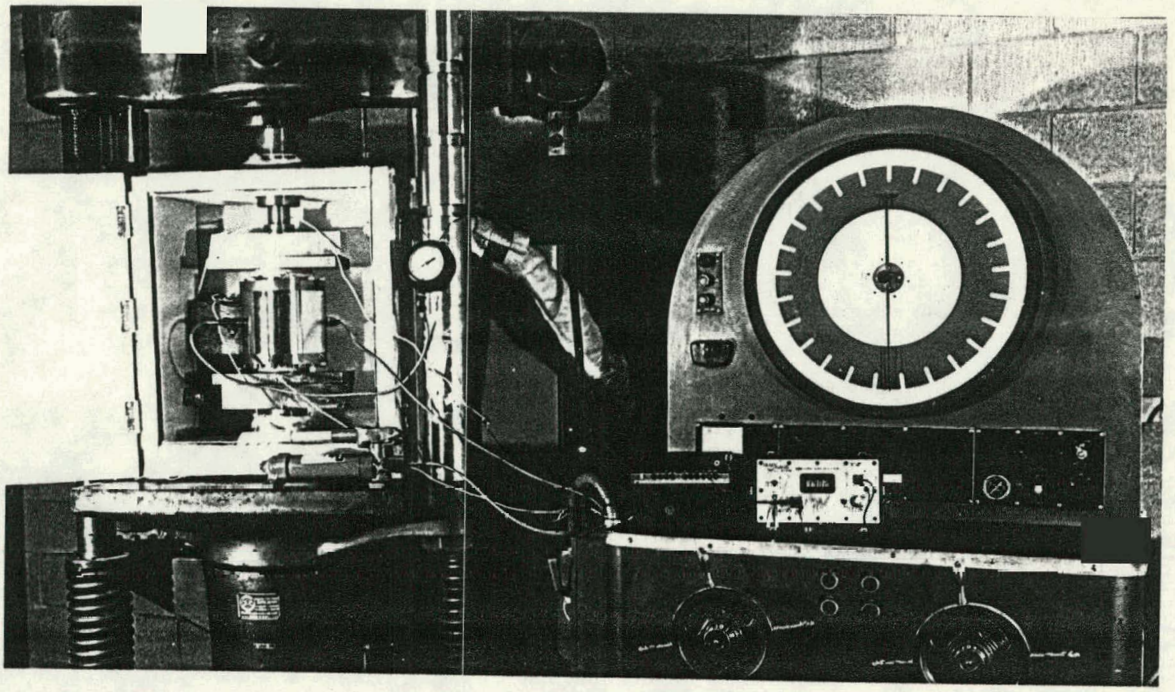

(a) Triaxial Test Setup

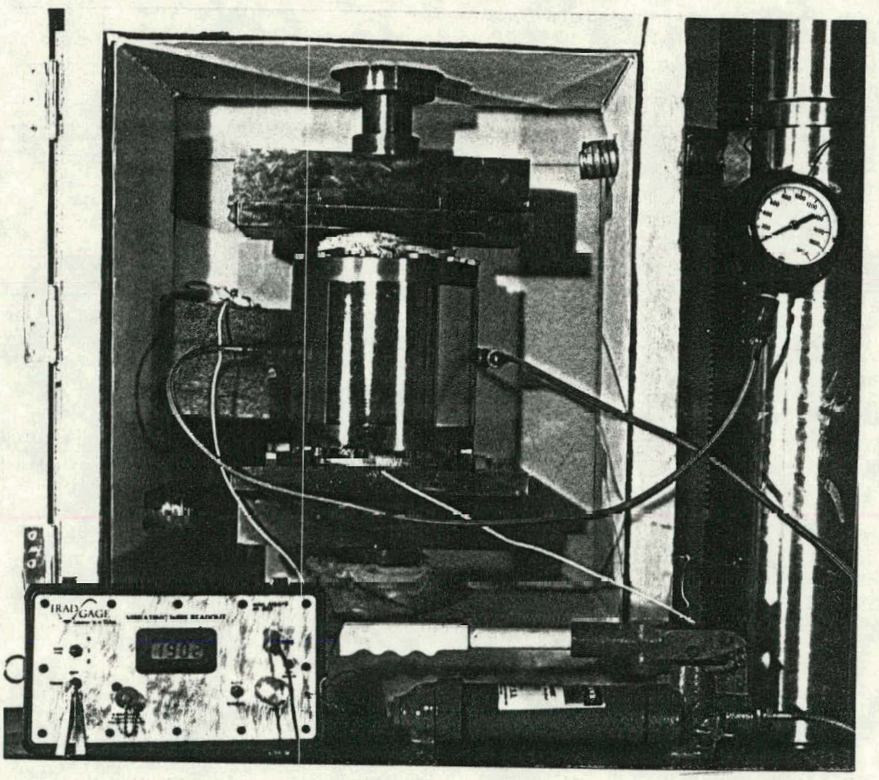

(b) Triaxial Test Setup (Close up)

Figure 16. Triaxial Testing at Elevated Temperatures

and test slab. The enclosure was constructed of Marinite I* and sealed with RTV. The temperature was monitored with Western Thermistors' No. 1C2001-A3 thermistors; 2 thermistors were mounted on each test slab above and below the borehole, one thermistor was inside the stressmeter, and a final thermistor monitored the air temperature inside the chamber. The thermal enclosure is shown in Figure 16 with the triaxial test setup.

The thermal gradient, across the test slab thickness, is computed by considering the linear flow of heat across a solid bounded by a pair of parallel planes. For a region $-\ell/2<x<+\ell/2$ with zero initial temperature and with the surfaces $x = \pm\ell/2$ kept at constant temperature V, for $t>0$ (t = time), the ratio of the mid slab temperature υ (at $x = 0$) to surface temperature (or air temperature), V, is defined by $\gamma = \frac{\upsilon}{V}$ and given by (Carslaw, et. al., 1959).

$$\frac{\upsilon}{V} = 1 - \frac{4}{\pi} \sum_{n=0}^{\infty} \frac{(-1)^n}{2n+1} e^{-(2n+1)^2\pi^2 t/4} \cos\left(\frac{2n+1}{2}\right) \pi \left(\frac{x}{\ell}\right)$$

To predict the time constant of Climax granite to achieve thermal stability, a determination of the temperature ratio, γ, ($\gamma = \frac{\text{mid-slab temperature}}{\text{air temperature}}$) vs time was computed. Figure 17 shows that, for 1.5 in. thick Climax granite, the mid-slab/surface slab temperature ratio is > 99% after 40 minutes. The minimum time allotted for each temperature change during testing was 90 minutes; therefore, uniform temperature equilibrium was assured.

Elevated temperature tests were performed in uniaxial, biaxial and triaxial modes. The maximum attainable temperature was 130°C. The test protocol was as follows:

(a) Uniaxial Tests

(1) The test slab was positioned in the thermal enclosure, initial load was applied, and the stressmeter was set to a predetermined preload. Four load/unload cycles were performed at room temperature.

(2) The temperature of the enclosure was raised to the next desired level by using the control on the oven. When equilibrium was reached, four load/unload cycles were repeated.

(3) Step 2 was repeated for the remaining temperature levels.

---

* Marinite I is a calcium silicate insulator manufactured by Johns-Manville, Denver, Colorado.

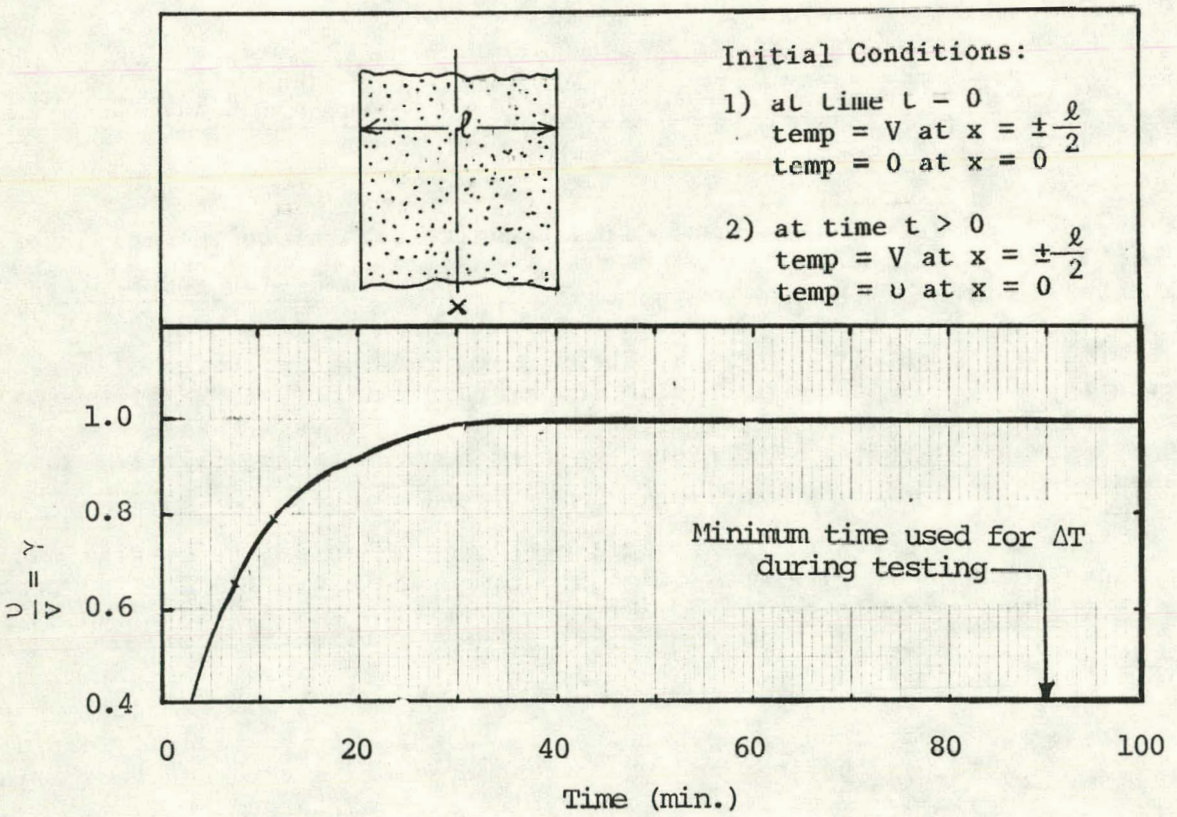

Figure 17. Time Required for Climax Granite Temperature Equilibrium

(b) Biaxial Tests

(1) The test core was installed in the biaxial test chamber, and the stressmeter was set to a predetermined preload. The test chamber was moved inside the BLUE-M oven.

(2) Four load cycles were performed at room temperature by applying hydrostatic pressure from the hydraulic jack.

(3) The temperature of the oven was raised, and the load/unload cycles were repeated after attaining thermal equilibrium.

(4) Step 3 was repeated for the remaining temperature levels.

(c) Triaxial Tests

Triaxial tests were carried out in the thermal enclosure.

(1) The test core was installed in the biaxial test chamber, and the stressmeter was set to a predetermined preload. The biaxial test chamber was then mounted in the thermal enclosure for application of end loads on the test core.

(2) With a constant predetermined end load, four hydrostatic load/unload cycles were applied at room temperature.

(3) The temperature of the enclosure was raised to a predetermined level and Step 2 was repeated.

(4) Step 3 was repeated for the remaining temperature levels.

(5) The procedures from Steps 2-4 were repeated for the remaining end loads.

4. TEST RESULTS

This section summarizes the experimental results. The IRAD GAGE vibrating wire readout (T) (related to wire stress) vs. applied rock stress (σ_r) is the direct experimental result. However, this relationship is not linear (see Section 2.3, Calibration Theory), and the most convenient way to determine the rock stress is to divide the wire stress by a calibration factor - defined as the sensitivity factor α, discussed earlier. Results are thus presented both in readout units (T) and in terms of the uniaxial stress sensitivity factor, α.

4.1 Influence of Sample Size

Calibration tests using two different sizes of samples were conducted with three different moduli materials: aluminum (E_r = 10 x 10^6 psi (69 GPa)), Barre granite (E_r = 6.2 x 10^6 psi (41.4 GPa)) and Lucite (E_r = 0.5 x 10^6 psi (2.76 GPa)). The Barre granite and aluminum samples are shown in Figure 18, and Table 8 is the summary of the results. Figure 19 is the plot of the results.

Table 8: Influence of Sample Size on Calibration Results

Material	Length/Width Ratio	Sensitivity Factor α	Percentage Variation
Aluminum	1.0	4.40	7.3
	2.0	4.08	
Barre Granite	1.0	6.52	3.1
	1.5	6.32	
Lucite	1.0	9.25	1.1
	2.0	9.15	

4.2 Stressmeter Stiffness

Tests were conducted to determine the stiffness of the stressmeter. Two types of stressmeter bodies (see Figure 20) were included in the test program: (1) the standard IRAD GAGE VBS-1HT stressmeter, and (2) a specially prepared body with an 0.005 in. (0.013 cm) plating of electroless nickel (referred to in this report as the UCL^3 type stressmeter). For the UCL^3 type system, a 0.005 in. (0.013 cm) thick electroless nickel-plated HR (hard rock type) platen was also provided. Table 9 gives the dimensions of the stressmeter bodies. In addition to electroless nickel plating, the UCL^3 type stressmeter was coated with a 0.0005 in. (0.0013 cm) thick layer of pyrolene-N, a polymer used to seal the stressmeter from moisture in use.

The stiffness results are based on compression testing the gage bodies between two flat ground stock platens and measuring the frequency output of the gage wire — and assuming that the deformation of the wire is the same as the gage. The details of the test are given in Appendix 3. Table 10 summarizes the results.

Table 10. Stiffness of the Stressmeter Bodies

Gage Type	Stiffness, K_g $lb_f/in.$ (N/cm)
Standard VBS-1HT (4 gages)	$7.1 \times 10^6 \pm 3\%$ $(1.24 \times 10^7) \pm 3\%$
UCL[3] type VBS-1HT (2 gages)	$7.5 \times 10^6 \pm 1\%$ $(1.29 \times 10^7) \pm 1\%$

Figure 21 illustrates that, for near identical conditions of stressmeter loading, in an aluminum slab, the two gages have near identical responses. The small variation in gage sensitivity between plated and non-plated gages is due to a difference in preloading rather than a difference in stiffness.

The influence of the 0.0005 in. (0.0013) thick pyrolene-N coating on the UCL[3] type stressmeter's response was negligible; and test comparisons on two rock types confirmed this. Table 11 gives the results of these tests.

Table 11: Influence of Pyrolene-N Coating on Stressmeter Performance

Test Sample	Uniaxial Stressmeter Sensitivity (α)	
	w/Pyrolene	w/o Pyrolene
Climax Granite	4.60	4.55
Barre Granite	6.39	6.36

4.3 Gage Reproducibility and Hysteresis Effect

The reproducibility of the stressmeter output was investigated under two conditions: (1) single setting with multiple load cycling and (2) multiple setting with single load cycling. Both the standard VBS-1HT and the UCL[3] type stressmeters were tested in Barre and Climax granites. Some tests were also made in aluminum and Lucite slabs.

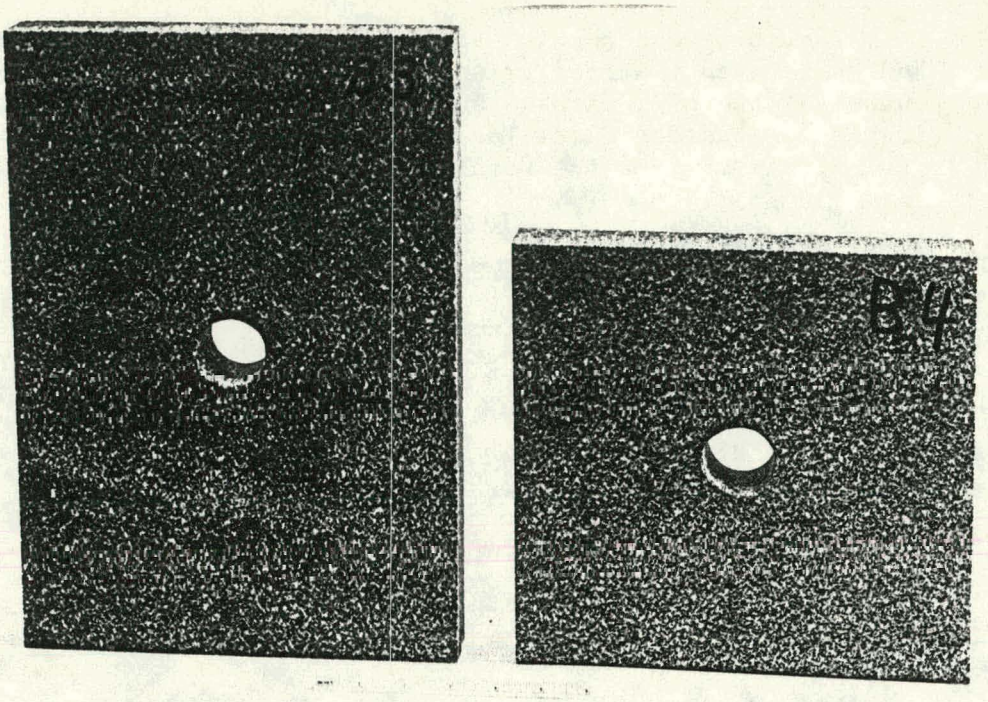

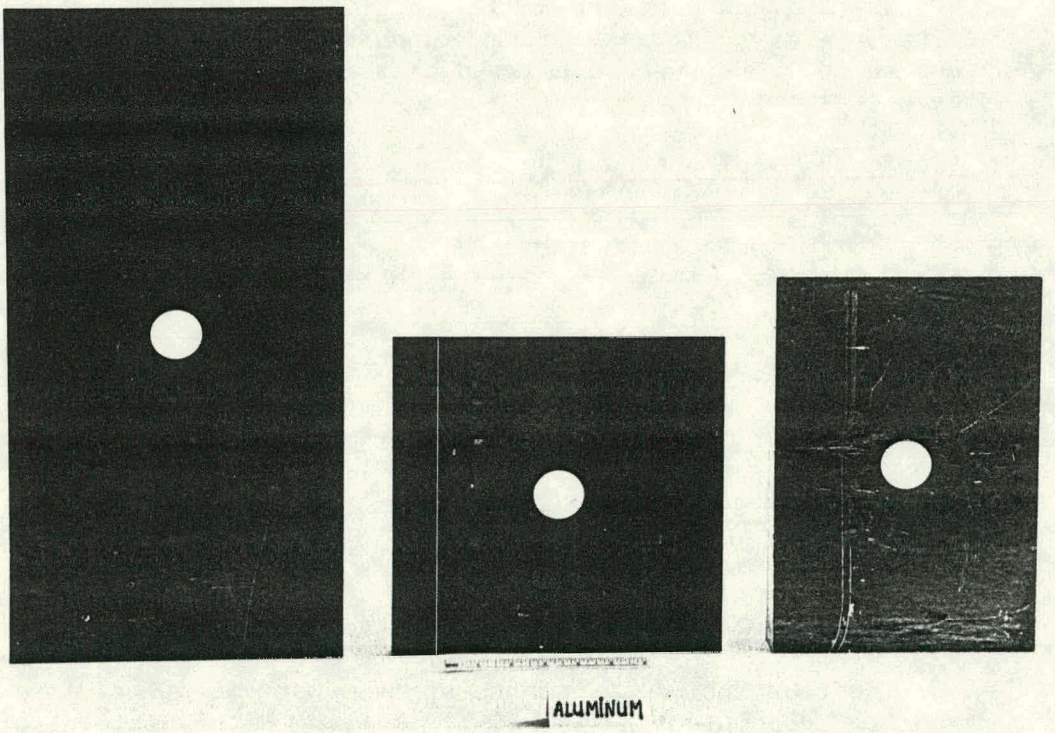

Figure 18. Uniaxial Test Samples of Different Sizes

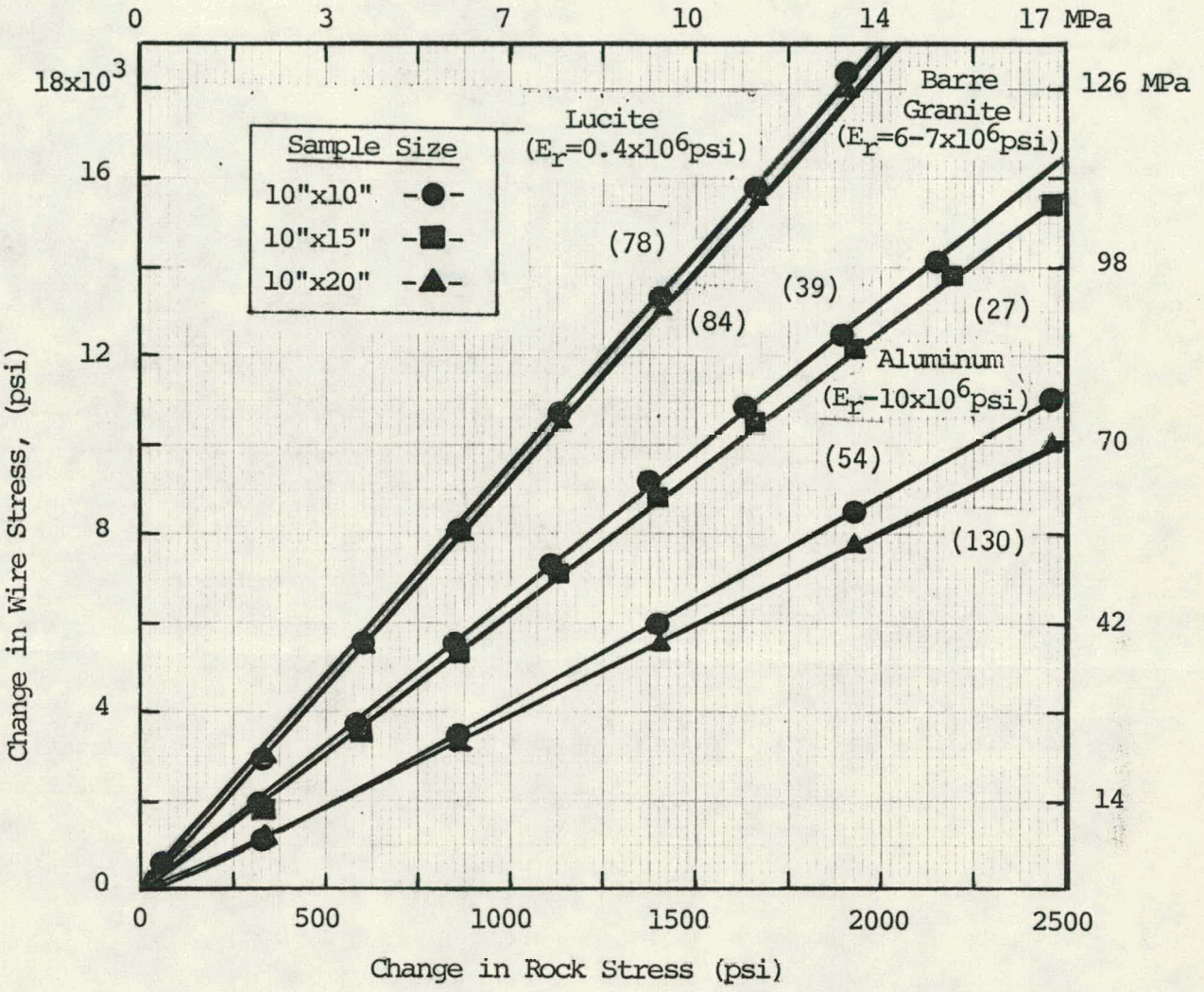

Figure 19. Influence of Sample Dimension on the Uniaxial Stress Sensitivity for Various Materials

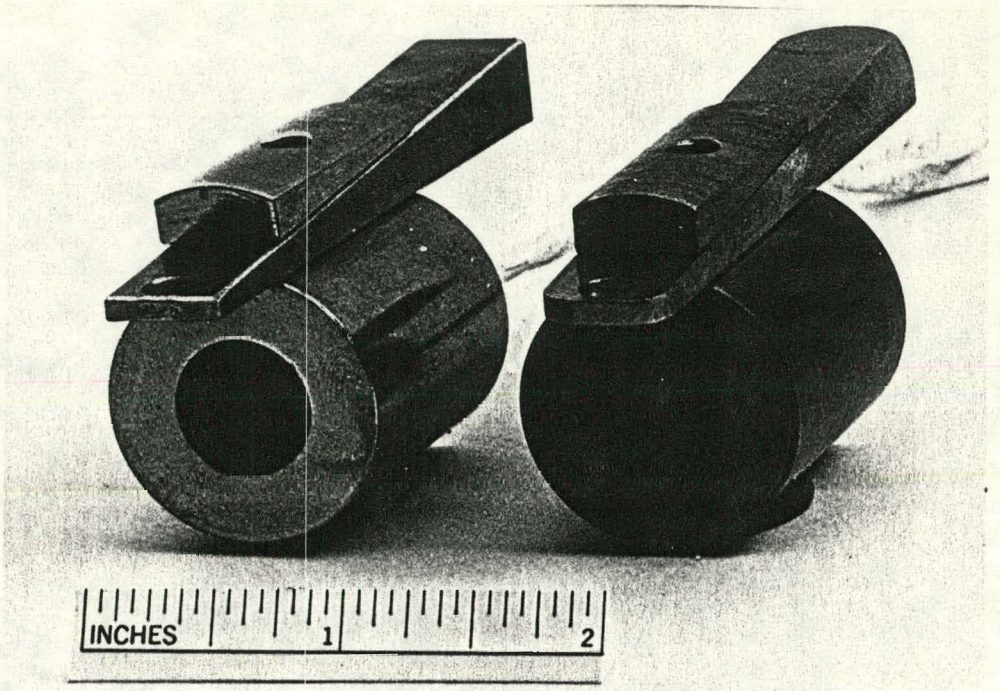

Figure 20. UCL[3] and Standard IRAD GAGE VBS-1HT Type Stressmeter

Table .9 Dimension of the Test Stressmeters

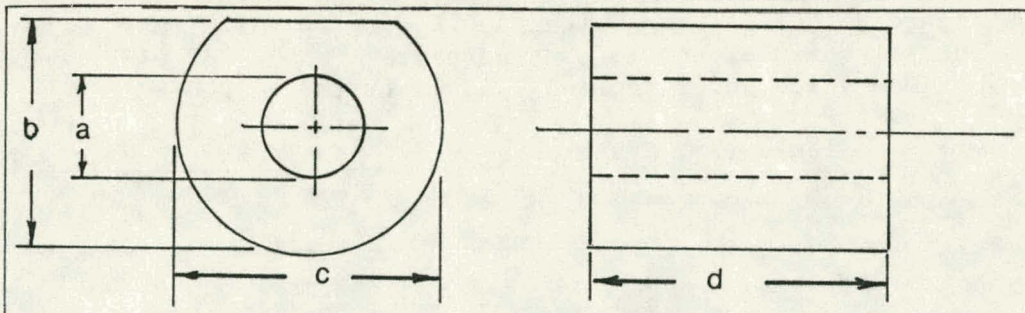

Stressmeter Body

	Condition	a (in.)	b (in.)	c (in.)	d (in.)
UCL³ type VBS	Pre-plate	0.510	1.062	1.115	1.490
	Post-plating + Heat Treat	0.502	1.068	1.123	1.498
	Plating Thickness	0.004	0.003	0.004	0.004
	Standard VBS-HT	0.502	1.066	1.125	1.500

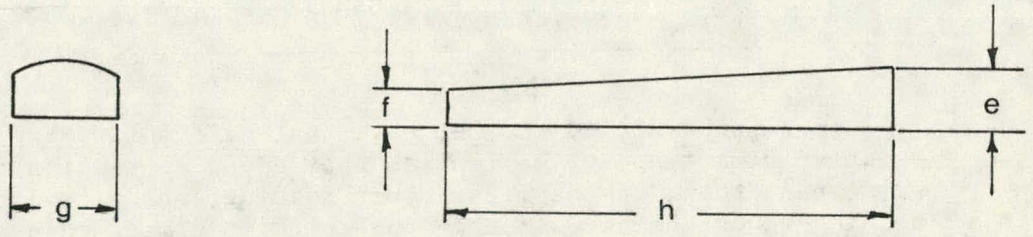

HR Platen

	Condition	e (in.)	f (in.)	g (in.)	h (in.)
UCL³ type VBS	Pre-plate	0.239	0.125	0.500	1.500
	Post-plating + Heat Treat	0.243	0.130	0.505	1.507
	Plating Thickness	0.002	0.0025	0.003	0.0035
	Standard VBS-HT	0.244	0.130	0.500	1.500

In all cases, a zero shift has been observed between the initial and the second load cycles. Figure 22 gives this result for aluminum, Figure 23 for Barre granite, and Figure 24 for Climax granite. The initial shift expressed as a percentage change of wire stress to its maximum value under applied load is listed in Table 12.

Table 12. Hysteresis Effect of the Stressmeter with HR Platen

Sample	Aluminum psi (MPa)	Barre Granite psi (MPa)	Climax Granite psi (MPa)
Maximum Applied Rock Stress (a)	5126 (35.4)	2150 (14.8)	2000 (13.8)
Maximum Wire Stress Change Corresponding to Maximum Applied Rock Stress (b)	25,496 (175.8)	8000 (55.2)	6011 (41.5)
Zero Shift in Wire Stress Following Maximum Applied Rock Stress (c)	-1800 (-12.4)	-1400 (-9.7)	-1100 (-7.6)
Zero Shift as Percentage of the Maximum Applied Wire Stress Change	7.06	17.5	18.3

In Figures 22, 23 and 24, note that zero shifts are all in the negative direction, which implies that the wire tension has increased. We suspect that, on the first cycle loading, there is a small degree of bedding-in of the stressmeter—the calculated magnitude of which, for the aluminum slab loaded to 1800 psi (12.4 MPa) wire stress change equivalent to the zero shift, is 46.8 microinch.

The results based on the second through fourth consecutive load cycles under identical testing conditions are presented in Figure 25 for the standard IRAD GAGE high temperature stressmeter, and in Figure 26 for the UCL[3] stressmeter in Climax granite. In both cases, the reproducibility is around + 3 digits (130 psi, 0.90 MPa)

The gage reproducibility for multiple settings in various materials has also been investigated. Figure 27 gives these results for the first cycle of each setting. The reproducibility with Barre granite is better than with Climax granite.

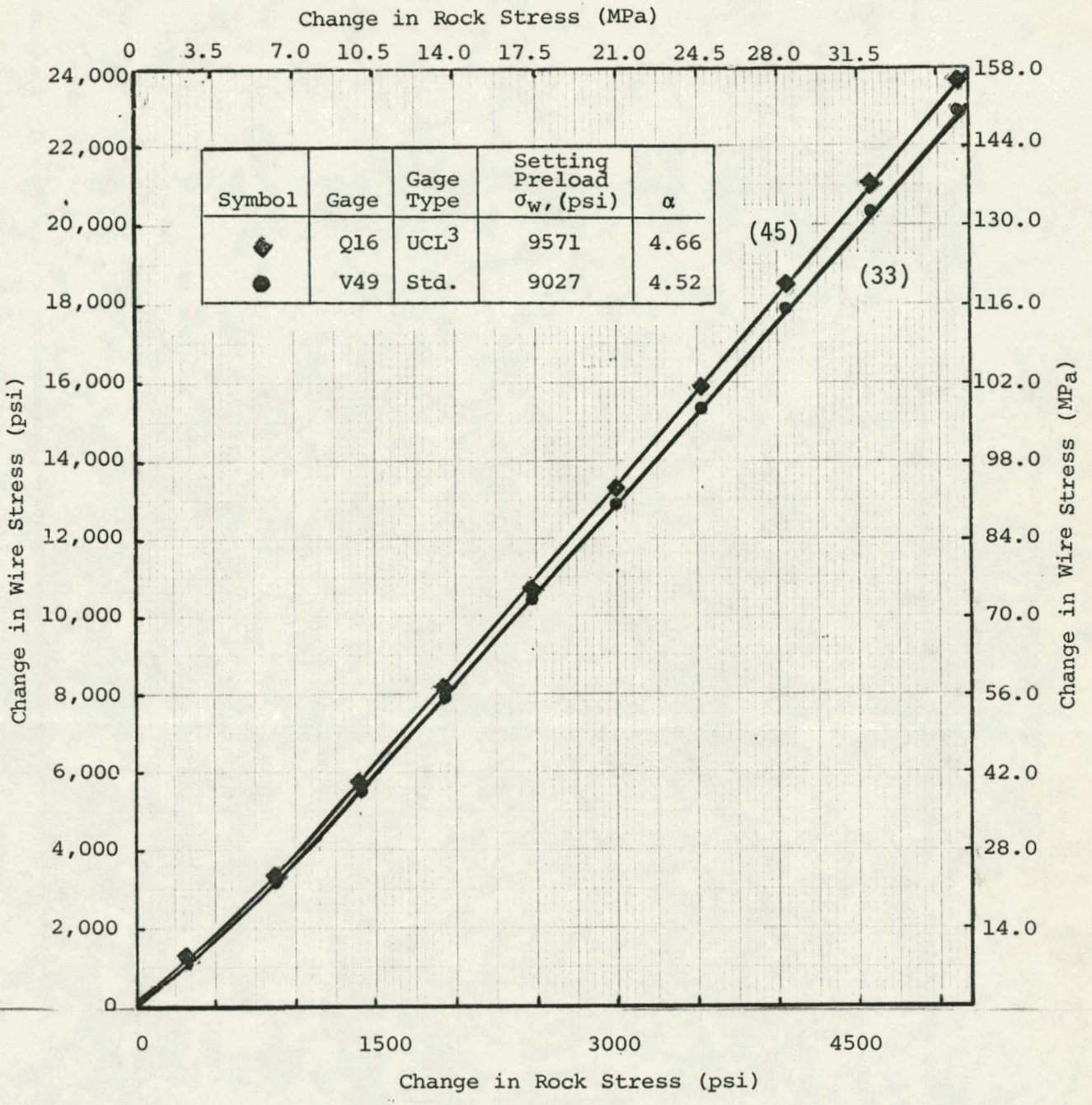

Figure 21. Comparison of Plated (UCL³ type) and Unplated (Standard) Stresmseter

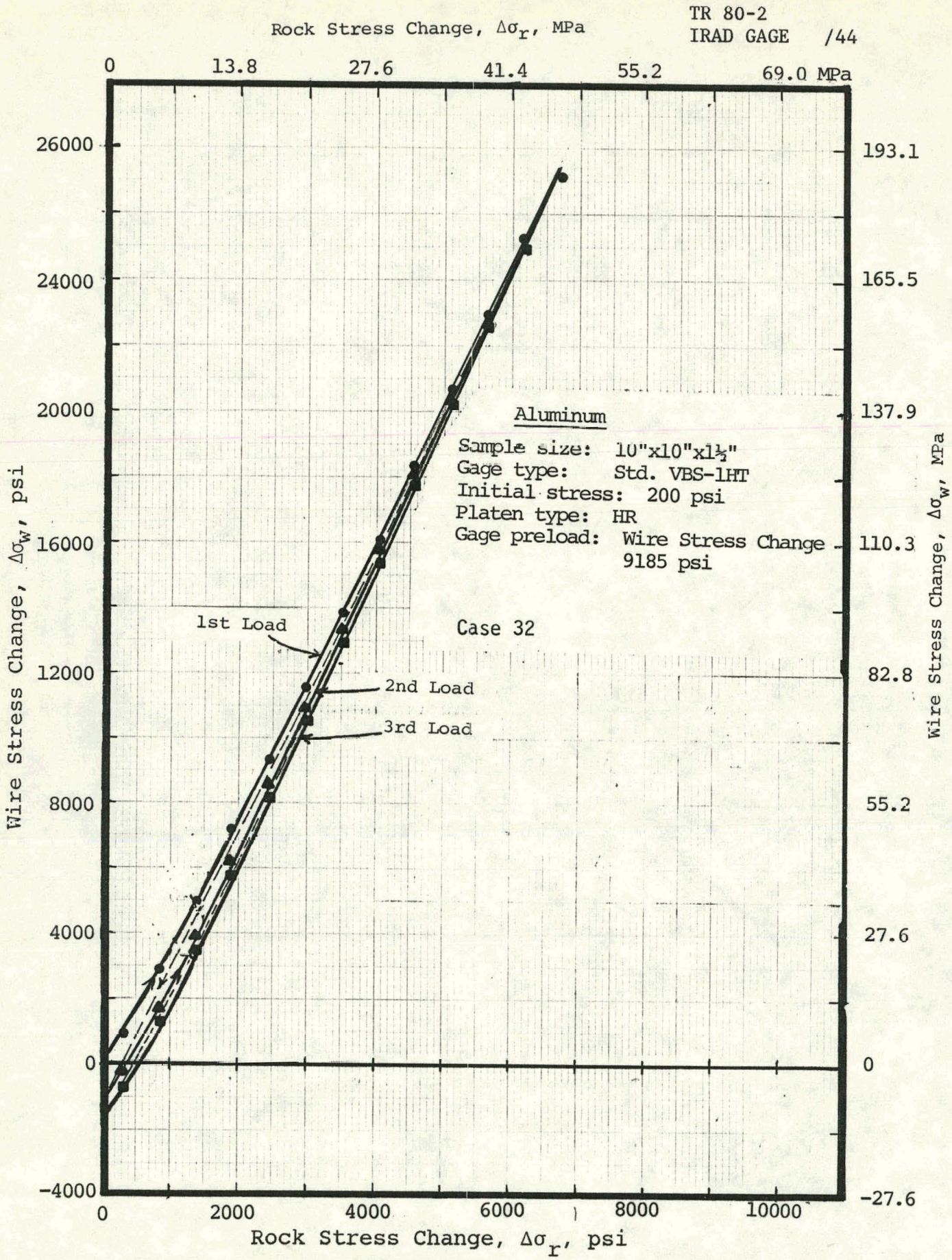

Figure 22. Stress Hysteresis in Aluminum Slab

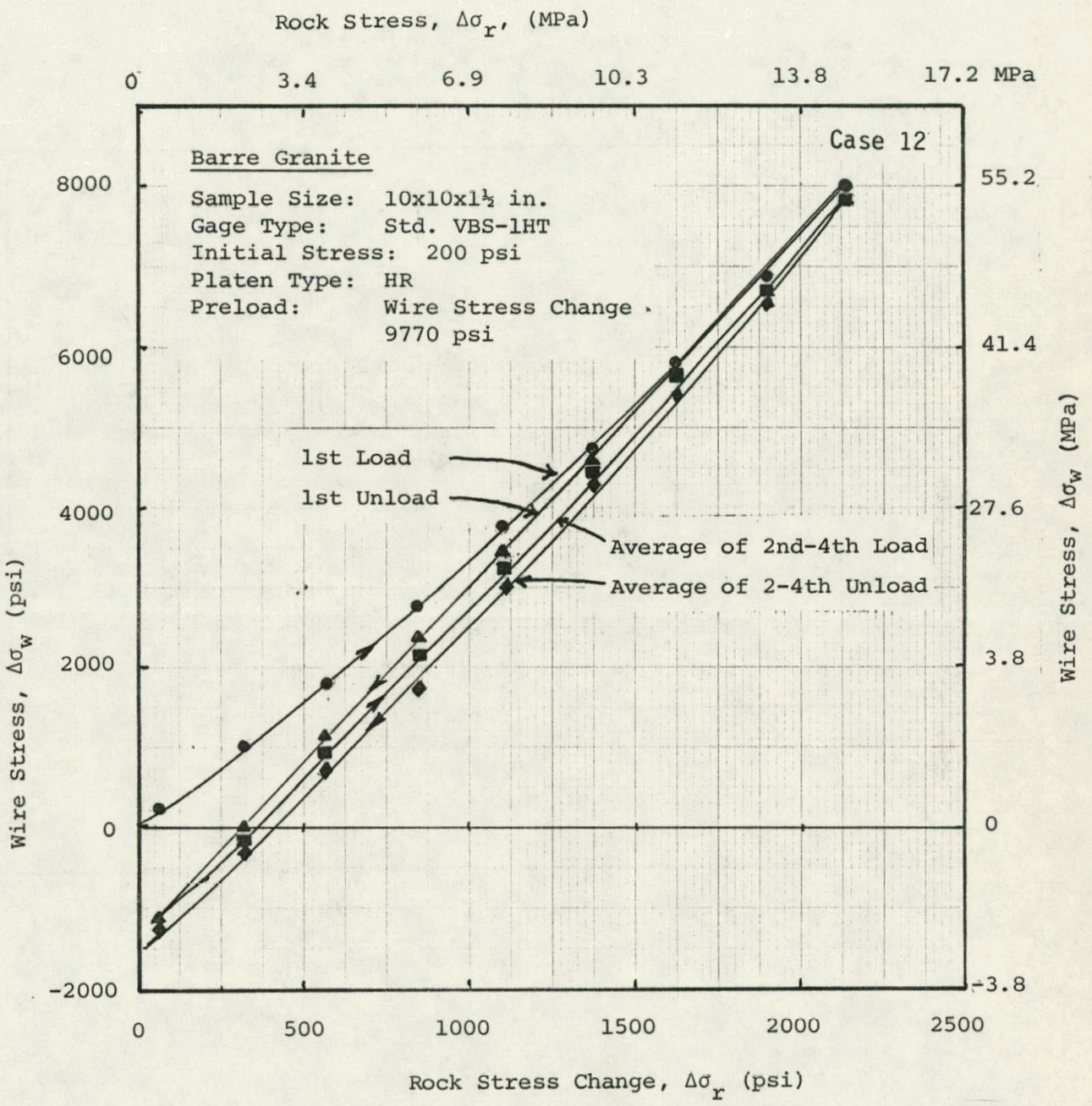

Figure 23. Stress Hysteresis in Barre Granite

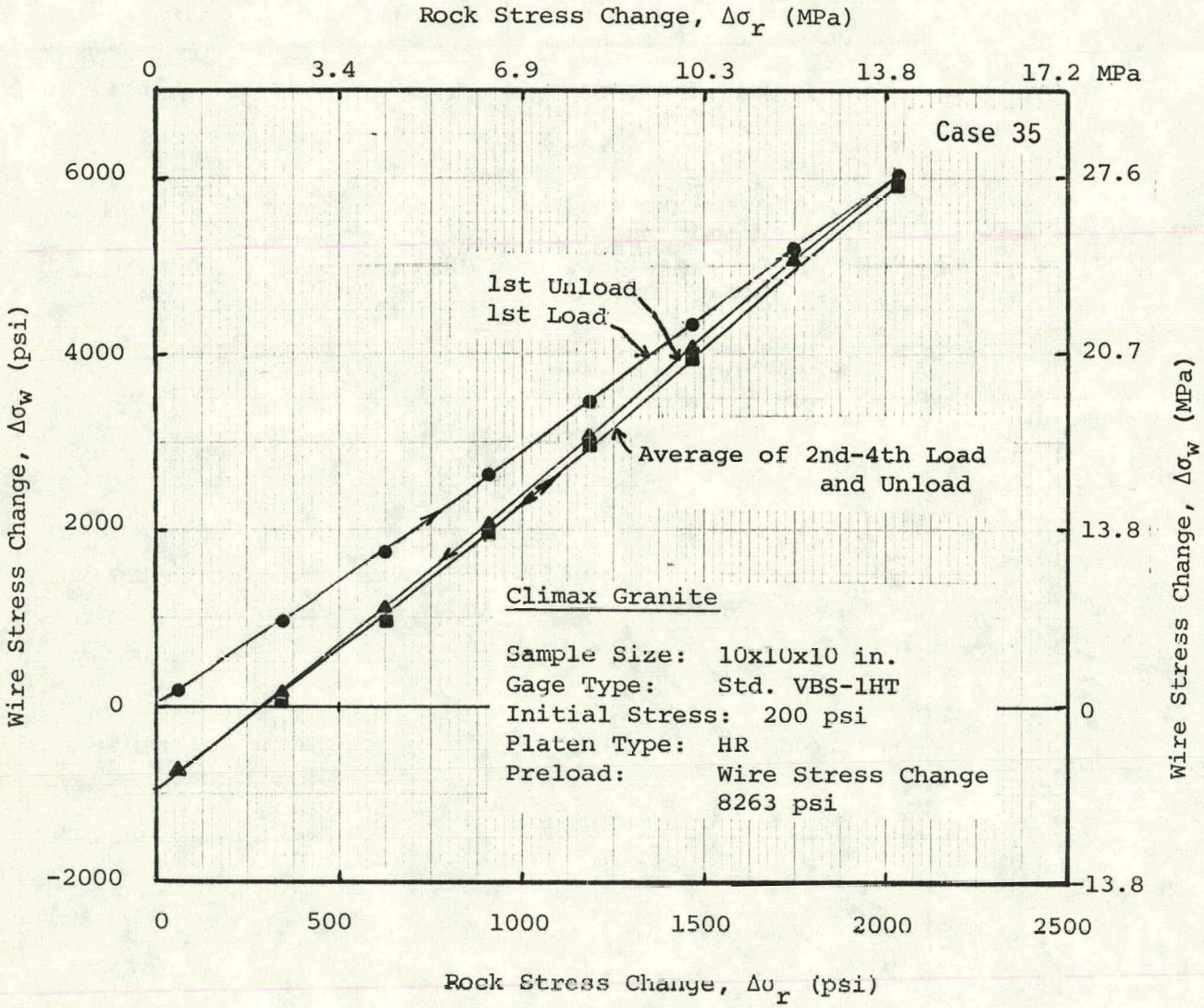

Figure 24. Stress Hysteresis in Climax Granite

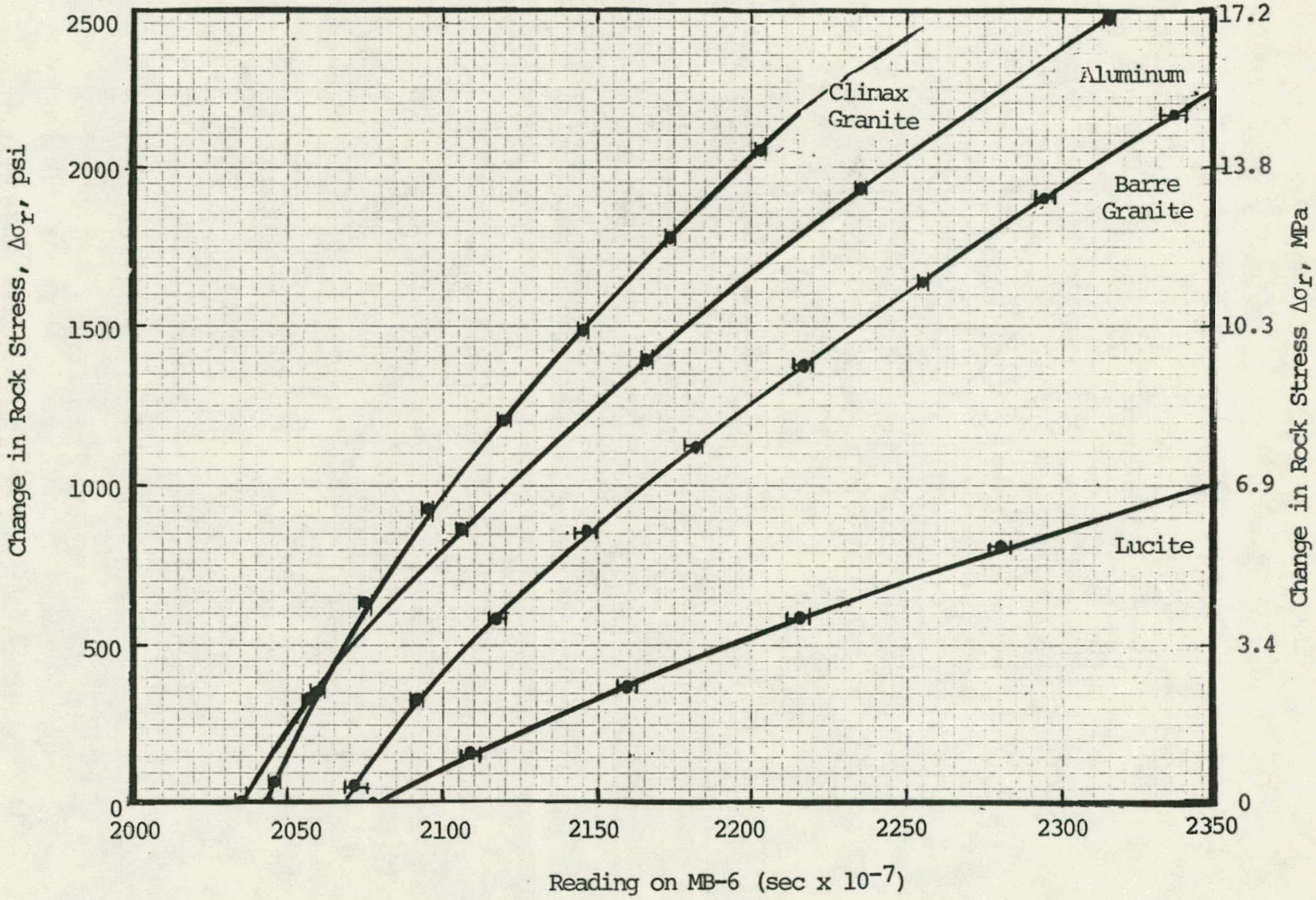

Figure 25. Reproducibility of Standard VBS-1HT Stressmeter for 2nd-4th Load Cycle

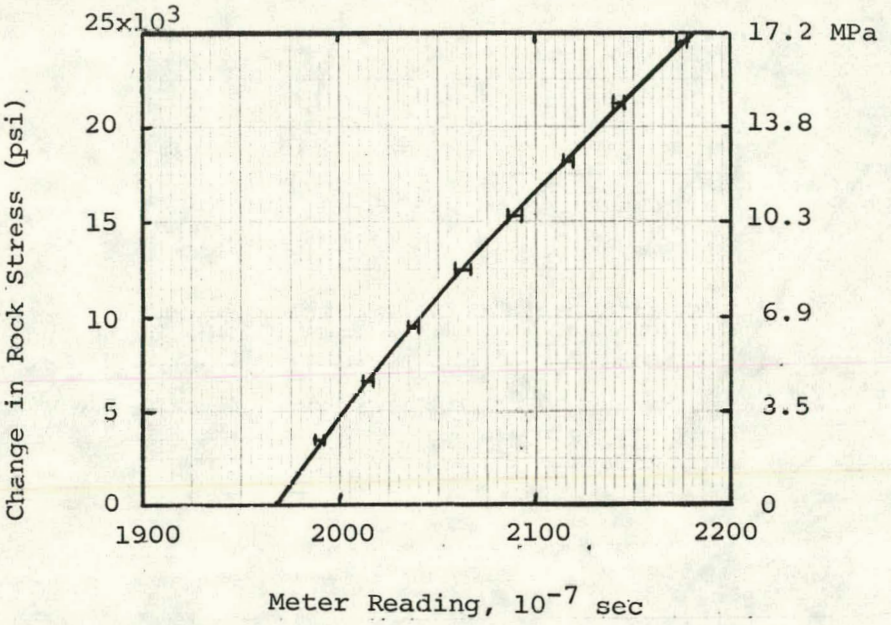

Figure 26. Reproducibility of UCL[3] Type Stressmeter in Climax Granite (2nd-4th Cycle)

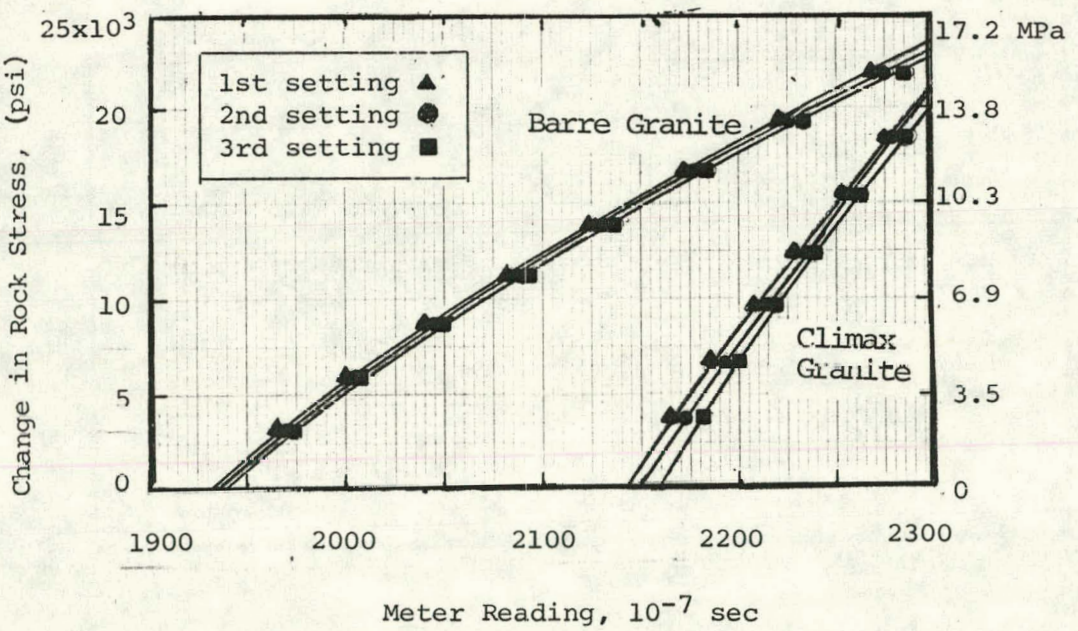

Figure 27. Reproducibility of 1st Load Cycle for 3 Multiple Sets

4.4 Influence of Gage Preload

Installation of an IRAD GAGE stressmeter is accomplished by pulling a wedge between a platen and stressmeter body. The setting load applied during installation is measured by the number of readout unit digit change between an unset gage bench reading and the final set gage readout. This difference is referred to as the gage preload. This difference expressed as wire stress change σ_w has also been used to provide a common reference for different initial readings of the stressmeter.

The amount of gage preload recommended varies with material and stressmeter system employed; it must be sufficient to satisfy two major criteria: (1) gage preload must be sufficient to ensure intimate, permanent contact between the stressmeter system and the borehole contacting surfaces, and (2) for applications involving measurement of tensile stresses (gage unloading), the gage preload must be sufficient to cover the entire anticipated range of tensile stress without losing the required intimate contact between gage system and borehole surfaces. It is, however, necessary to limit the preload value to prevent tensile cracking of the material on the surface of the hole.

The results of varying gage preload tests for all four materials are summarized in Figure 28. These results show that α value becomes constant above a threshold preload. Figure 28 shows that, for Climax granite samples, the threshold gage preload was approximately +170 digits (equivalent to wire stress change of 10,090 psi). HR platens were used in these tests.

4.5 Influence of Initial Stress Field

The underground locations in which the University of California, Lawrence Livermore Laboratory has planned to set their stressmeters provides an initial stress field range from 500-1200 psi (3.5-8.3 MPa) [Ramspott et al (1979)]. To determine the influence of the initial stress field on α, a Climax slab with initial stress fields ranging from 200-1300 psi (1.4-9.0 MPa) was studied, using the UCL^3 type stressmeter. The results are given in Figure 29. The results show that the effect of initial stress field on gage sensitivity is negligible.

4.6 Influence of Platen Geometry

Table 13 includes the dimensional specifications of the three platen geometries investigated, with a photograph of these platens mounted on the stressmeters. Experiments were performed with two different moduli materials to determine the influence of platen geometry on sensitivity. These results are summarized in Table 14.

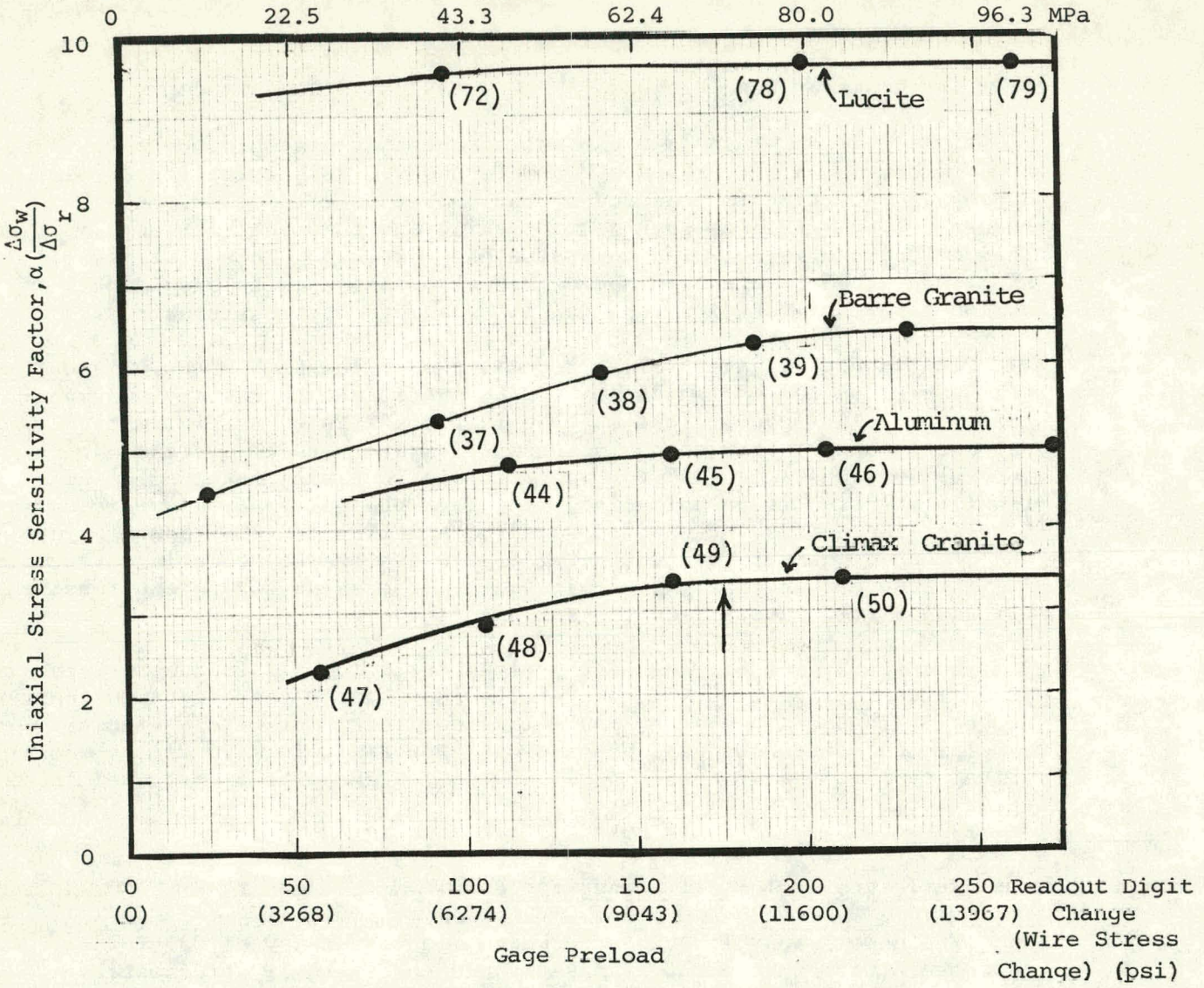

Figure 28. Influence of Gage Preload on uniaxial Stress Sensitivity (HR Platen)

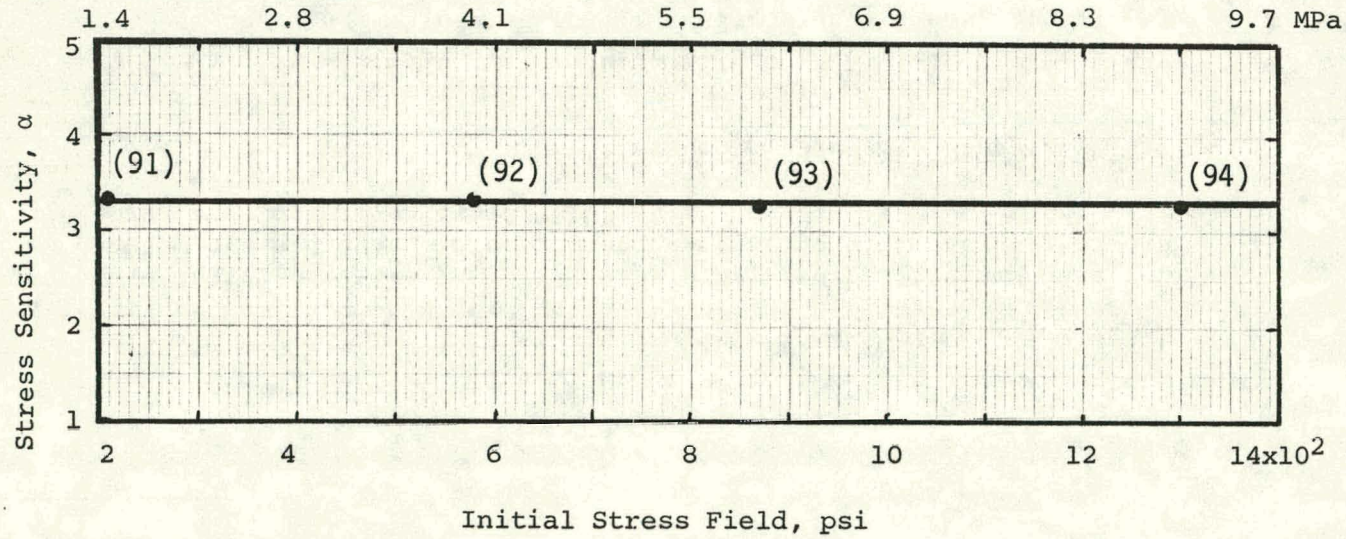

Figure 29. Influence of Initial Stress Field on Uniaxial Stress Sensitivity

Table 13. Dimensional Specifications of the Three Platen Geometries

HR Platen (Hard Rock Platen)	MSR Platen (Modified Soft Rock Platen)	SR Platen (Soft Rock Platen)
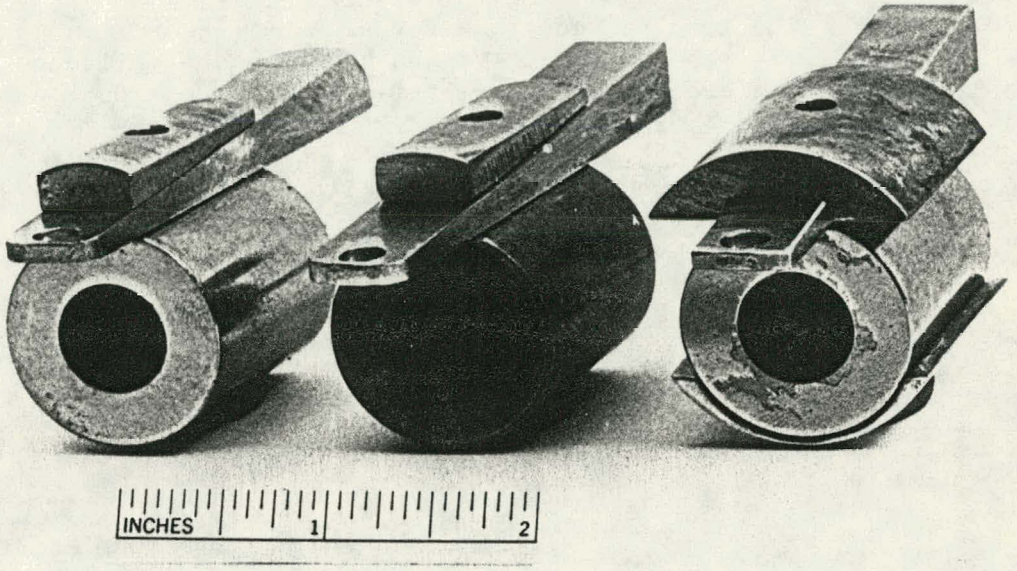		
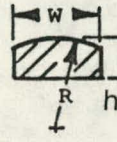	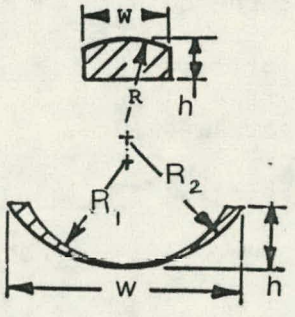	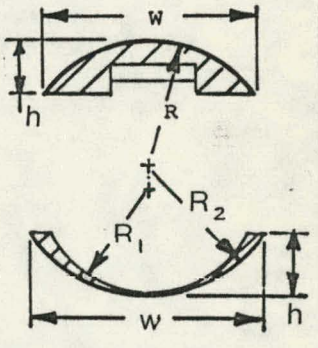
Upper Platen w = 0.500-.010 h = 0.244-.005 R = 0.56	Upper Platen w = 0.500-.010 h = 0.244-.005 R = 0.75	Upper Platen w = 1.25-.010 h = 0.375-.015 R = 0.75
	Lower Platen w = 1.250-.010 h = 0.375-.005 R_1 = 0.56 R_2 = 0.75	Lower Platen w = 1.250-.010 h = 0.375-.005 R_1 = 0.56 R_2 = 0.57

Table 14. Influence of Platen Geometry on the Uniaxial Stress Sensitivity

Test Material	Uniaxial Stress Sensitivity α		
	HR	MSR	SR
Aluminum	4.50	5.25	5.50
Lucite	9.35	-	9.80

The results show that for aluminum or Lucite, the SR platen is more sensitive than the HR. Figure 30 shows the influence of variable preload with different platen geometries.

4.7 Influence of Platen Orientation

If α_o = uniaxial stress sensitivity with wire positioned in the loading direction,
and α_{90} = uniaxial stress sensitivity of a stressmeter set at 90° to the loading direction. From elasticity theory, it is expected that

$$\frac{\alpha_o}{\alpha_{90}} = -3$$

To check the validity of the above, the gage response when mounted perpendicular and parallel to the direction of loading was taken; Figure 31 summarizes the results of such an experimental arrangement for a Climax granite slab with a UCL[3] type stressmeter at two gage preload values. Table 15 summarizes these results. Note that the α_o/α_{90} ratio is not exactly -3*; this is probably due to the non-linearity of the gage response at low rock stress values.

Table 15. Influence of Stressmeter Orientation

	Gage Preload psi (MPa)	α_o	α_{90}	α_o/α_{90} Test	α_o/α_{90} Theory
Case 1	9779 (67) 9623 (66)	4.56	-1.39	-3.28	-3
Case 2	13,269 (91) 11,991 (83)	4.65	-1.64	-2.84	-3

* See Appendix 6

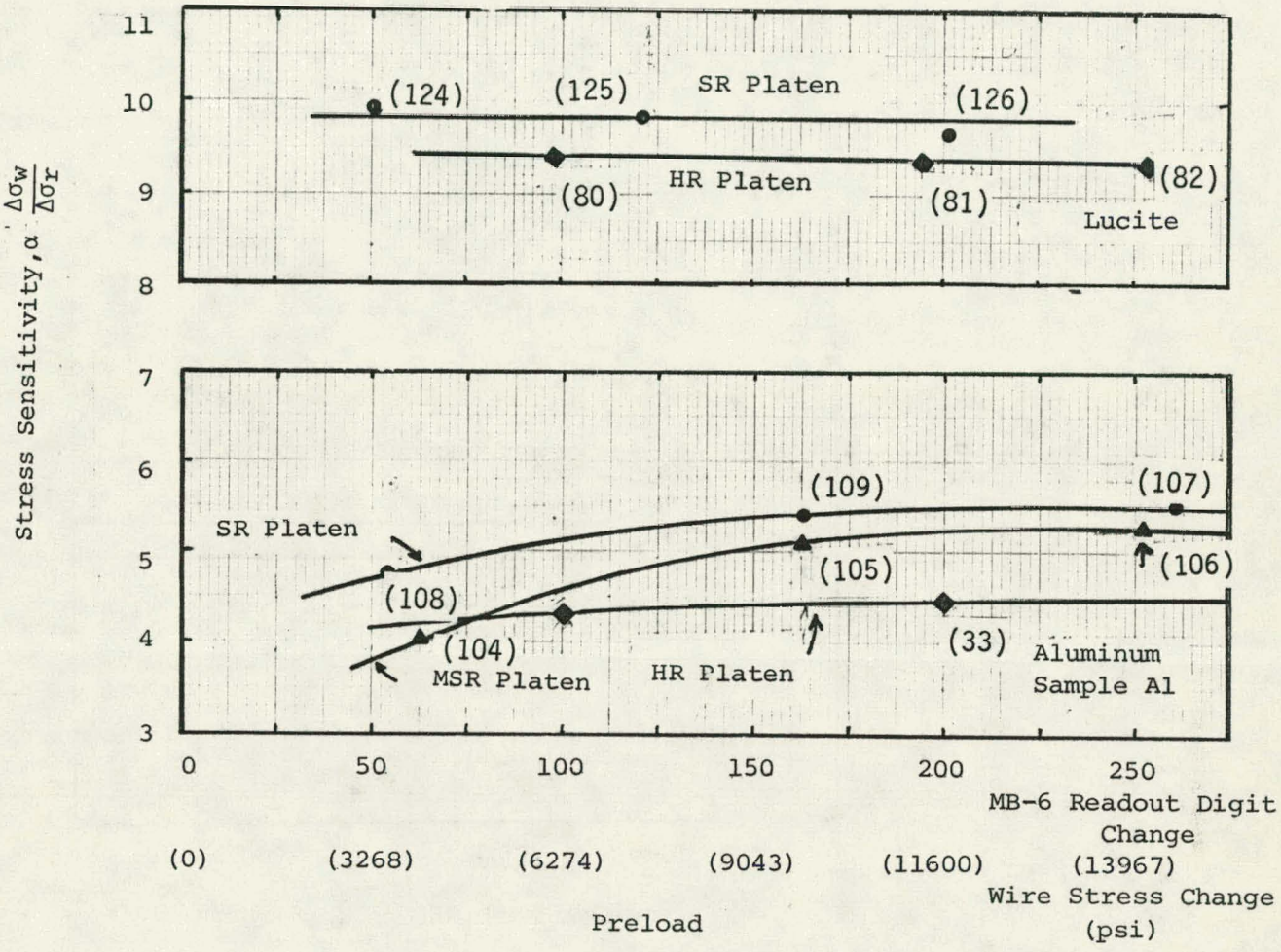

Figure 30. Influence of Platen Geometry on Stressmeter Sensitivity

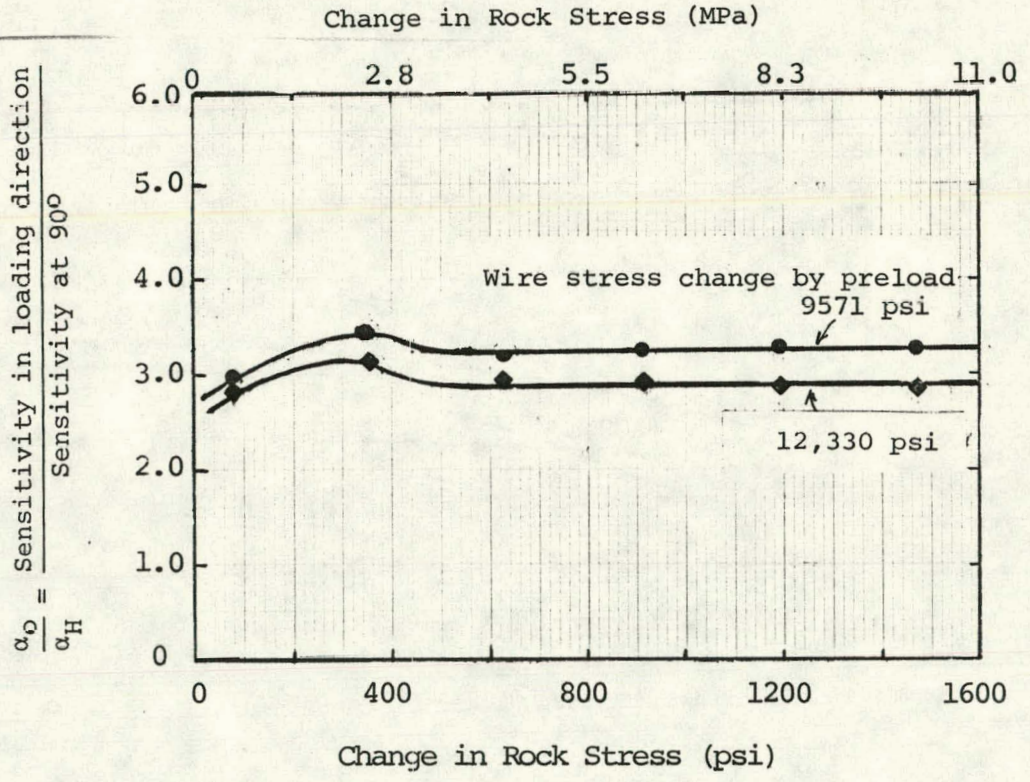

Figure 31. Influence of Gage Orientation on Uniaxial Sensitivity for Climax Granite

4.8 Influence of Elevated Temperature; Uniaxial, Biaxial, Triaxial

The results of high temperature tests in the three modes of load application, uniaxial, biaxial and triaxial, are given in Figures 32, 33 and 34.

Prior to shipment of the twenty electroless nickel-plated VBS-1HT stressmeters to the University of California, Lawrence Livermore Laboratory, the unset gage thermal offsets were measured (Figure 35). All the gages increased their readings as temperature increased; for the twenty gages fabricated, the average unset thermal offset was 0.21 ± 0.08 units change in readout/°C .

The thermal offset of a stressmeter set in rock is greater than that of an unset meter (see Section 2.5). The measured thermal offset (given as wire stress) of a plated VBS-1HT stressmeter in various loading modes in Climax granite is given in Table 16 and illustrated in Figure 36.

Table 16. Thermal Offset of the VBS Stressmeter Set in Climax Granite

Loading Mode	Rock Stress Range (σ_r) psi (MPa)	Thermal Offset as Wire Stress (σ_w) psi/°C (MPa/°C)	Gage Preload	
			Wire Stress psi (MPa)	Reading Change
Uniaxial	0-1751 (12.1)	59 ± 1 (0.41)	11,502 (79.3)	+198
Biaxial	0-1390 (9.6)	55 ± 1 (0.38)	10,955 (75.6)	+187
Triaxial	0-634 (4.4) (end loading) 205-1230 psi 1.4-8.5 MPa)	56 ± 2 (0.39)	11,796 (81.4)	+204

Figures 37 a-e are the plots of the test data for the three modes of stress application. The slope of these curves give the uniaxial stress sensitivity of the stressmeter, which is plotted in Figure 38. Figure 38 also shows that the effect of end loading is very small on the sensitivity in triaxial loadings. As temperature increases, the sensitivity remains approximately constant, until around 60°C, where sensitivity begins to increase.

Within the test range (0-100°C approx.), the effect of temperature on uniaxial stress sensitivity is negligible. The sensitivity predicted by biaxial and triaxial testing is consistent with uniaxial data (following conversion of hydrostatic pressure to applied rock stress, as discussed in Section 2.2).

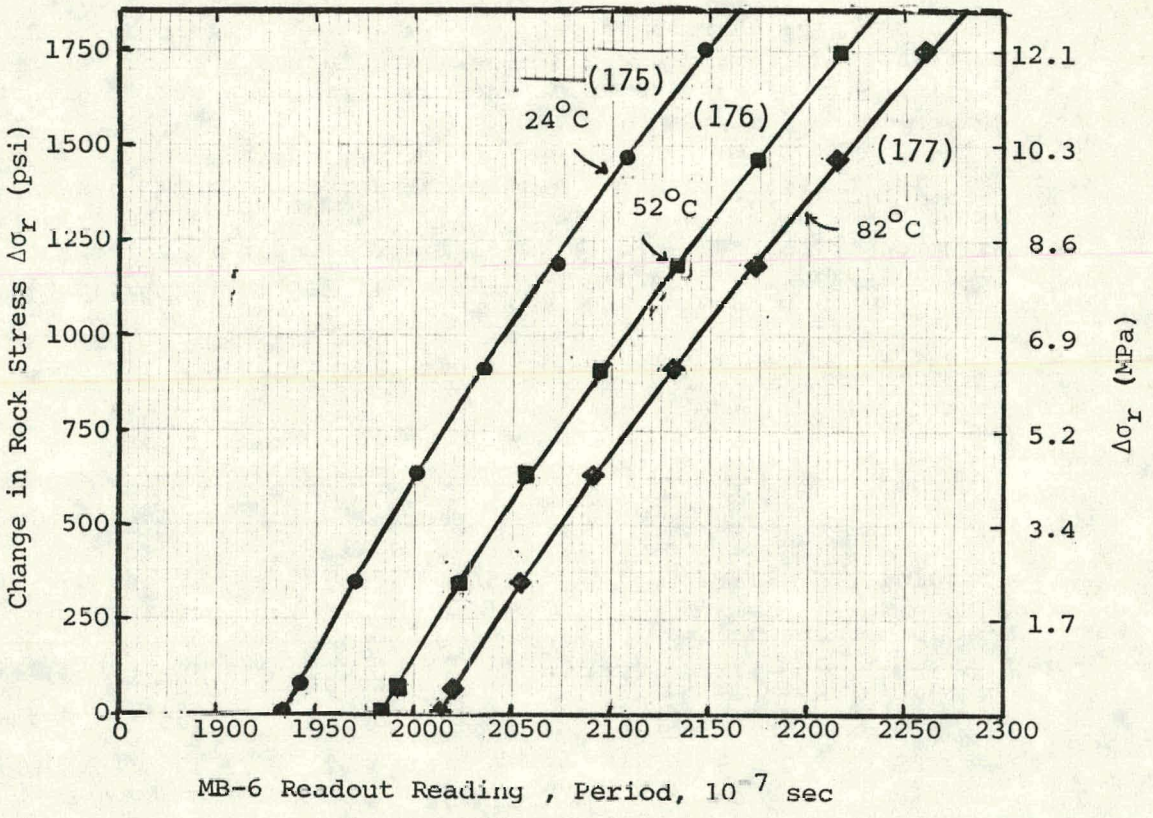

Figure 32. Uniaxial Temperature Test Results (Climax Granite, Stressmeter Preloaded to Wire Stress Change 11403 psi)

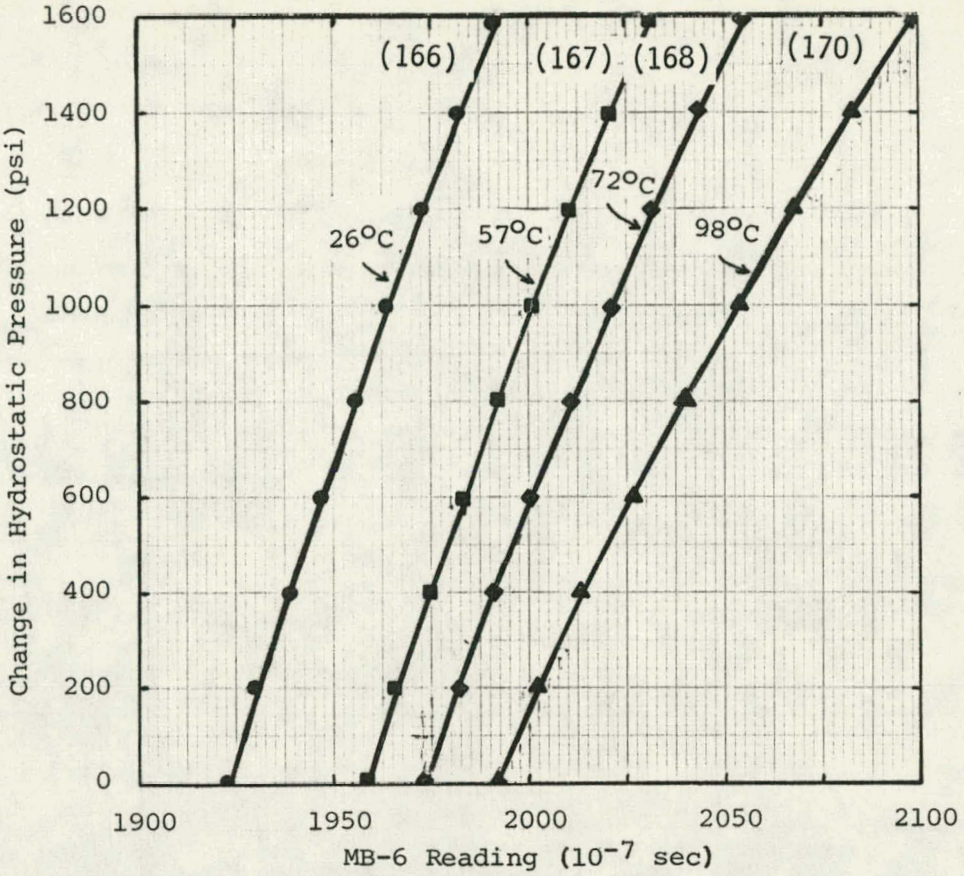

Figure 33. Biaxial Temperature Test Results in Climax Granite (Preload Wire Stress = 11403 psi)

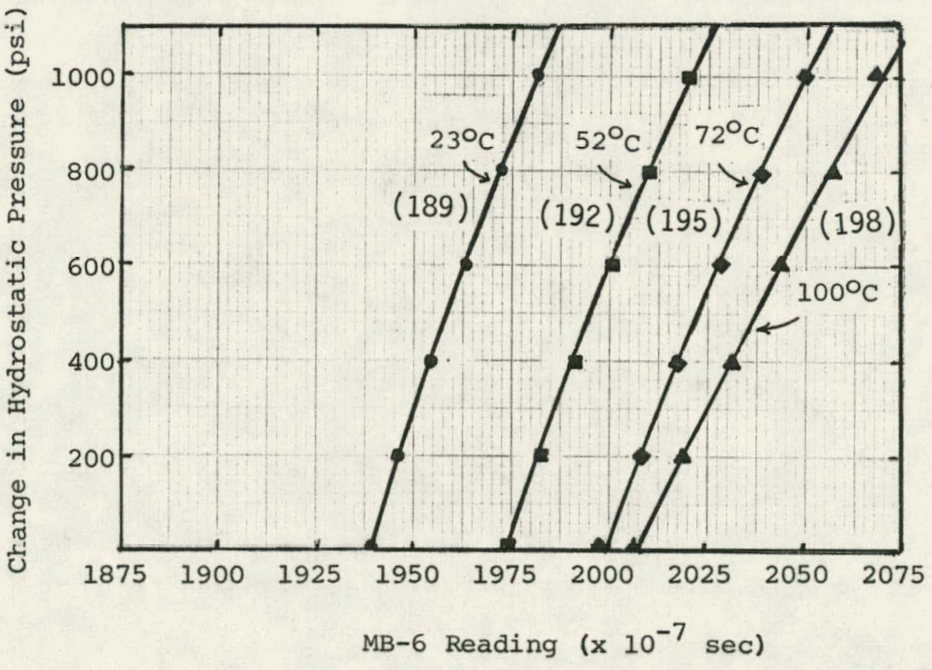

Figure 34. Triaxial Temperature Test Results in Climax Granite (Preload Wire Stress 11796 psi, End load 615 psi)

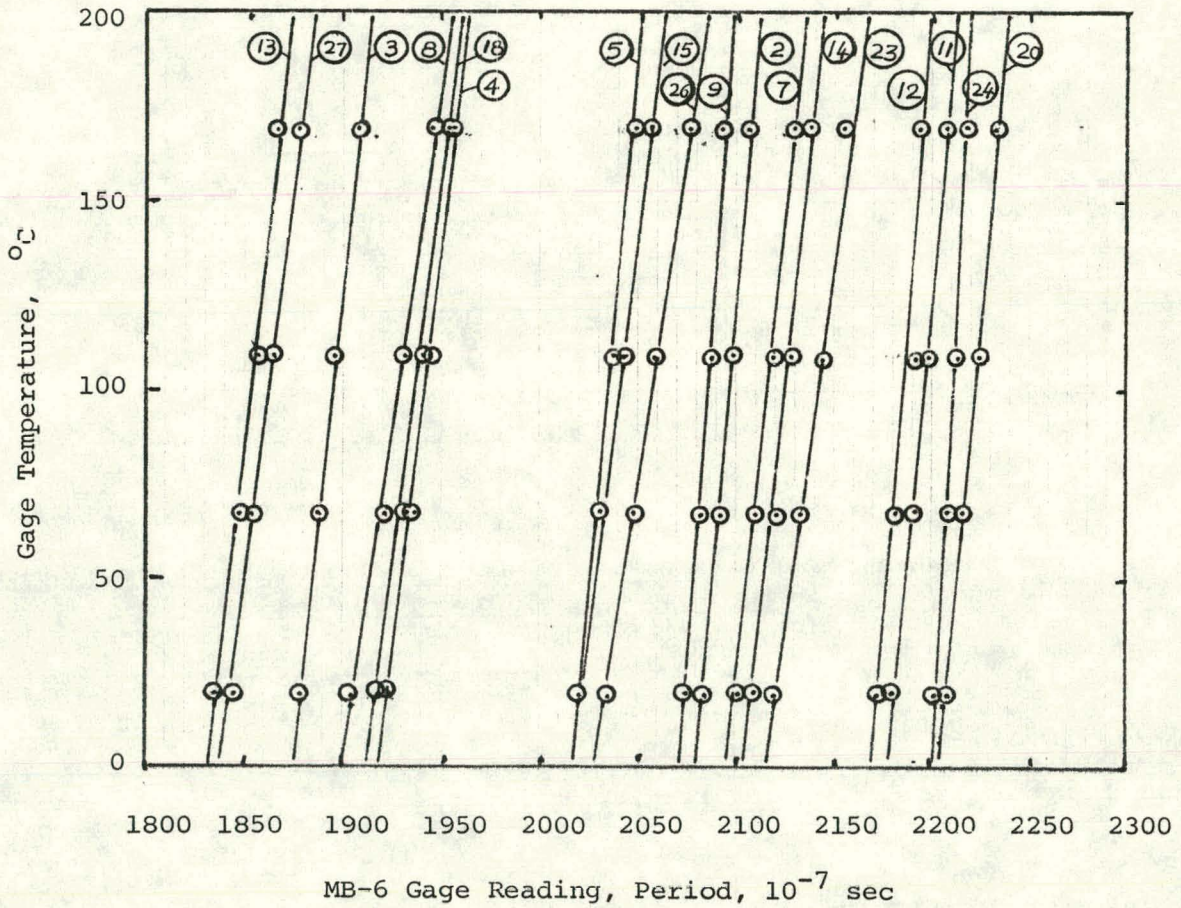

Figure 35. Temperature vs Reading Change of Unset UCL^3 Type Stressmeter

(Stressmeter ID ◯ Numbers)

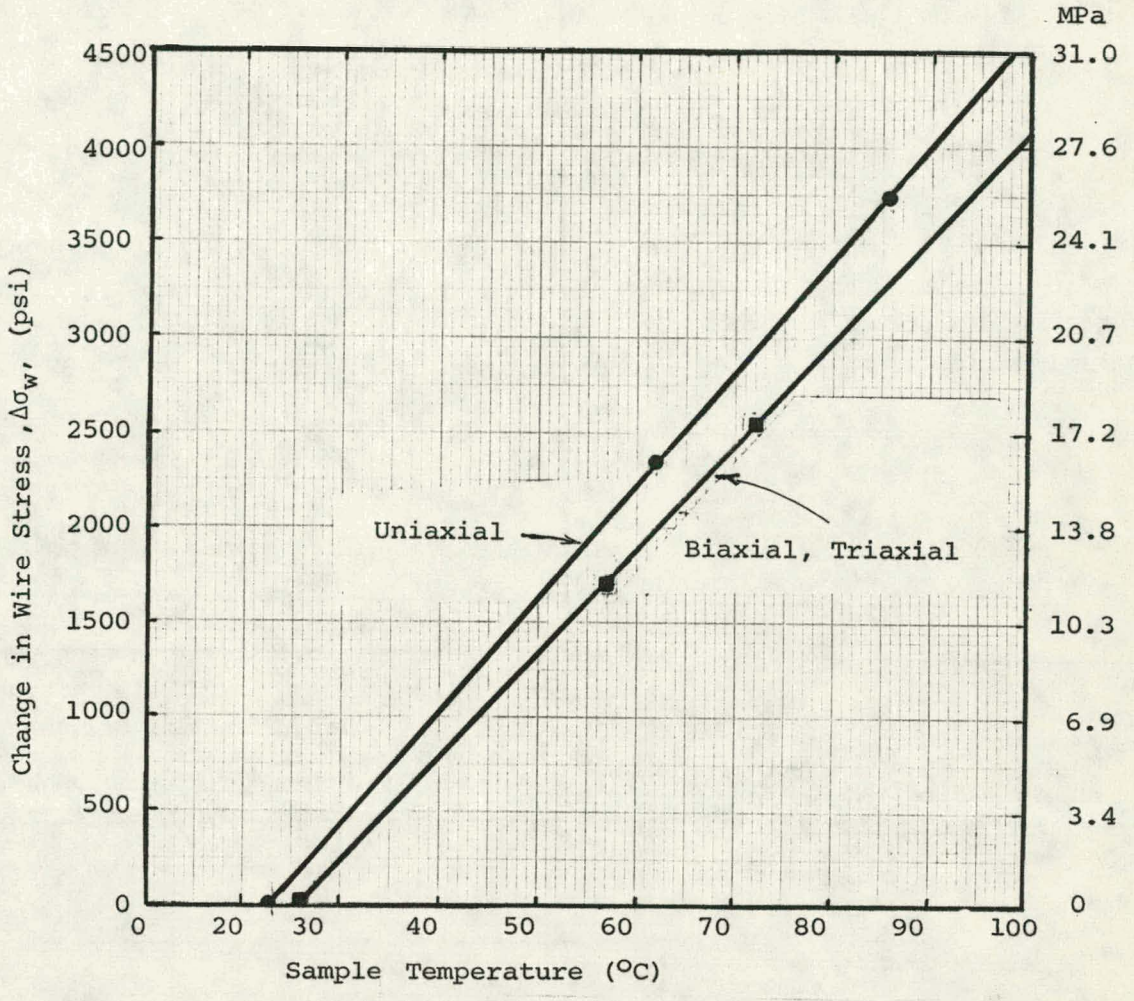

Figure 36. Change in Wire Stress of a Set Stressmeter in Climax Granite Under Elevated Temperature

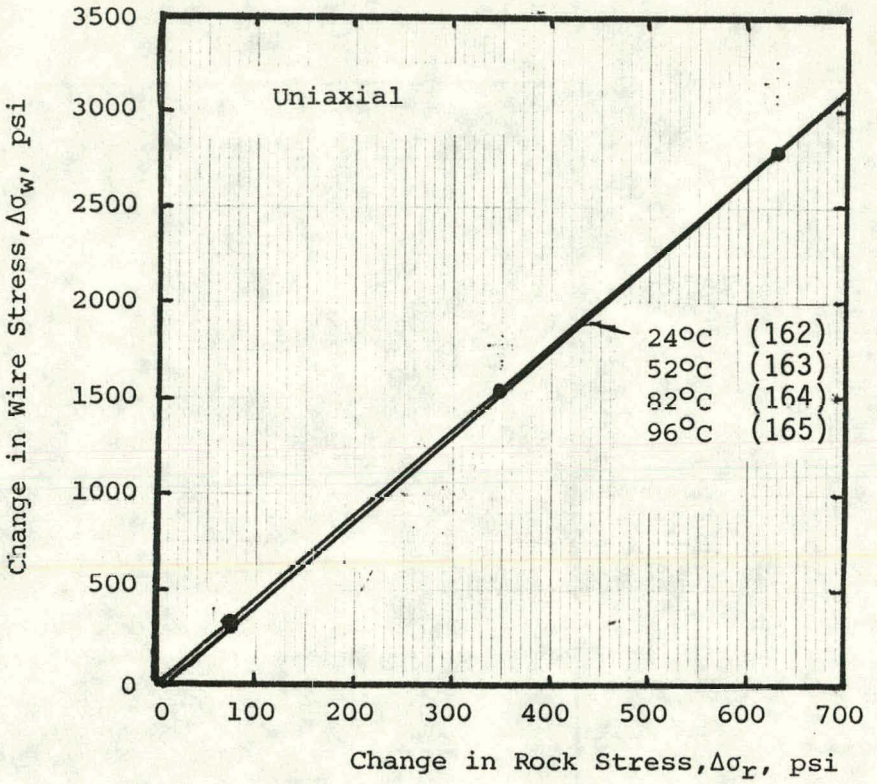

(a) High Temperature Stressmeter Sensitivity Under Uniaxial Loading

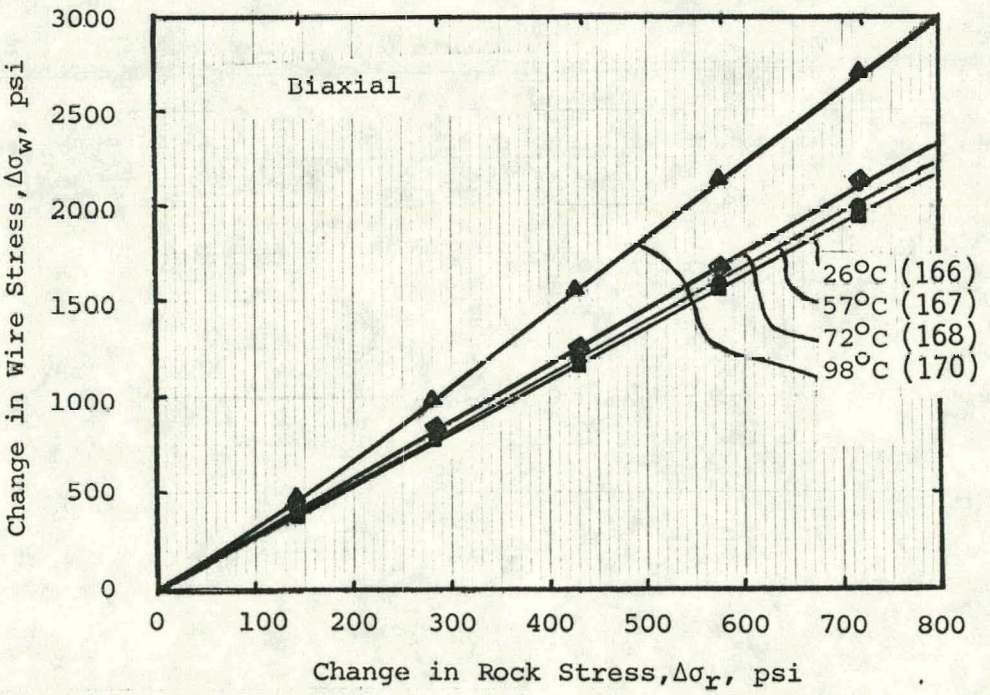

(b) High Temperature Stressmeter Sensitivity Under Biaxial Loading

Figure 37. (a and b)

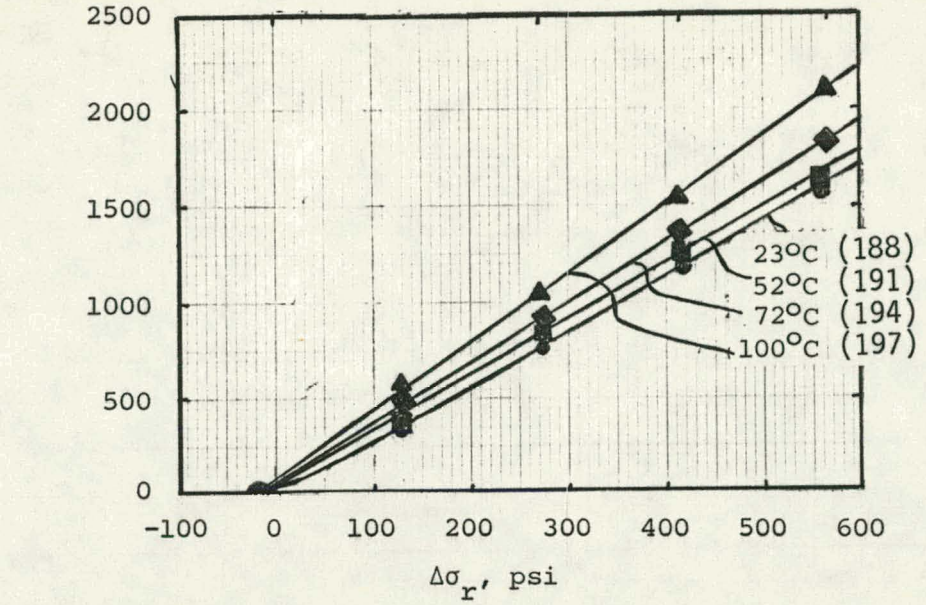

(c) End Load = 225 psi (1.55 KPa)

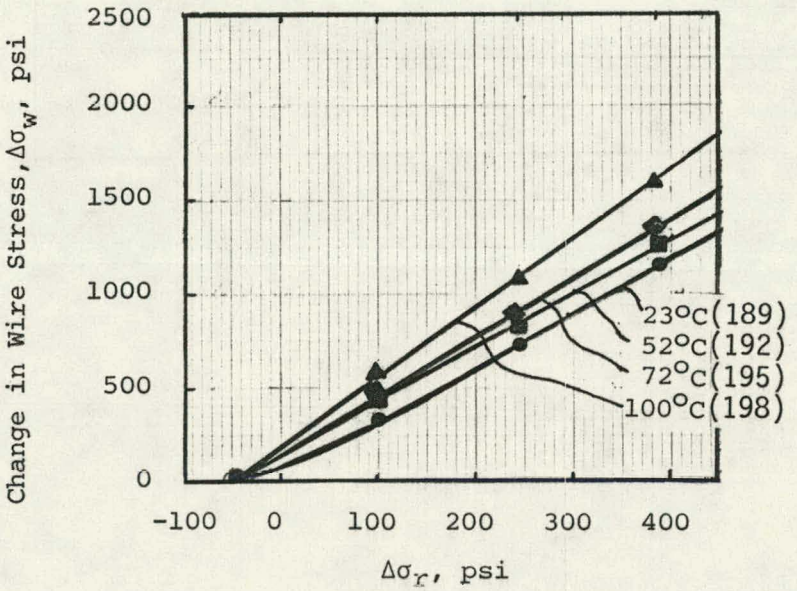

(d) End Load = 615 psi (4.24 KPa)

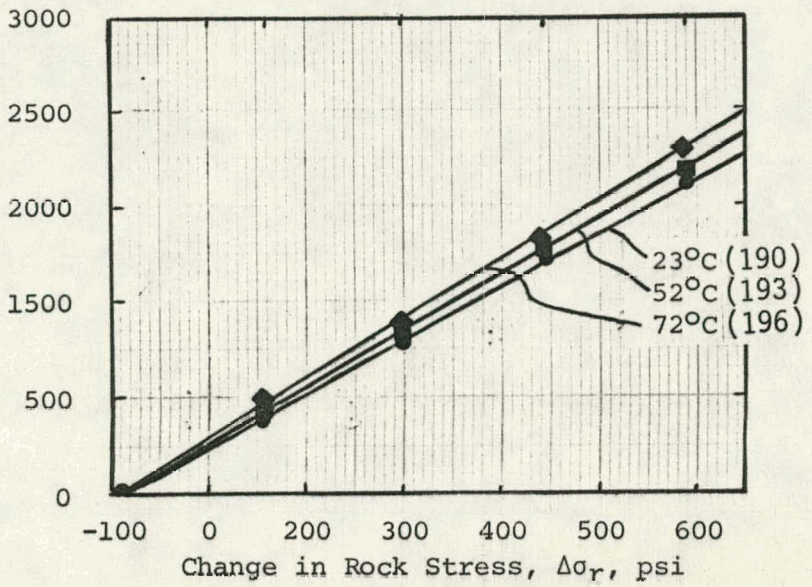

(e) End Load = 1230 psi (8.5 KPa)

Figure 37. (c-e)
High Temperature Stressmeter Sensitivity Under Triaxial Loading

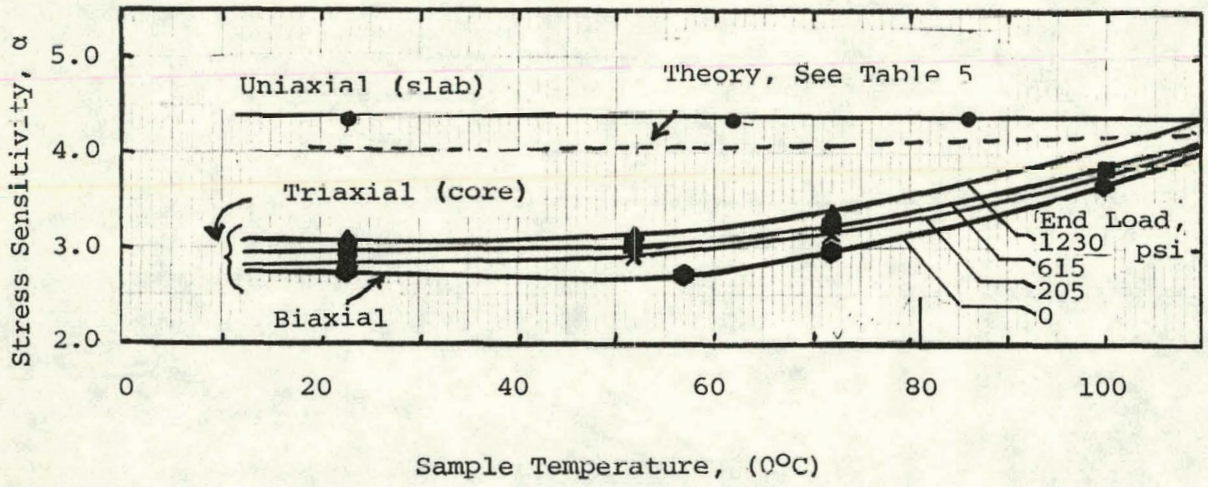

Figure 38. Influence of High Temperature on Stress Sensitivity Factor (Rock: Climax Granite, UCL[3] Type Stressmeter, Preload: 11403 psi Wire Stress

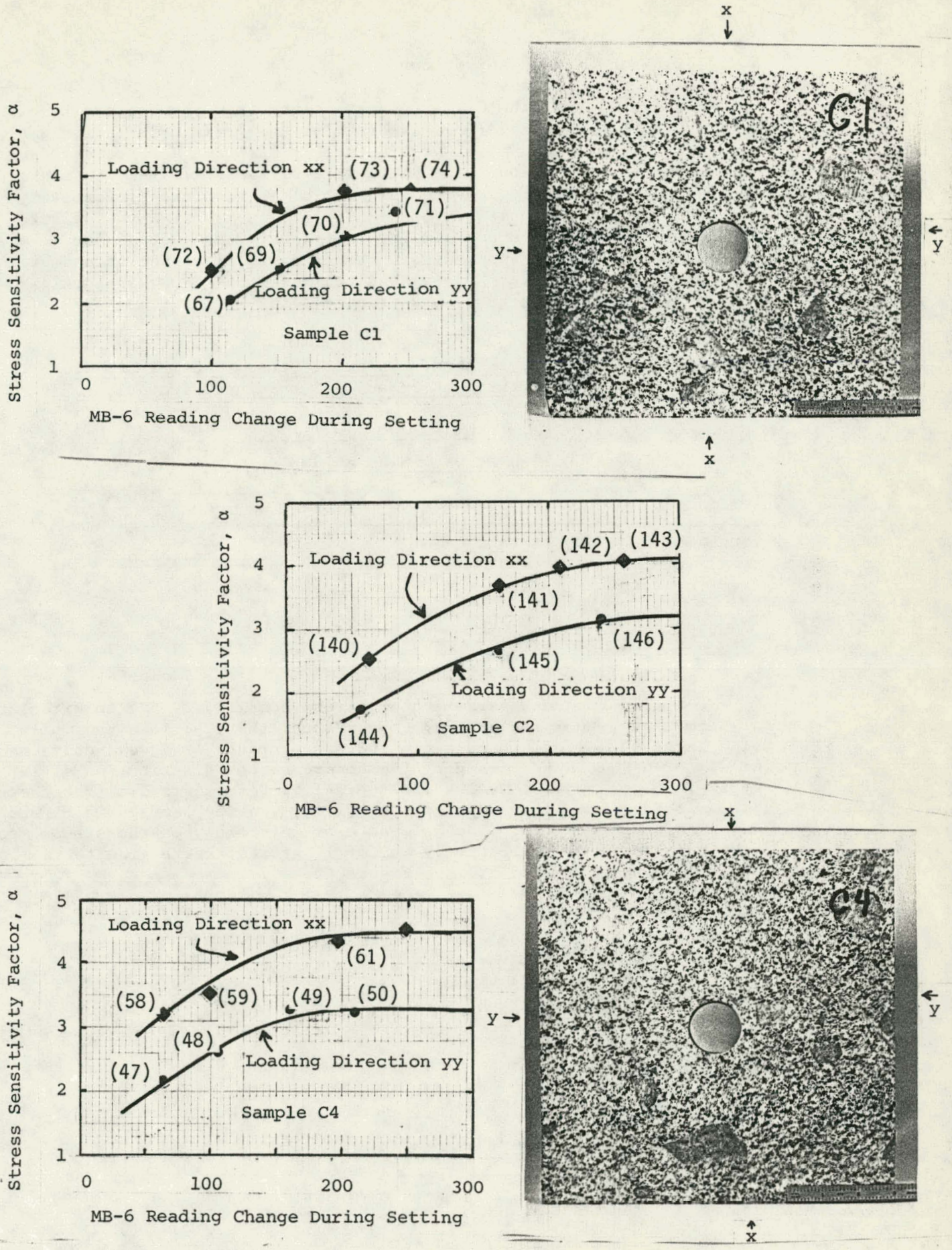

Figure 39. Influence of Climax Granite Rock Anisotropy on Stressmeter Sensitivity

4.9 Influence of Rock Anisotropy

Upon receipt of the Climax granite slabs from the University of California, Lawrence Livermore Laboratory, the grain orientation was studied; however, each slab was arbitrarily assigned a "vertical" and "horizontal" orientation. The slabs were all approximately square (10" x 10" x 1.5") facilitating the measurement of a "vertical" sensitivity, α_v, and a "horizontal" sensitivity, α_H. Table 17 summarizes the measured sensitivities. (Note under similar test conditions that α_v and α_H are all measured with the applied rock stress parallel to the stressmeter wire orientation. Figure 39 (a) and (b) shows the α vs gage preload characteristics for three Climax granite slabs.

Table 17. Anisotropy Effect: Uniaxial Stress Sensitivity of Climax Granite at 0° and 90° Loading Orientation

Slab No.	Slab at 0°	Slab at 90°	(% Change)
	α_v	α_H	$\frac{\alpha_v - \alpha_H}{\alpha_v} \times 100$
C1	3.80	3.40	11.0
C2	4.00	3.10	22.0
C4	4.50	3.30	27.0

The apparent variation of stress sensitivity due to orientation of Climax granite is around 25%. We suspect that, besides the influence of a large number of closed micro and macro cracks, this extensive variability of α values is caused by the heterogeneous distribution of large grain (0.5 to 1.0 in.) inclusions typical to Climax granite (see the inclusions in the photographs of the Climax granite samples in Figure 39 and also in Figure 11). The influence of anisotropy on the stress sensitivity factor α of a relatively uniformly grained Barre granite is much less, being only around 8%; see Figure 40.

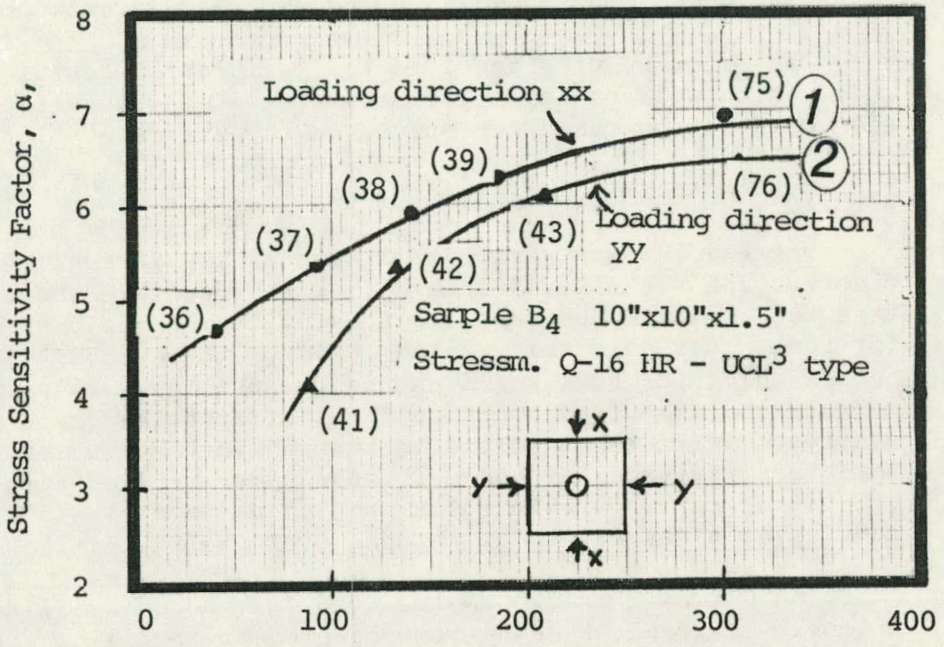

Figure 40. Influence of Anisotropy on Barre Granite Stress Sensitivity Factor

5. DISCUSSION AND CONCLUSIONS

When the IRAD GAGE stressmeter was originally developed, calibration data were intended primarily to give general, rather than detailed, values relating meter readings to the stress changes in surrounding rocks. In view of the widespread success of the meter as a stability indicator, and its growing use as a scientific instrument, there is a need for a complete review of the stressmeter behavior and performance. This investigation, which was aimed at meeting the Lawrence Livermore Laboratory's data interpretation requirements, is an effort in that direction.

The major conclusions from the calibration test results are summarized under three categories: (1) Host material characteristics, (2) Gage design and construction characteristics and (3) Stress environment.

5.1 Host Material Characteristics:

Because the material composition of the stressmeter (steel) and its construction are always identical, a reproducible response is always expected when the host material has uniform elastic properties. However, for rock, such uniformity seldom exists; the composition varies widely. For example, the quartz content in granite may vary by a factor of three or more and elastic properties from different geographical areas may vary considerably. Cracks (micro and macro) in the rock may reversibly and sometimes irreversibly open or close under applied stress, resulting in non-linear stress-strain relationships and hysteresis loops; the static modulus of elasticity also changes over the stress range.

The Climax granite samples used for the uniaxial tests were cut from a single large block. The removal process (drilling and blasting) probably induced large cracks into the specimen, and slab samples larger than the 10 in. x 10 in. size could not be prepared. A variable number of closed micro cracks are also suspected to be present in these slabs. All samples contained an assorted size (maximum 1½ in. diameter) of pink alkali feldspar crystals (see Figure 11). The physical properties of the Climax granite are summarized in Table 18. Note that the porosity varies about 40% and Young's modulus around 12%. It is important to take into consideration the influence of these variabilities in rock properties when interpreting stressmeter data.

Young's Modulus:

Earlier in Section 2.3, it has been discussed that Hawkes et al (1973) predicted a linear relationship between the material moduli and gage sensitivity α. Fossum's (1977) analytical and experimental results showed that this relationship is non-linear.

In the test program, uniaxial stress sensitivity factor, α, was determined for four materials, aluminum, Barre granite, Climax granite and Lucite, of equal sample size (10" x 10" x 1.5") (the samples are shown in Figure 41).

Table 18: Physical Properties of Climax Granite (Source: Ramspott et al (1979))

Property		Value
Dry density	lb/ft^3	163-166
	g/cm^3	2.6-2.66
Porosity (%)		0.7-1.1
Compressive Strength	psi	30500
	MPa	210
Young's Modulus	psi	$8.9\text{-}10.1 \times 10^6$
	GPa	61.4-69.7
Poisson's ratio		0.21-0.22
Thermal conductivity (W/mk)		3.0

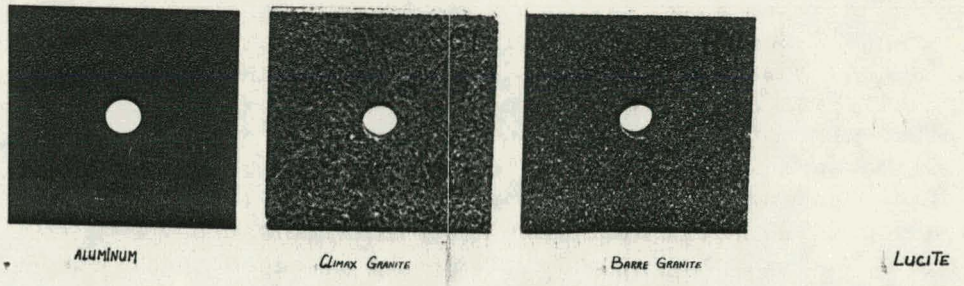

Figure 41. Slab Samples for Uniaxial Stress Sensitivity Determination Tests

Figure 42 shows a plot of the current test results plotted on the theoretical curves predicted by Equation (16) for various platen/rock contact angles. The data for Climax granite were plotted with the assumed value $E_r = 10 \times 10^6$ psi.

It is seen that an increase in contact angle either by preload, applied stress or platen geometry produces a larger change in sensitivity factor α for low modulus material than in high modulus material.

Over the modulus range of the materials tested (0.4 - 10 x 10^6 psi), the sensitivity factor changed around 44%. Had the stressmeter been an ideal stress gage, there would be no change in the sensitivity. The stressmeter sensitivity factor is indeed non-linear with Young's modulus change and is also a complex function of the platen contact angle and, hence, the preload. Thus, in order to use the vibrating wire stressmeter as a precise tool for stress measurement, the change in sensitivity α with modulus change should be precisely determined through laboratory calibration for the host materials of interest.

Anisotropy, Petrofabric, Creep and Uniaxial Compressive Strength:

Table 17 gives three sets of values of α determined in mutually perpendicular directions for three Climax granite slabs. In the mutually perpendicular directions α varied by 11 to 27%; the heterogeneous distribution of the large inclusions, the closed micro and macro cracks, and the general anisotropy of the materials are the suspected causes of this extensive variability. For comparison in a relatively uniformly grained Barre granite, the stress sensitivity factor, α, changed only 8% in the two mutually perpendicular directions.

No measurement of Climax granite creep was made, nor was its influence on stressmeter output determined.

In all tests, a zero shift has been observed between the initial and the second load cycles. Between the second and subsequent load cycles, the shift was negligible. The shift, as a percentage of the maximum applied wire stress, was 7% in aluminum, 16% in Barre granite, and 18% in Climax granite. The contact stress between gage and sample at the maximum loading in aluminum was 74,000 psi (510 MPa), in Barre granite 41,029 psi (283 MPa), and in Climax granite 45,680 psi (315 MPa)*. It appears in all cases they have locally exceeded their compressive strength (for the three materials studied, the compressive strengths are 55,000 psi (379 MPa), 29,300 psi (145 MPa), and 30,500 psi (210 MPa), respectively) and permanent local deformation has set in, which is responsible for the zero shift. Further discussion of the contact stress problem is made later under preload.

---

* See Appendix 7

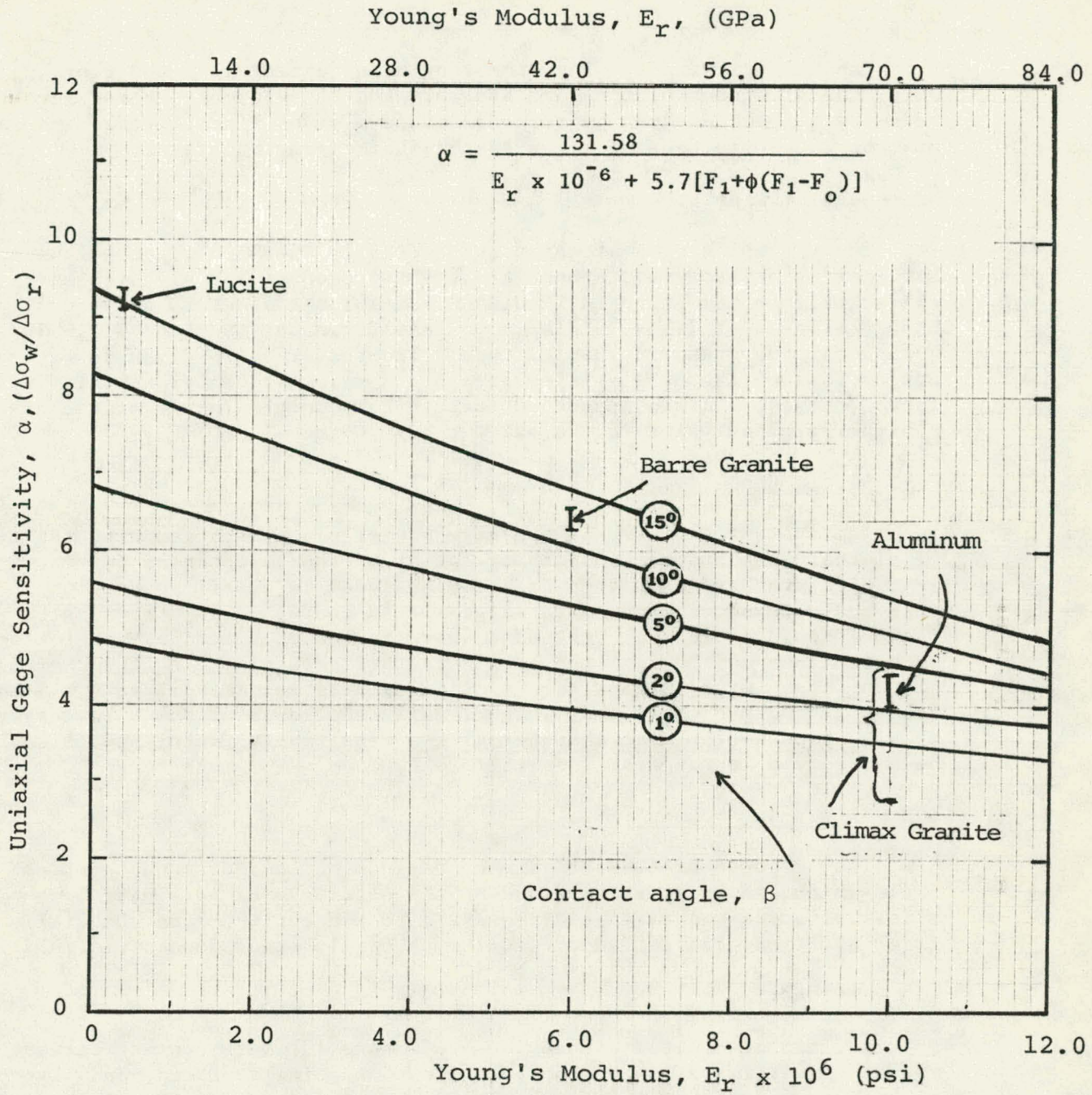

Figure 42. Influence of Contact Angle on the Stressmeter Sensitivity

5.2 Gage Design and Construction Characteristics:

The initial wire tension, the length and diameter of the vibrating wire, the stiffness of the gage assembly and the platen/rock contact geometry determine the gage response under a given load (wire length and diameter and wire tension are predetermined during manufacture).

Gage Stiffness:

The vibrating wire stressmeters specially prepared for the Lawrence Livermore Laboratory had a heat treatment procedure and electroplating different from the standard IRAD GAGE VBS-1HT stressmeter, and had a gage body stiffness of 7.5×10^6 lb/in. slightly greater than the 7.1×10^6 lb/in. for the standard VBS-1HT type. The test results given in Figure 21 appear to show that the stiffer gage has a slightly higher sensitivity factor; however, it is suspected that this is only a result of the use of a higher preload value in the stiffer gage test.

Platen Geometry:

The contact geometry of the stressmeter platen changes with the type of platen. The stress sensitivity factor of the stressmeter for the IRAD GAGE standard HR platen has been analyzed in detail in Section 2.3; this analysis shows that, with large platen contact area, the sensitivity factor should increase. Test data shown in Table 14 indicate that, for both aluminum and Lucite, the larger contact area of the soft rock (SR) platen indeed gives higher values of uniaxial stress sensitivity. A modified soft rock (MSR) platen, which ideally should match the hole curvature, is also expected to give a higher stress sensitivity factor and this has been observed in the test results for aluminum.

5.3 Stress Environment

The response of the stressmeter depends on the surrounding stress field which, in turn, is governed by the setting preload, initial in-situ stress, loading range, gage orientation to the applied load, biaxial and triaxial stress fields and the influence of elevated temperature.

Preload:

An initial preload is provided to ensure intimate contact between the stressmeter system and the borehole contacting surfaces, and also to maintain permanent contact for measuring tensile stress (gage unloading). Now the preload operation increases the gage contact area and this, as discussed in the analysis section (Section 2.3), will cause an increase in sensitivity factor, α. The stress sensitivity factor, α, computed from Equation (16) with contact angle 2β increasing from 1° to 20°, is shown in Figure 43 for a material of an assumed elastic constant E_r = 6×10^6 psi (4.1×10^4 MPa), typical of Barre granite. The trend of this curve is similar to the experimental data plotted in Figure 28, which shows that α increases much more under low preload values than under higher preload values — implying that a high preload is desirable to attain a small variation in α under "set" conditions. In fact, the data show that a minimum preload value should be used, above which the sensitivity α is essentially constant.

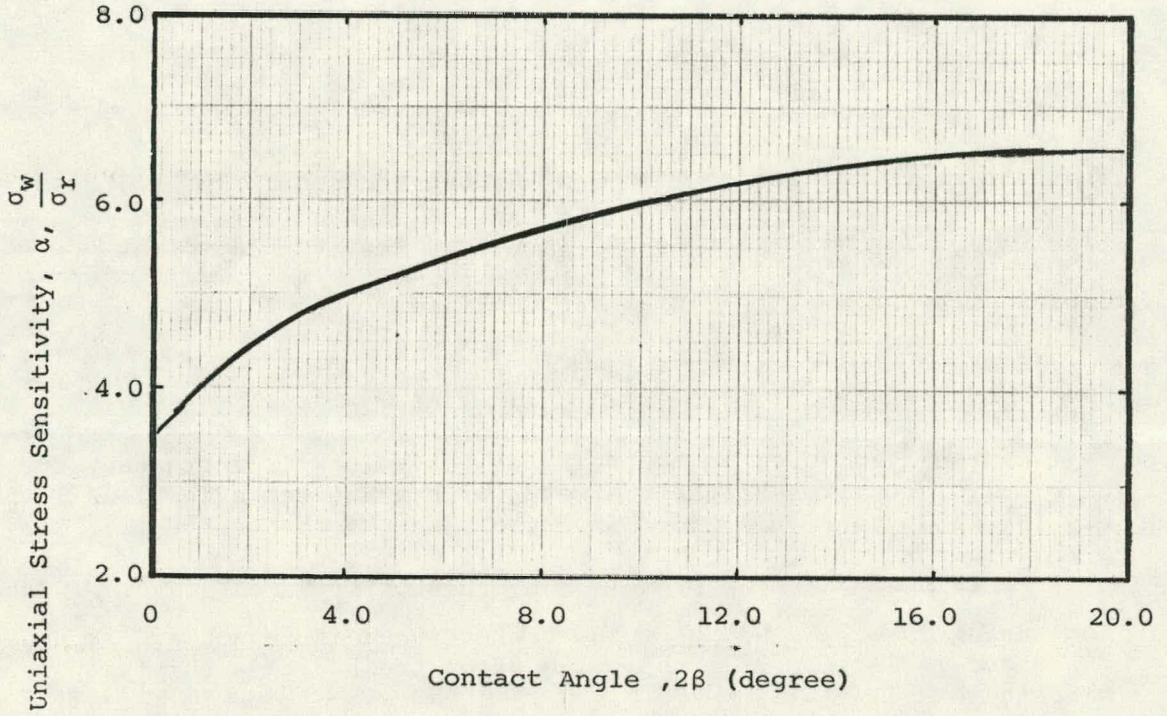

Figure 43. Influence of Contact Angle 2β on The Sensitivity Factor, α

Initial Stress Field:

A borehole drilled in a rock mass under a high state of stress will be deformed, and the response of the gage set in such an environment has been, prior to these tests, largely unknown. Test results shown in Figure 29 for gages set in a Climax granite slab with initial stress levels up to 1300 psi (9 MPa) indicate that the influence of the initial stress level within test range is negligible.

Gage Orientation:

If the preloading direction (wire axis) differs from the loading direction of the slab by an angle θ, and the rock stress in the preload direction is σ_o, and in the loading direction σ_θ, then

$$\sigma_\theta = \frac{\sigma_o}{3} (1+2 \cos 2\theta)$$

Tests to check the ratio $\frac{\alpha_o}{\alpha_{90}} = -3$ with the gage set at 90° to the direction of loading were carried out in Climax granite. A very close correlation with the result $\frac{\alpha_o}{\alpha_{90}} = -3$ was obtained.

Load Range:

As the load level on the uniaxial test block is increased, the curve of σ_w vs σ_r concaves slightly upward, with a knee at a low load level, e.g. as shown in Figure 21. Since the slope of this curve is $\alpha = \frac{\sigma_w}{\sigma_r}$, this can also be explained by the contact area effect. With increasing load, the width of the contact area increases and hence, as discussed in Section 2.3, the value of α, the stress sensitivity factor, also increases.

Biaxial and Triaxial Stress Field:

The influence of biaxial and triaxial loading on the uniaxial stress sensitivity factor is shown in Figure 38. An analytical approach to this problem, presented earlier in Section 2.4, shows that, with a hydrostatic loading configuration, the biaxial and triaxial mode of loading can be related to the uniaxial stress sensitivity factor through the formulae presented in Table 3.

Results summarized in Figure 38 show, for Climax granite, that the equivalent uniaxial stress sensitivity factors , based on the equivalent rock stress formulae from Table 3 under biaxial and triaxial loading are within a range of 2.7-3.2 at room temperature. Referring to Table 17, it will be seen that uniaxial sensitivity factor, α, for Climax granite ranged from 3.1 to 4.5 depending on the sample used and direction of applied loading. The biaxial and triaxial values of α (α = 2.7-3.2),

therefore, lie well within the data scatter of the stress sensitivity factor determined under uniaxial loading on the four Climax granite slabs. It is concluded that biaxial and triaxial loading do not significantly affect the stress sensitivity factor.

Temperature:

The influence of temperature on a stressmeter set in rock is complicated, and an approach to the problem is discussed in Sections 2.5.

For both a set and an unset gage, the readings increase with temperature. For an unset gage, the increase in reading is caused by differential expansion of the wire and the body; for the set gage, the increase in reading is caused by differential expansion of the wire and the rock.

The analytical solution, given in Section 2.5.2, also shows that the uniaxial stress sensitivity factor α will increase with temperatures. The dotted line in Figure 38 represents the theoretical data calculated for uniaxial tests, as given in Table 4 for Climax granite. The theory predicts only a very small increase of α with temperature, which is borne out by experiment. Under biaxial and triaxial loading, the test data, however, show a more pronounced increase in α values (approximately 25%).

The principal conclusion of this study is that the uniaxial stress sensitivity factor for the Climax granite varied over a wide margin — from 2.7 to 4.5. A large number of factors listed earlier influence the stressmeter response. In interpreting the field data, influence of each factor needs to be carefully evaluated.

The algorithm for conversion of measured readings into rock stress changes is given in Appendix 8. Appendix 9 gives the raw data of the tests performed in the calibration study.

REFERENCES

1. Carslaw, H. S. and Jaeger, J. G.; ' Conduction of Heat in Solids', Oxford University Press, 1959, pp 99-105.

2. Coutinho, A.; 'Theorie de la Determination Experimentale des Contraintes par une Methode n'exigeant pas la Connaissance Précise du Module de l'élasticite', Int. Assoc. Bridge and Structure Eng. Cong., 1949, p. 83.

3. de la Cruz, R. V., Goodman, R. E.; 'The Borehole Deepening Method of Stress Measurement', Paper No. 7, Int'l Symp. on the Determination of Stresses in Rock Masses, Lisboa, 1969.

4. Fossum, A. F., Russell, J. E., Hansen F. D.; 'Calibration Analysis for the In-Situ Response of a Vibrating-Wire Stress Gauge in Soft Rock', 1976 SESA Spring Meeting, Silver Spring.

5. Hast, N.; 'The Measurement of Rock Pressure in Mines', Sveriges Geologiska Undersöking, Generalstabens Litografiska Anstalts Förlag, Drottninggatan 20 Stockholm 16, 1958.

6. Hawkes, I.; 'Theory of the Photoelastic Biaxial Gauge and Its Applications in Rock Stress Measurements', Strain, Vol. 3, July, 1967.

7. Hawkes, I.; 'Design, Develop, Fabricate, Test and Demonstrate Permissible Low Cost Cylindrical Stress Gages and Associated Components Capable of Measuring Change in Stress as a Function of Time in Underground Coal Mines', USBM Contract Report (HO220050), 1973.

8. Jaeger, J. C. and Cook, N. G. W.; 'Fundamentals of Rock Mechanics', Methuen & Co. Ltd., 1969, pp 242-245.

9. Jordan, D. W.; 'Strains in an Annular Rock Dynamometer', Journal of Strain Analysis, Vol. 1., No. 1., 1965.

10. Nichols Jr., T. C., Abel, J. F. and Lee, F. T.; 'A Solid-Inclusion Borehole Probe to Determine Three-Dimensional Stress Changes at a Point in a Rock Mass', Geological Survey Bulletin 1258-C, 1968.

11. Pariseau, W. G., et al, 'Coal Pillar Strength Study (The Design of Production Pillars in Coal Mines)', prepared for USBM, pp 396-417, NTIS PB-274900.

12. Ramspott, L. D., Ballou, L. B., Carlson, R. C., Montan, D. N., Butkovich, T. R., Duncan J. E., Patrick W. C., Wilder, D. G., Brough, W. G., and Mayer, M. C.; 'Technical Concept for a Test of Geological Storage of Spent Reactor Fuel in the Climax Granite, Nevada Test Site, June, 15, 1979, p. 11.

13. Roark, R. J. and Young, W. C.; 'Formulas for Stress and Strain', McGraw Hill Book Company, New York, 1975, p. 518.

14. Roberts, A; 'In-Situ Stress Determination in Rock Masses-A Review of Progress in the Application of Some Techniques', Paper No. 9., Int'l Symp. on the Determination of Stresses in Rock Masses, Lisboa, 1969.

15. Rocha, M. and Silverio, A.; 'A New Method for the Complete Determination of the State of Stress in Rock Masses', Paper No. 18, Int'l Symp. on the Determination of Stresses in Rock Masses, Lisboa, 1969.

APPENDIX 1

Deformation of Borehole Under Preloading of Stressmeter

APPENDIX 1

Deformation of a Borehole Under Preloading of Stressmeter

Jaeger and Cook (Reference 8) have shown that for an applied pressure p on a borehole wall (Figure A.1) and plane stress condition:

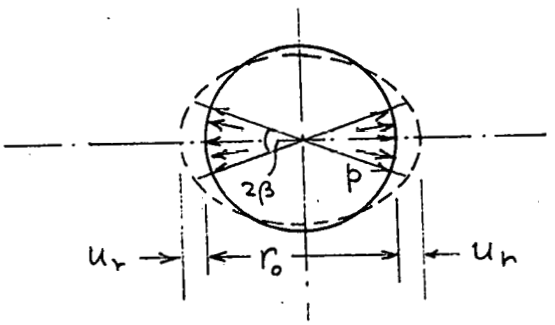

Figure A.1. Borehole Deformation Under Internally Applied Pressure.

$$\frac{2\pi G u_r}{r_o p} = -2\beta - k\left[\frac{\pi}{2}\cos\beta + \sin\beta \ln\cot\frac{\beta}{2} - \frac{\pi}{2} + \beta\right] - \left[\frac{\pi}{2} - \beta - \frac{\pi}{2}\cos\beta + \sin\beta \ln\cot\frac{\beta}{2}\right]$$

where $G = \frac{E_r}{2(1+\nu_r)}$, $k = \frac{3-\nu_r}{1+\nu_r}$ and $p = \frac{P}{2\beta r_o t}$

From above

$$\delta = 2u_r = -2\frac{\beta r_o p}{\pi G} - k\frac{r_o p}{\pi G}\left[\frac{\pi}{2}\cos(\beta) + \sin(\beta)\ln\left\{\cot\frac{\beta}{2}\right\} - \frac{\pi}{2} + \beta\right] - \frac{r_o p}{\pi G}\left[\frac{\pi}{2} - \beta - \frac{\pi}{2}\cos(\beta) + \sin(\beta)\ln\left\{\cot\frac{\beta}{2}\right\}\right]$$

$$= A + B + C \qquad (A\text{-}1.1)$$

where $A = \frac{-2\beta r_o p}{\pi G} = -\frac{2\beta r_o p}{\pi \cdot \frac{E_r}{2(1+\nu_r)}} = \frac{-2P(1+\nu_r)}{\pi t E_r}$

$$B = K \frac{r_0 P}{\pi G}\left[\frac{\pi}{2}\cos(\beta) + \sin(\beta)\ln\left\{\cot\frac{\beta}{2}\right\} - \frac{\pi}{2} + \beta\right]$$

$$= \frac{3-\nu_r}{1+\nu_r} \times \frac{r_0}{\pi G} \times \frac{P}{2\beta r_0 t} \times \frac{2(1+\nu_r)}{E_r}\left[\frac{\pi}{2}\cos(\beta) + \sin(\beta)\right.$$
$$\left.\ln\left\{\cot\frac{\beta}{2}\right\} - \frac{\pi}{2} + \beta\right]$$

$$= \frac{P(3-\nu_r)}{\beta\pi t E_r}\left[\frac{\pi}{2}\cos(\beta) + \sin(\beta)\ln\left\{\cot\frac{\beta}{2}\right\} - \frac{\pi}{2} + \beta\right]$$

$$C = \frac{r_0 P}{\pi G}\left[\frac{\pi}{2} - \beta - \frac{\pi}{2}\cos(\beta) + \sin(\beta)\ln\left\{\cot\frac{\beta}{2}\right\}\right]$$

$$= r_0 \frac{P}{2\beta r_0 t} \cdot \frac{2(1+\nu_r)}{\pi E_r}\left[\frac{\pi}{2} - \beta - \frac{\pi}{2}\cos(\beta) + \sin(\beta)\ln\left\{\cot\frac{\beta}{2}\right\}\right]$$

$$= \frac{P(1+\nu_r)}{\pi t \beta E_r}\left[\frac{\pi}{2} - \beta - \frac{\pi}{2}\cos(\beta) + \sin(\beta)\ln\left\{\cot\frac{\beta}{2}\right\}\right]$$

Rewriting eq. A-1.1

$$\delta = \frac{-2P(1+\nu_r)}{\pi t E_r} - \frac{P(3-\nu_r)}{\beta\pi t E_r}\left[\frac{\pi}{2}\cos(\beta) + \sin(\beta)\ln\left\{\cot\frac{\beta}{2}\right\}\right.$$
$$\left. - \frac{\pi}{2} + \beta\right] - \frac{P(1+\nu_r)}{\pi t \beta E_r}\left[\frac{\pi}{2} - \beta - \frac{\pi}{2}\cos(\beta) + \sin(\beta)\left\{\cot\frac{\beta}{2}\right\}\right]$$

$$= \frac{P}{E_r}\cdot\frac{2}{\pi t}\left[-1-\nu_r - \frac{3-\nu_r}{2\beta}\left[\frac{\pi}{2}\cos(\beta) + \sin(\beta)\ln\left\{\cot\frac{\beta}{2}\right\} - \frac{\pi}{2} + \beta\right]\right.$$
$$\left. - \frac{(1+\nu_r)}{2\beta}\left[\frac{\pi}{2} - \beta - \frac{\pi}{2}\cos(\beta) + \sin(\beta)\ln\left\{\cot\frac{\beta}{2}\right\}\right]\right.$$

$$= \frac{2P}{\pi E_r t}\left\{-1-\nu_r-\frac{3}{2\beta}\left[\frac{\pi}{2}\cos\beta+\sin(\beta)\ln\cot\left(\frac{\beta}{2}\right)-\frac{\pi}{2}+\beta\right]\right.$$
$$+\frac{\nu_r}{2\beta}\left[\frac{\pi}{2}\cos(\beta)+\sin(\beta)\ln\cot\left(\frac{\beta}{2}\right)-\frac{\pi}{2}+\beta\right]$$
$$-\frac{1}{2\beta}\left[\frac{\pi}{2}-\beta-\frac{\pi}{2}\cos(\beta)+\sin(\beta)\ln\cot\left(\frac{\beta}{2}\right)\right]$$
$$\left.-\frac{\nu_r}{2\beta}\left[\frac{\pi}{2}-\beta-\frac{\pi}{2}\cos(\beta)+\sin(\beta)\ln\cot\frac{\beta}{2}\right]\right\}$$

$$= \frac{2P}{\pi E_r t}\left[-1-\frac{3}{2}+\frac{1}{2}-\nu_r+\frac{\nu_r}{2}+\frac{\nu_r}{2}-\frac{3\pi}{4\beta}\cos(\beta)+\frac{\pi}{4\beta}\cos(\beta)\right.$$
$$-\frac{3}{2\beta}\sin\beta\ln\cot\frac{\beta}{2}-\frac{1}{2\beta}\sin(\beta)\ln\cot\frac{\beta}{2}$$
$$+\frac{3\pi}{4\beta}-\frac{\pi}{4\beta}+\frac{\nu_r\pi}{4\beta}\cos(\beta)+\frac{\nu_r\pi}{4\beta}\cos(\beta)$$
$$\left.-\frac{\nu_r\pi}{4\beta}-\frac{\nu_r\pi}{4\beta}\right]$$

$$= \frac{2P}{\pi E_r t}\left[-2-\frac{\pi}{2\beta}\cos(\beta)-\frac{2}{\beta}\sin(\beta)\ln\cot\frac{\beta}{2}+\frac{\pi}{2\beta}+\frac{\nu_r\pi}{2\beta}\cos(\beta)-\frac{\nu_r\pi}{2\beta}\right]$$

$$= \frac{-2P}{\pi E_r t}\left[2+\frac{\pi}{2\beta}\cos(\beta)+\frac{2}{\beta}\sin(\beta)\ln\cot\frac{\beta}{2}-\frac{\pi}{2\beta}-\frac{\nu_r\pi}{2\beta}\cos(\beta)+\frac{\nu_r\pi}{2\beta}\right]$$

$$= \frac{-2P}{\pi E_r t}\left[1+\frac{1}{\beta}\left\{\frac{\pi}{2}\cos(\beta)-\frac{\pi}{2}+\beta\right\}-\frac{\nu_r}{\beta}\left\{\frac{\pi}{2}\cos(\beta)-\frac{\pi}{2}+\beta\right\}\right.$$
$$\left.+\nu_r+\frac{2}{\beta}\sin(\beta)\ln\cos\frac{\beta}{2}\right]$$

$$= -\frac{2P}{\pi E_r t}\left[1+\nu_r+\frac{1-\nu_r}{\beta}\left\{\frac{\pi}{2}\cos(\beta)-\frac{\pi}{2}+\beta\right\}+\frac{2}{\beta}\sin(\beta)\ln\cot\left(\frac{\beta}{2}\right)\right]$$

(A.1.2)

APPENDIX 2

Calculation of the Uniaxial Stress Sensitivity Factor, α

APPENDIX 2

Calculation of the Uniaxial Stress Sensitivity Factor, α

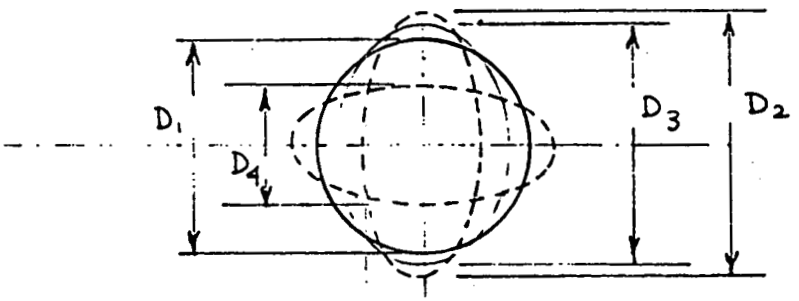

Figure A.2.1. Borehole Deformation Under Stressmeter Setting and Loading

Using the nomenclature of Section 2.3,

$$\delta_{po} = D_2 - D_1 = \frac{P_o}{E_r} f(\beta_o, \nu_r, t) \qquad (A2.1)$$

$$\delta_p = D_2 - D_3 = \frac{P}{K_{ga}} = \frac{K_g \delta_w}{K_{ga}} = \frac{K_g \ell_w \sigma_w}{K_{ga} E_w} \qquad (A2.2)$$

$$\delta_e = D_1 - D_4 = \frac{3 D_1 \sigma_r}{E_r} \qquad (A2.3)$$

and $$\delta = D_3 - D_4 = \frac{P_o + P}{E_r} f(\beta, \nu_r, t) \qquad (A2-4)$$

Simplifying and combining

$$\delta = \delta_e - \delta_p + \delta_{po} \qquad (A2-5)$$

From Sec. 2.3. $$P = K_g \delta_w = K_g \frac{\ell_w \sigma_w}{E_w}$$

$$P_o = K_g \delta_{w_o} = K_g \frac{\ell_w \sigma_{w_o}}{E_w}$$

Let $\frac{P_o}{P} = \frac{\Delta\sigma_{wo}}{\Delta\sigma_w} = \phi$

Therefore $P_o = P\phi$ (A2-6)

Substituting the expressions in eq. A2-5

$$\frac{P_o + P}{E_r} f(\beta, \nu_r, t) = \frac{3D_1\sigma_r}{E_r} - \frac{K_g l_w \sigma_w}{K_{ga} E_w} + \frac{P_o}{E_r} f(\beta_o, \nu_r, t)$$

or $$\frac{P_o}{E_r}\left[f(\beta, \nu_r, t) - f(\beta_o, \nu_r, t)\right] + \frac{P}{E_r} f(\beta, \nu_r, t) + \frac{K_g l_w \sigma_w}{K_{ga} E_w} = \frac{3D_1\sigma_r}{E_r}$$ (A2-7)

Let $F_1 = f(\beta, \nu_r, t)$

and $F_o = f(\beta_o, \nu_r, t)$

Eq. A2-7 rewritten:

$$\frac{K_g l_w \sigma_w \phi}{E_w E_r}\left[F_1 - F_o\right] + \frac{K_g l_w \sigma_w}{E_r E_w} \cdot F_1 + \frac{K_g l_w \sigma_w}{K_{ga} E_w} = \frac{3D_1\sigma_r}{E_r}$$

or $$\sigma_w\left\{\frac{K_g l_w}{E_w E_r}\left[\phi(F_1 - F_o) + F_1\right] + \frac{K_g l_w}{K_{ga} E_w}\right\} = \frac{3D_1\sigma_r}{E_r}$$

$$\text{or} \quad \frac{\sigma_w}{\sigma_r} = \frac{3 D_1}{E_r \left\{ \frac{K_g \ell_w}{E_w E_r} \left[\phi (F_1 - F_0) + F_1 \right] + \frac{K_g \ell_w}{K_{ga} E_w} \right\}}$$

$$= \frac{3 D_1}{\frac{K_g \ell_w}{E_w} \left[\phi (F_1 - F_0) + F_1 \right] + \frac{E_r}{K_{ga}}}$$

$$= \frac{3 D_1 E_w}{K_g \ell_w E_r \left[\frac{\phi (F_1 - F_0) + F_1}{E_r} + \frac{1}{K_{ga}} \right]} \qquad (A2-8)$$

By definition, $\alpha = \frac{\sigma_w}{\sigma_r}$

Therefore,

$$\alpha = \frac{3 D_1 E_w}{K_g \ell_w E_r \left[\frac{\phi (F_1 - F_0) + F_1}{E_r} + \frac{1}{K_{ga}} \right]} \qquad (A2-9)$$

For VBS-1HT stressmeter

$D_1 = 1.5$ in.

$E_w = 30 \times 10^6$ p.s.i

$K_g = 7.5 \times 10^6$ lb/in.

$K_{ga} = 5.7 \times 10^6$ lb/in.

$\ell_w = 0.780$ in.

which gives

$$\alpha = \frac{131.58}{E_r \times 10^{-6} + 5.7\left[F_1 + \phi\left(F_1 - F_0\right)\right]} \qquad (A2\text{-}10)$$

APPENDIX 3

Experimental Results of Stiffness Testing of the VBS-1HT

APPENDIX 3

Experimental Results of Stiffness Testing of the VBS-1HT

A test to determine the gage stiffness, Kg, was performed with the test setup depicted in Figure A.3.1. The stressmeter was captured between flat ground surfaces, and loaded through a column including a spherical seat (to centralize the load).

An initial test was performed to determine the stiffness of the load system. An LVDT was employed to determine deflection.

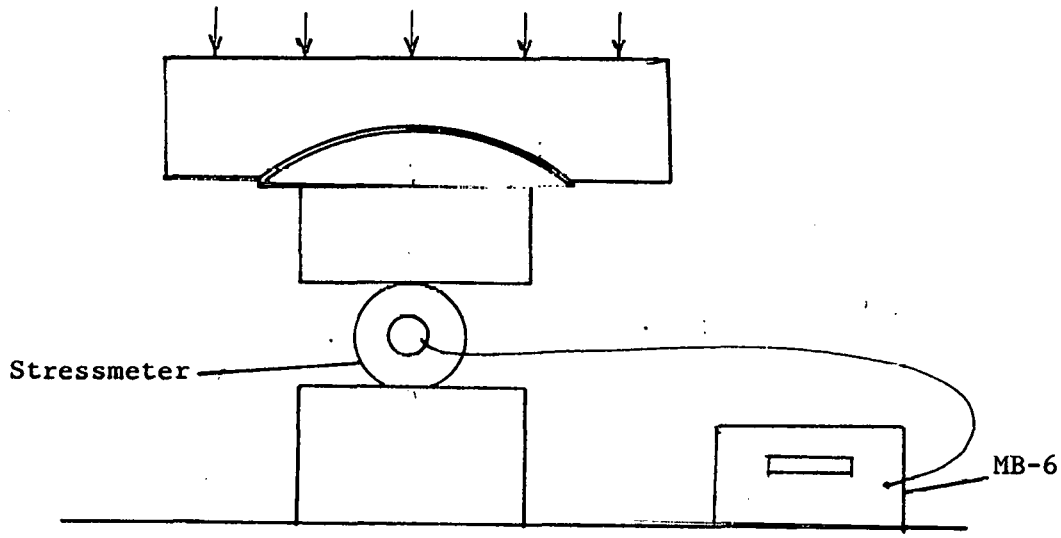

Figure A.3.1. Test Setup for Stiffness Testing of the Gage.

To determine gage stiffness, the gage output vs applied load are measured and recorded. The change in wire length was assumed to be the same as the gage body deformation. The change in gage reading is then converted to a change in wire length by Equation A3-1.

$$E_w = \frac{\Delta\sigma_w}{\Delta\varepsilon_w} = \frac{\Delta\sigma_w \ell_w}{\Delta\ell_w}$$

$$\Delta\ell_w = \frac{\Delta\sigma_w \ell_w}{E_w}$$

Substitute $\Delta\sigma_w = 1.78 \times 10'' \cdot [\ \frac{1}{T_1^2} - \frac{1}{T_0^2}\ ]$

Therefore,

$$\Delta\ell_w = 1.78 \times 10'' \cdot [\ \frac{1}{T_1^2} - \frac{1}{T_0^2}\ ] \frac{\ell_w}{E_w} \qquad \text{(A3-1)}$$

The results are then plotted as applied load vs change in wire length (interpreted as change in body dimension) and the stiffness is determined. A sample case is given below:

Stressmeter No. Q8

Applied Load (lb_f)	Wire Period $T(sec^{-1})$	Wire Length Change $\Delta\ell$(in.)
0	T_o = 1923	0
600	1977	6.76×10^{-5}
1000	2024	1.22×10^{-4}
1600	2103	2.06×10^{-4}
2000	2158	2.58×10^{-4}
2600	2253	3.41×10^{-4}
3000	2324	3.96×10^{-4}

The results are plotted in Figure A.3.2. The determined gage stiffness, Kg, was 7.5×10^6 lb_f/in. for the test cases performed.

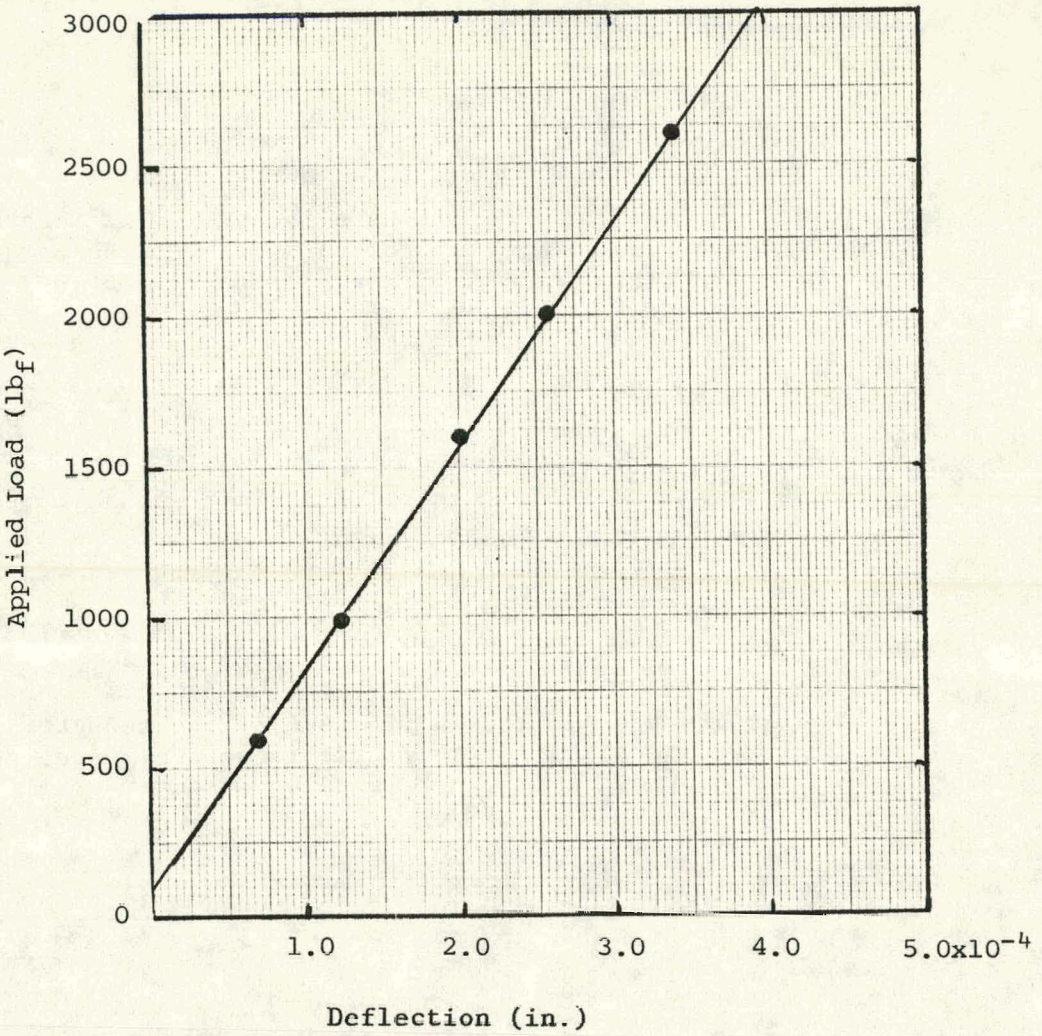

Figure A.3.2. Results of Gage Stiffness Tests

APPENDIX 4

Influence of Biaxial and Triaxial Loading on the Uniaxial Stress Sensitivity Factor

APPENDIX 4

Influence of Biaxial and Triaxial Loading on the Uniaxial Stress Sensitivity Factor

The following discussion establishes the equivalence between the hydrostatic pressure induced stress change to an overcore rock mounted in the IRAD GAGE Biaxial modulus chamber, and the uniaxial applied rock stress (defined as applied load divided by contact area) on a 1.5 in. thick test slab mounted in uniaxial compression, starting from the assumtion that equal borehole deformation produced equal stressmeter response.

Several authors (Obert and Duvall, 1967) have assumed that hydrostatic pressure is equivalent to a biaxial stress field in the plane of the borehole. This would be correct if $\frac{b}{a} \to \alpha$ (a = borehole radius, b = cylinder radius). However, for the current test, the rock specimen radius was $\cong$ 2.75 in. and hole radius $\cong$ 0.75 in.

Uniaxial

Consider a test slab, under uniaxial compression, as in Figure A1.

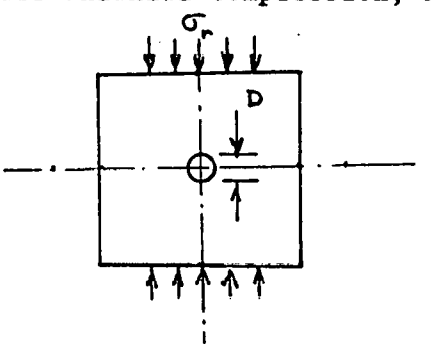

Figure A.4.1 Uniaxial Loading

The empty borehole diametral deformation, δ_e, is equal to

$$\delta_e = \frac{3 D \sigma_r}{E_r} \qquad \text{(A1)}$$

where D = borehole diameter (in.)
σ_r = applied rock stress (σ_r = P/A) (psi)
E_r = rock modulus (psi)

Biaxial

Consider an overcore sample under hydrostatic pressure, P_o, as in Figure A2.

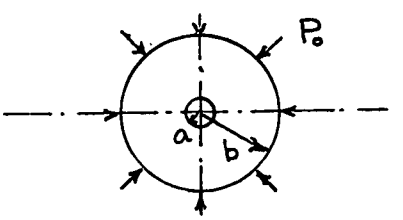

Figure A.4.2 Hydrostatic Loading

The empty borehole radial deformation, u, is equal to

$$u = \frac{2ab^2 P_o}{E_r(b^2 - a^2)} \tag{A2}$$

where a = inner radius (in.)
b = outer radius (in.)
P_o = hydrostatic pressure (psi)
E_r = rock modulus (psi)

Assuming that $P_o = K\sigma_r$, the proportionality constant, K, is determined from

$$\delta_e = 2 \cdot u$$

$$\text{or} \quad \frac{3D\sigma_r}{E_r} = 2 \cdot \frac{2ab^2 P_o}{E_r(b^2 - a^2)} \tag{A3}$$

setting D = 2a, and assuming the overcore and test slab are identical materials, Equation (A3) simplifies

$$K = \frac{P_o}{\sigma_r} = \frac{3}{2}\left[\frac{b^2 - a^2}{b^2}\right] \tag{A4}$$

Figure A3 shows the proportionality constant, K, vs core outer radius, b, based on Equation (A4). For the test case used b = 2.75 in., a = 0.75 in. Substituting into Equation (A4)

$$\frac{P_o}{\sigma_r} = 1.389 \quad ; \quad \sigma_r = \frac{P_o}{1.389} \tag{A5}$$

The uniaxial gage sensitivity, α, is ,therefore, equal to:

$$\alpha = \frac{\Delta\sigma_w}{\Delta\sigma_r} = \frac{\Delta\sigma_w}{\frac{P_o}{1.39}} = 1.39\,\frac{\Delta\sigma_w}{P_o} \tag{A6}$$

Equation (A6) defines the uniaxial gage sensitivity, α, in terms of hydrostatic pressure, P_o, for the biaxial test case.

Triaxial

The above derivation is correct for the triaxial case, with a modification to Equation (A2). The empty borehole radial deformation, u, for the triaxial case, is equal to:

$$u = \frac{2ab^2 P_o}{E_r(b^2 - a^2)} - \frac{\upsilon a P_z}{E_r} \tag{A7}$$

where P_o, a, b, E_r are as defined in Equation (A2), and

υ = Poisson's ratio
P_z = end loading (psi)

Using the same logic as the biaxial case, we seek proportionality constant, K, where $P_o = K\sigma_r$, and $\delta_e = 2.u$. Setting D = 2a, Equations (A1) and (A7) reduce to

$$\sigma_r = P_o \left[\frac{2}{3} \cdot \frac{b^2}{b^2 - a^2} \right] - \frac{\upsilon}{3} P_z \qquad \text{(A8)}$$

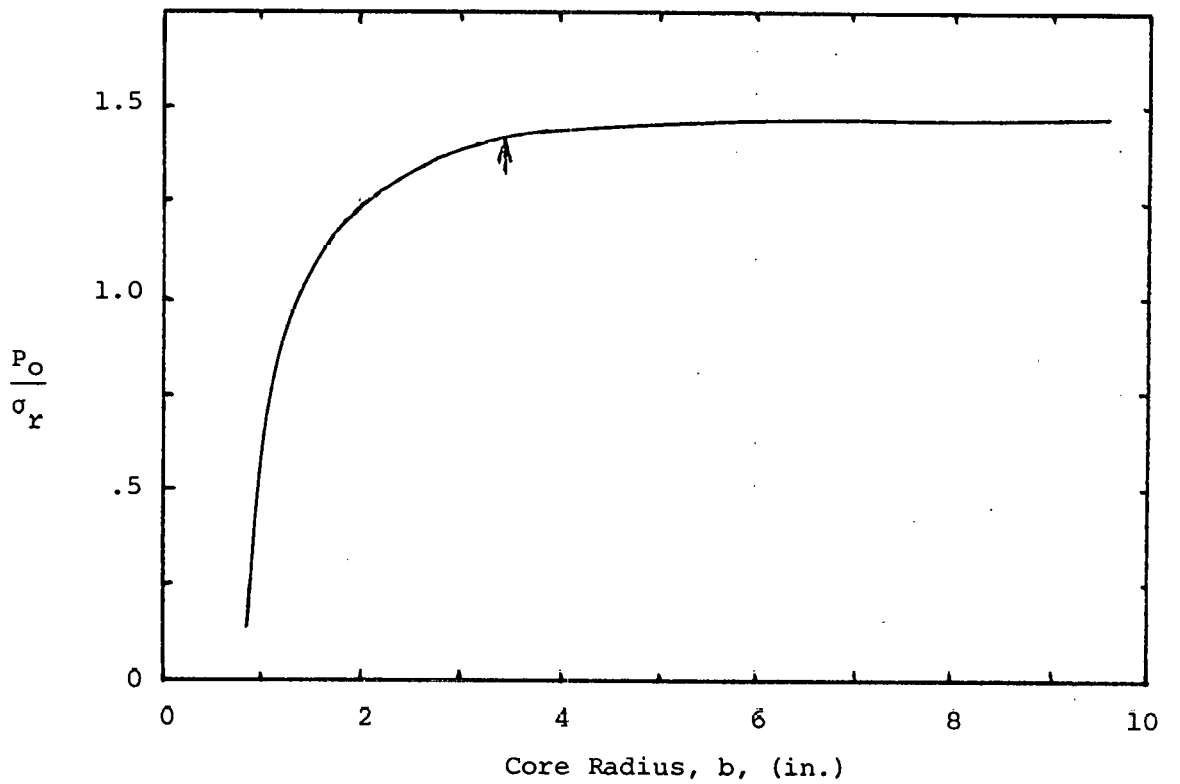

Figure A.4.3 Relationship Between Uniaxial Stress σ_r and Hydrostatic Pressure

APPENDIX 5

Calibration of Baldwin Testing Machine

TR 80-2
IRAD GAGE /93

APPENDIX 5

SATEC Systems, Inc. Grove City, Pa. 16127

Certificate of Calibration

This is to certify That *the following described machine has been calibrated in accordance with ASTM-E4 and found to be within a tolerance of* 1.0 %.

Location Creare Inc.
Hanover, NH

Machine Baldwin
(Model) UTE
(Ser. No.) 372033

Machine Range:

MACHINE READING	RING READING	MACHINE ERROR LB.	MACHINE ERROR %	P. R. CODE
600	595	4.0	.66	1
1200	1195	5.0	.42	1
2400	2390	10.0	.42	2
3600	3585	15.0	.42	2
4800	4789	11.0	.23	2
6000	5990	10.0	.17	2

Machine Range:

MACHINE READING	RING READING	MACHINE ERROR LB.	MACHINE ERROR %	P. R. CODE

Machine Range:

MACHINE READING	RING READING	MACHINE ERROR LB.	MACHINE ERROR %	P. R. CODE
2400	2379	21.0	.87	2
4800	4759	41.0	.85	2
9600	9561	39.0	.41	2
14400	14470	70.0	.49	2
19200	19290	90.0	.47	2
24000	24168	168.0	.7	3

Machine Range:

MACHINE READING	RING READING	MACHINE ERROR LB.	MACHINE ERROR %	P. R. CODE

Machine Range:

MACHINE READING	RING READING	MACHINE ERROR LB.	MACHINE ERROR %	P. R. CODE
12000	11910	90.0	.75	2
24000	23810	190.0	.79	3
48000	47698	302.0	.63	3
72000	71816	184.0	.26	3
96000	95711	289.0	.3	3
120000	119650	350.0	.29	3

CALIBRATING APPARATUS

P. R. CODE	SER. NO.	CAPACITY	LAB NO.	CALIBRATION DATE
1	480	2000	SJT.01/101268	4/78
2	1197	20000	SJT.01/101369	9/78
3	1623	200000	SJT.01/101368	9/78
4				
5				
6				

LOAD VALUES CORRECTED FOR TEMP. OF 70 °F.

Method of verification and pertinent data is in accordance with A.S.T.M. Specification E4 and SATEC Systems, Inc. "Procedure for Calibrating Tension and Compression Testing Machines" dated 9-16-68. The testing device(s) used for this calibration have been verified per A.S.T.M. Specification E74 and are directly traceable to the U. S. Bureau of Standards.

Date of Calibration OCT. 30, 1979

By J. M. [illegible]
Service Engineer

75-11S

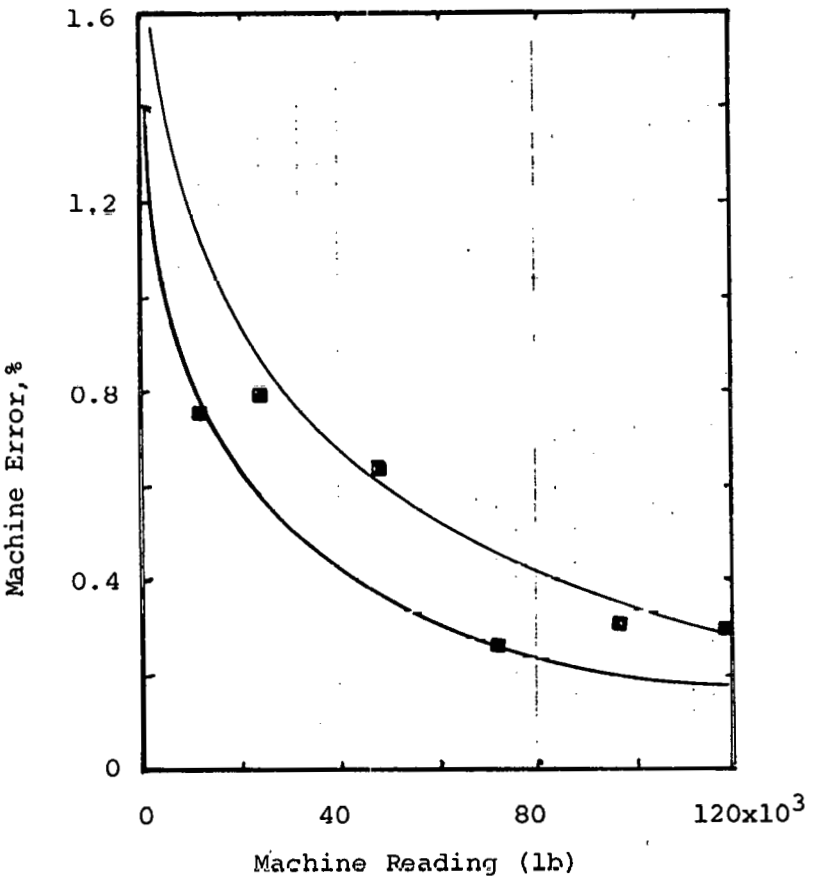

Figure A.5.1. Baldwin Testing Machine Error Band

APPENDIX 6

Biaxial Stress Changes

APPENDIX 6

Biaxial Stress Changes

The analysis of biaxial stress changes in the plane of a bore hole, in cases where the stress directions are unknown, requires the use of three gauges set at predetermined angles to each other.

The relationship between the radial deformation of a boro hole, U, and the magnitude of the two principal stresses in the plane of the bore hole has been given by

For plane stress:

$$U = \frac{D}{E_r} \left[(\sigma_1 + \sigma_2) + 2 (\sigma_1 - \sigma_2) \cos 2\theta \right] \qquad (A1)$$

where:

σ_1 and σ_2 are the principal stresses in the plane of the bore hole

θ is the angle measured counterclockwise from the direction of σ_1

D is the diameter of the bore hole

(In practice, plane strain usually applies, but as the difference between the two cases is very small, plane stress is ucually assumed). Hast (1958) has shown that Equation A1 also applies for a unidirectional stressmeter if the term $\frac{D}{E_r}$ is replaced by some other constant which is a function of E_r and the stiffness of the meter.

In applying the general form of Equation A1 to stressmeters a basic assumption is made that the force measured across the stressmeter platens is proportional to the deformation that would have occurred in this direction had the stressmeter not been there.

With respect to the Vibrating Wire Stressmeter it is convenient to express Equation A1 in the form;

$$\sigma_R = \frac{1}{3}(\sigma_1 + \sigma_2) + \frac{2}{3}(\sigma_1 - \sigma_2)\cos 2\theta$$

where:

σ_R is the radial stress in the direction θ, calculated, as explained earlier, as if the stress change were uniaxial and in the direction of θ.

For example, if this were actually the case then $\cos 2\theta = 1$; $\sigma = 0$ and

$$\sigma_R = \frac{1}{3}\sigma_1 + \frac{2}{3}\sigma_1 = \sigma_1$$

(The calculated value of σ_R is, of course, the principal stress σ_1.)

If the stress change was known to be uniaxial and at 90° to the preload direction of the gauge, then

$\cos 2\theta = -1$, $\sigma_2 = 0$ and

$$\sigma_R = \frac{1}{3}\sigma_1 - \frac{2}{3}\sigma_1 = -\frac{\sigma_1}{3}$$

i.e. $$\sigma_1 = -3\,\sigma_R$$

The stress change would be three times the value calculated using the uniaxial α and of the opposite sign. The negative sign arises because the measured, σ_R, value would be tensile when σ_1 is compressive.

APPENDIX 7

Calculation of Contact Stress

APPENDIX 7

Calculation of Contact Stress

From Roark (1975) contact stress σ_c is given by

$$\sigma_c = 0.798 \sqrt{\frac{p}{K_D C_E}}$$

where $K_D = \frac{D_1 D_2}{D_1 - D_2}$

and $C_E = \frac{1-\nu^2}{E_1}_1 + \frac{1-\nu^2}{E_2}_2$

From Table 2:

	Aluminum	Barre Granite	Climax Granite
K_D	4.5	4.5	4.5
C_E	1.18×10^{-7}	1.92×10^{-7}	1.26×10^{-7}

From Equation (24): Load on gage body P

$$P = 3.4792 \times 10^{10} \left[\frac{1}{T_2}^2 - \frac{1}{T_1}^2\right]$$

T_2 and T_1 are the Readout readings

$p = \frac{P}{1.5}$ = load per unit length

Therefore,

$$p = \frac{3.4792}{1.5} \times 10^{10} \left[\frac{1}{T_2}^2 - \frac{1}{T_1}^2\right]$$

σ_c for Aluminum

$T_1 = 1884$
$T_2 = 3535$

$p = 4679$ lb/in.

$\sigma_c = 74{,}909$ psi $\quad y_s = 50{,}000$ psi

σ_c for Barre Granite

$T_1 = 1884$
$T_2 = 2336$

$p = 2284$ lb/in.
$\sigma_c = 41{,}029$ psi
$y_s = 30\text{-}40{,}000$

σ_c for Climax Granite

$T_1 = 1884$
$T_2 = 2227$

$p = 1858$ lb/in.
$\sigma_c = 45{,}680$ psi
$y_s = 30\text{-}40{,}000$

APPENDIX 8

Algorithm Development

APPENDIX 8

Algorithm Development

A change of rock stress $\Delta\sigma_r$ in the direction of wire orientation is given by:

$$\Delta\sigma_r = \frac{1.78422 \times 10^{11} \left[\frac{1}{T_3^2} - \frac{1}{T_2^2} \right]}{\alpha} \qquad \text{(A8-1)}$$

where T_2 = stressmeter reading after setting of the meter in the borehole

T_3 = stressmeter reading after the rock stress has changed

α = uniaxial stress sensitivity factor of the meter

$$\left(\alpha = \frac{\Delta\sigma_w}{\Delta\sigma_r} = \frac{\text{Wire stress change}}{\text{Rock stress change}}\right)$$

The values of T_2, T_3 and α are sensitive to temperature change. Experiments were performed to determine the values of α for a range of temperature in Climax granite under uniaxial, biaxial and triaxial loadings.

Uniaxial Loading

Under unaxial loading, the experimental results, which are summarized in Figure 37a of the main text, show that α remains constant at a value of 4.43 for the range of temperature used; i.e., 20°C to 100°C. This value should be used for uniaxial loading situation. The rock stress change determined from Equation (A8-1) is

$$\Delta\sigma_r = 4.0275847 \times 10^{10} \left[\frac{1}{T_3^2} - \frac{1}{T_2^2} \right] \qquad \text{(A8-2)}$$

It is to be noted that the initial MB-6 reading of the set gage denoted by T_2 in the above equation will change with the ambient temperature of the gage and the rock. Laboratory test results of stressmeters set in Climax granite which was elevated to higher temperature (test Nos. 162, 163, 164 and 165) are summarized in Table A8.1 and in Figure 9 of the main text.

The thermal offset is given by the following equation:

$$T_2 - T_1 = 1.55\ (t_2 - t_1) \qquad \text{(A8-3)}$$

TABLE A8.1

RESPONSE OF UCL³ TYPE STRESSMETER SET IN CLIMAX GRANITE AT HIGH TEMPERATURE

Test No.	Temperature °C	Reading of the Set Gage
162	24	1938
163	52	1985
164	82	2035
165	96	2047

Thus, if a gage is set at temperature t_1, but loading (or rock stress change) on that gage has started at t_2 temperature, then $\Delta\sigma_r$, the rock stress change, will be determined as per the following equation:

$$\Delta\sigma_r = 4.0275847 \times 10^{10} \left[\frac{1}{T_3^2} - \frac{1}{[T_1 + 1.55\ (t_2 - t_1)]^2} \right]$$

Example:

Suppose a stressmeter was set in Climax granite at 20°C. The temperature of the rock subsequently increased to 25°C and the rock stress also changed because of mining operation. Readings of the stressmeter after setting was 2010 at 20°C and 2450 at 85°C. Determine the change in rock stress due to mining operation.

$T_1 = 2010$

$T_3 = 2450$

$t_2 = 25°C$

$t_3 = 85°C$

$$\Delta\sigma_r = 4.0275847 \times 10^{10} \left[\frac{1}{T_3^2} - \frac{1}{[T_1 + 1.55\ (t_2 - t_1)]^2} \right]$$

$$= 4.0275847 \times 10^{10} \left[\frac{1}{(2450)^2} - \frac{1}{[2010 + 1.55\ (85 - 25)]^2} \right]$$

$$= 2397 \text{ psi}$$

Biaxial and Triaxial Loading

For biaxial and triaxial loading, the results are given in Figures 37a through 37e in the main text, Section 4.8. These results are summarized in Table A8.2. The average values of α are plotted against temperature in Figure A.8.1. In triaxial use of the gage, data from this curve should be used for α.

TABLE A8.2

VALUES OF α FOR BIAXIAL AND TRIAXIAL LOADING

End load psi / KPa	0 / 0	225 / 1.55	615 / 4.24	1230 / 8.50	
Temp °C					Average
23 } 26 }	2.75	2.82	2.78	3.00	2.84
52 } 57 }	2.81	2.90	2.80	3.20	2.93
72	2.88	3.06	3.20	3.33	3.12
98	3.75	3.60	3.70	-	3.69

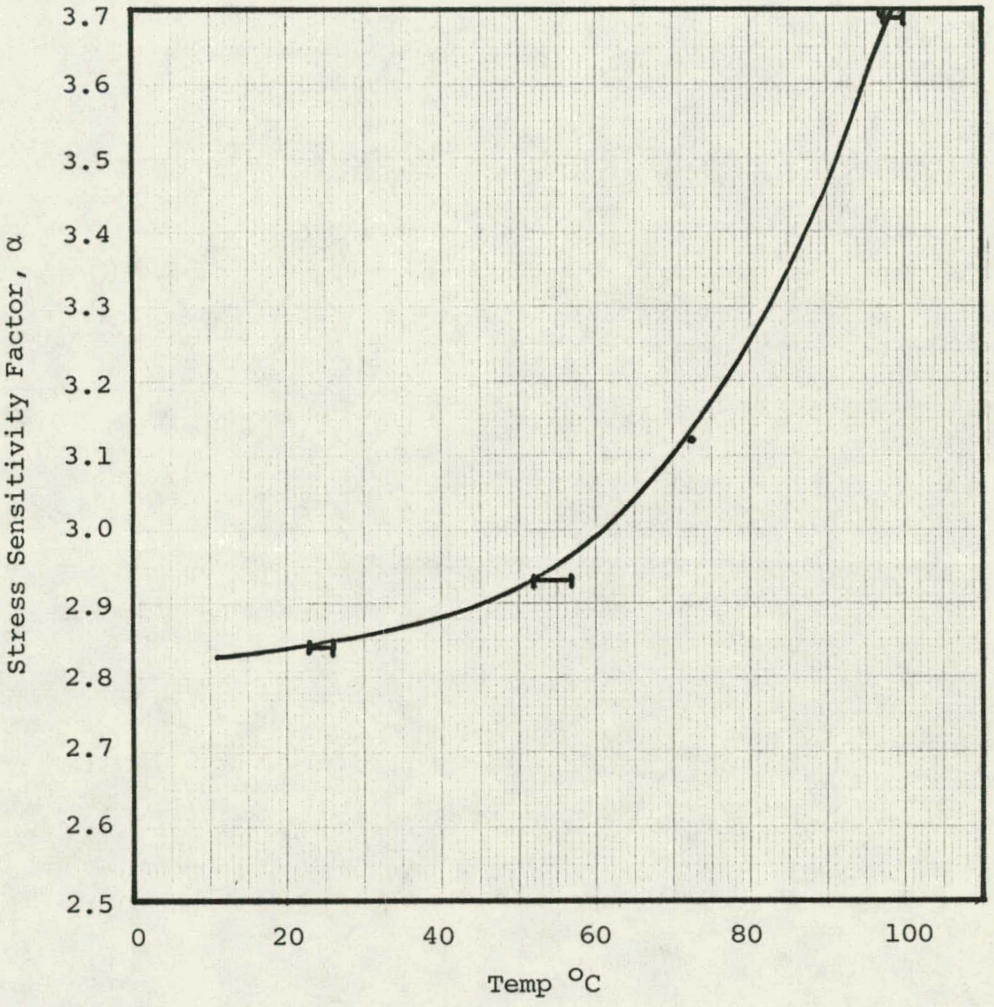

Figure A.8.1. Change of α with Temperature in Triaxial Loading of Climax Granite.